

## RESPONSE TO REVIEWERS

21 June 2019

Kelvin H. Bates and Daniel J. Jacob

We sincerely appreciate the time and effort expended by the reviewers in helping us improve and refine this lengthy manuscript. We have responded to each of the reviewers' suggestions in detail below. In the following pages, the reviewer comments are shown in italics, while our responses are shown in plain text. Throughout the responses below and the attached revised manuscript, added text is highlighted in red, while removed text is greyed and crossed out. We hope these revisions have fully addressed the concerns of the reviewers.

### REVIEWER 1

*I found that I wanted a little more explanation of the underlying reasons for presented differences in performance of RCIM compared with the detailed MCM scheme, i.e. (i) are they due to different fundamental assumptions in MCM and the Wennberg et al. (2018) comprehensive mechanism; or (ii) do they result from simplifications made in RCIM compared with the Wennberg et al. (2018) comprehensive mechanism? If the former, are the differences because there is currently no experimental information to base the chemistry on, and different assumptions have been made?*

Very few of the differences in performance presented herein are due to changes from the comprehensive (full, explicit) mechanism to the reduced (RCIM) mechanism. The Reduced mechanism was made concurrently with the full in Wennberg *et al.* (2018) and was designed to keep final product yields of known compounds the same. Where such products and reaction pathways weren't known, the authors sought to apply reasonable assumptions, extrapolations from similar compounds, and structure-activity relationships. Thus, most of the differences presented here are due to fundamental differences between the chemistry in RCIM and that in MCM and the GEOS-Chem v11-02c mechanisms, which we seek to describe along the way as we present the differences in model outcomes.

For the most part, the simplifications made from the full mechanism to the RCIM are detailed in Wennberg *et al.* (2018), and we avoid rehashing them here in this already length paper. To clarify these points, we have added the following to the first paragraph in the "Chemical mechanism" section (2.1): "RCIM is v4.1 of the "Reduced-plus" mechanism found in the Wennberg *et al.* (2018) mechanism repository (DOI 10.7907/Z9S75DHB). It includes the oxidation of isoprene by OH, ozone, and NO<sub>3</sub> and condenses the ensuing oxidation cascade for the practical range of atmospheric conditions. The mechanism includes 148 species and 412 reactions representing the complete isoprene oxidation cascade (~~full conversion to CO<sub>2</sub>~~), in contrast to the 385 species and 810 reactions in the Wennberg *et al.* (2018) full explicit mechanism, which did not seek to provide loss processes for compounds without experimental constraints, and therefore did not represent a complete oxidation cascade (i.e. full conversion to CO<sub>2</sub>). RCIM was compiled concurrently with the full explicit mechanism and was designed to

keep product yields of known compounds the same, with minimal simplifications beyond lumping of isomeric compounds with similar reaction pathways and removal of especially minor (<1% yield) pathways. Under atmospheric conditions, early-generation compound yields and mixing ratios in simulations with RCIM therefore closely track those of the full explicit mechanism. Major deviations occur only for later-generation compounds for which minimal experimental evidence exists to constrain reactive pathways, and for the proposed products of these reactions. For such compounds, the authors applied a self-consistent set of assumptions (Section 2 in Wennberg *et al.*, 2018) based on extrapolation from similar compounds and structure-activity relationships. While these assumptions were grounded in experimental evidence, they necessarily include high levels of uncertainty, which are discussed in greater detail in Section 8 of Wennberg *et al.* (2018).”

*a) Page 11, glyoxal section: The peak production of glyoxal at low [NO] from RCIM is explained by “. . .contributions from ISOPOO H-shifts and the degradation of IEPOX”, and contrasted with that from MCM. Inspecting Figs. 3 and 8 of Jenkin et al. (2015), it appears that MCM does have routes to glyoxal (and methyl glyoxal) from both ISOPOO1,6 H-shifts and the degradation of IEPOX, with this chemistry informed by mechanistic information presented by Peeters et al. (2014) and Bates et al. (2014). However, they rely on RO<sub>2</sub> to RO conversion and therefore require reaction of RO<sub>2</sub> with NO, NO<sub>3</sub> or RO<sub>2</sub>. At low [NO] these processes are generally outrun by competing 1,4 formyl H atom shifts or reaction with HO<sub>2</sub>. Wennberg et al. (2018) assume very high propagating channel branching ratios for the reactions of HO<sub>2</sub> with RO<sub>2</sub> radicals formed from OH + IEPOX, and those formed following the 1,6 ISOPOO H-shifts. These reactions provide additional RO<sub>2</sub> to RO conversion routes at low [NO], with associated formation of glyoxal (and methyl glyoxal) and OH. This assumption may or may not prove to be correct, but at present there is no evidence from elementary kinetics studies of RO<sub>2</sub> + HO<sub>2</sub> reactions to support propagating branching ratios as high as some of those applied.*

The discrepancies in glyoxal between GEOS-Chem v11-02c and RCIM are among the most striking in this manuscript, and they do therefore deserve particular attention, as the reviewer points out. Glyoxal yields were a point of strong disagreement between MCM and GEOS-Chem to begin with (fig S18-19); while MCM predicts higher glyoxal than RCIM under NO-dominated conditions, lower glyoxal under HO<sub>2</sub>-dominated conditions, and about the same under isomerization-dominated conditions, GEOS-Chem predicts about the same under all conditions except isomerization-dominant, under which conditions it predicts much more glyoxal. This derived largely from the observational constraints presented in Chan Miller *et al.* (2017), who sought to reconcile high observed glyoxal in isomerization-dominated conditions by increasing second-generation production from the products of isomerization (HPALD, DHDC). While RCIM retains some second-generation formation from the non-HPALD products (namely via HPETHNL from the assumed rapid photolysis of the C<sub>4</sub> dihydroperoxy carbonyls) and later-generation formation (via glycolaldehyde and the C<sub>4</sub> tetrafunctional compounds), the yield through these pathways is greatly reduced from Chan Miller's work. As pointed out by the reviewer, deviations from MCM derive largely from the radical-propagating channels of RO<sub>2</sub> + HO<sub>2</sub>, which are assumed to be greater in RCIM than in MCM.

In an already lengthy paper, we sought to avoid discussing specific points of uncertainty in the mechanism when such details are already covered in the initial mechanism description in Wennberg *et al.* (2018), but we agree that pointing out the conjectural pathways that prove particularly important to model outcomes of interest may be a beneficial way to direct future research to the most important remaining uncertainties, and will help the reader understand which aspects of these model outcomes are more or less constrained. As such, we have added a brief discussion of the uncertainties in the Wennberg *et al.* (2018) mechanism to Section 2.1 (described in the response to the previous reviewer comment; the radical propagating channels of HO<sub>2</sub> + RO<sub>2</sub> reactions were highlighted as one such uncertainty), and have revised the glyoxal subsection of Section 5.1 as follows:

"Glyoxal (C<sub>2</sub>H<sub>2</sub>O<sub>2</sub>) is also measured by satellites (Vrekoussis *et al.*, 2009; Alvarado *et al.*, 2014; Chan Miller *et al.*, 2014), and different yields relative to formaldehyde can discriminate between emissions of different VOCs (Chan Miller *et al.*, 2016). Past mechanisms have provided differing estimates on which isoprene oxidation pathways produce the most glyoxal (Li *et al.*, 2016), and comparisons with field measurements show that glyoxal production is higher under low-NO conditions than most mechanisms predict (Li *et al.* 2016, Chan Miller *et al.*, 2017). ~~RCIM yields of glyoxal from isoprene peak at 10% under low-NO conditions (Figure 10), reflecting contributions from ISOPOO H-shifts and the degradation of IEPOX.~~ In contrast, glyoxal yields in MCM are highest at high NO. Our diurnal steady-state box model simulations show that the RCIM glyoxal/formaldehyde ratio remains in the 2-3% range over the ensemble of atmospheric conditions (see Figure S21), in line with field observations for isoprene-dominated environments (Kaiser *et al.*, 2015; Chan Miller *et al.*, 2017).

RCIM yields of glyoxal from isoprene peak at 10% under low-NO conditions (Figure 10), while glyoxal yields in MCM are highest under high-NO conditions, and yields in the GEOS-Chem v11-02c mechanism are even higher than RCIM under low-NO conditions (Figures S18-S19). Mechanistically, these differences primarily reflect changes in the contributions from two low-NO pathways in RCIM relative to MCM and v11-02c: the products of Z- $\delta$ -ISOPOO H-shifts, and the reactions of IEPOX-derived peroxy radicals with HO<sub>2</sub>. While both MCM and RCIM include moderate yields of glyoxal (largely via hydroperoxyethanal) from the C<sub>4</sub>-dihydroperoxy-carbonyl products of Z- $\delta$ -ISOPOO H-shifts, GEOS-Chem v11-02c incorporates much higher second-generation glyoxal yields from these H-shift pathways (primarily via HPALD and dihydroperoxy-dicarbonyl compounds), consistent with field observations (Chan Miller *et al.*, 2017). For the reactions of IEPOX-derived peroxy radicals with HO<sub>2</sub>, both RCIM and GEOS-Chem v11-02c include moderate yields of glyoxal presumed to form in the radical-propagating reaction channel (RO<sub>2</sub> + HO<sub>2</sub>  $\rightarrow$  RO + OH + O<sub>2</sub>), as suggested in Bates *et al.* (2014) and implemented in Wennberg *et al.* (2018), while MCM includes no glyoxal formation under low-NO conditions from IEPOX-derived peroxy radicals. Both the atmospheric fates of C<sub>4</sub>-dihydroperoxy-carbonyl compounds and the radical-propagating channels of non-acyl RO<sub>2</sub> + HO<sub>2</sub> reactions are poorly constrained (Wennberg *et al.*, 2018), and the glyoxal yields from these pathways therefore remain uncertain.

We find in GEOS-Chem that many glyoxal precursors (IEPOX, nitrates, and tetrafunctional C<sub>5</sub> compounds) are lost to aerosol or deposition before they can react in the gas phase, depressing the glyoxal yield relative to the box model simulations where aerosol/deposition effects are not included. This results in a global glyoxal yield from isoprene of 2% in GEOS-Chem with RCIM, only half that reported recently by Muller *et al.* (2019) and even lower than in some past simulations (Fu *et al.*, 2008; Myriokefalitakis *et al.*, 2008; Taraborrelli *et al.*, 2009). We find a reduction in global tropospheric glyoxal loading of 60% relative to the GEOS-Chem v11-02c mechanism. However, Miller *et al.* (2017) found good agreement between glyoxal simulated by GEOS-Chem v11-02c and aircraft observations in the Southeast United States. This suggests that RCIM may underestimate glyoxal yields from isoprene."

*Rapid exclusive photolysis of di-HPCARBs is assumed (instantaneous in RCIM) leading significantly to methylglyoxal formation, and some glyoxal formation (via HOOCH<sub>2</sub>CHO) in conjunction with substantial OH formation. Wennberg *et al.* (2018) indicate that "No experimental evidence exists to constrain these rates and products, so the mechanisms shown here are strictly conjectural". Because the di-HPCARBs do not contain a conjugated C=C double bond, it is likely that their photolysis is not exceptionally rapid, and MCM logically represents competitive loss by reaction with OH. This reduces the yield, and delays formation, of methylglyoxal and glyoxal. It therefore appears that at least some of the higher formation of glyoxal in RCIM at low [NO] results from assumptions that differ from those in MCM, which may or may not be correct. This therefore highlights areas of uncertainty in understanding, where more information is required, and this should probably be made clearer.*

The uncertainties in this pathway do indeed merit greater attention, and we thank the reviewer for the detailed assessment of this reaction channel. We highlight these uncertainties and their importance for both glyoxal production and OH regeneration in our responses to the previous reviewer comment (glyoxal, Section 5.1) and the next reviewer comment (OH, section 4.1).

*It should probably be made clearer that the higher OH at low [NO] in RCIM results at least partly from the assumed choice of processes that maximize HO<sub>x</sub> regeneration, rather than from recent advances in understanding that are reported in Wennberg *et al.* (2018) and not considered in earlier mechanisms.*

This process is indeed a major source of the increased OH in RCIM under low-NO conditions, and we thank the reviewer for drawing more attention to this uncertainty. As described above, we have included additional discussion of the relative certainty and uncertainty of specific aspects of the Wennberg *et al.* (2018) mechanism in Section 2.1, which touches on this point. We have also added the following to the "Effects on HO<sub>x</sub> radicals" section (4.1) to clarify the uncertainty surrounding the fate of the C<sub>4</sub> dihydroperoxy-carbonyl species: "The initial H-shift of the Z-δ-4-OH-ISOPOO radical (the dominant ISOPOO H-shift pathway) is highly temperature-dependent and regenerates one equivalent of HO<sub>x</sub> (0.6 OH + 0.4 HO<sub>2</sub>) concurrently with the first generation of non-radical products. In RCIM, the C<sub>4</sub>-dihydroperoxy-carbonyl compounds (top right of Figure 6) produced in this reaction are assumed to rapidly photolyze as postulated in

Wennberg *et al.* (2018), which produces an additional 1.2 HO<sub>x</sub> equivalents, for a total HO<sub>x</sub> regeneration of 2.2 equivalents (1.5 OH + 0.7 HO<sub>2</sub>) from the 1,6 H-shifts of Z- $\delta$ -ISOPOO isomers. Reaction with OH could possibly provide a competitive loss pathway for the C<sub>4</sub>-dihydroperoxy-carbonyl compounds, which would result in lower net HO<sub>x</sub> production."

*The use of the "fixed radical box modeling" method would benefit from further justification of why it is of value. At present, it seems to be justified by the following sentence: "This method serves to remove most nonlinearities and feedbacks inherent in the isoprene oxidation mechanism, so as to isolate the effects of the radicals on the oxidation pathways." Surely, the non-linearities and feedbacks (i.e. on HO<sub>x</sub> and NO<sub>x</sub>) exemplify the major differences between the mechanisms and contribute to the "effects of the radicals on the oxidation pathways" in the different mechanisms. While I understand that you can look at the OH-initiated oxidation alone (i.e., without O<sub>3</sub>- and NO<sub>3</sub>-initiated oxidation), it is quite difficult to understand how heavily constraining the system provides reliable information on comparative mechanism performance.*

Our goal in including the fixed-radical box models was to provide quantitative product yields, particularly of organic products, under specific ambient conditions; their use is intended primarily for the reader who has observed isoprene oxidation in a chamber or the atmosphere at quantified NO and HO<sub>2</sub> conditions to look up an expected yield from these plots. We acknowledge in the text that this is an unrealistic way to compare the effects of isoprene oxidation on oxidant cycling and overall (e.g. global) outcomes across mechanisms, but we still find utility in answering the question: "Under a given observed level of (e.g.) OH, NO, and HO<sub>2</sub>, light, and temperature, what can I expect the yield of (e.g.) formaldehyde to be from OH-initiated isoprene oxidation in RCIM, and how does that compare to MCM and GC v11?" In an effort to clarify this point, we have expanded the sentence questioned by the reviewer to read: "This method serves to remove most nonlinearities and feedbacks inherent in the isoprene oxidation mechanism, so as to isolate the effects of the radicals on the oxidation pathways, and provides a quantitative reference of organic product yields from OH-initiated isoprene oxidation under fixed ambient conditions."

*> 10 ppb NO is stated to be "not of general atmospheric relevance". However, the fixed box model outputs in the SI present results and comparisons up to 100 ppb NO, with some of the largest differences occurring between 10 ppb and 100 ppb.*

We believe these may still be a useful reference to some readers, particularly because while such conditions are not of general atmospheric relevance, they have been used in chamber experiments to constrain product yields. The comparisons in, e.g., Figure S14 therefore allow a reader with some specific curiosity about these conditions to identify the potential disparities in outcomes between the mechanisms compared here. We have updated the relevant sentence from "Here, the reduced model deviates substantially from reality and from the explicit model, but these conditions are rarely relevant in the atmosphere." to "Here RCIM deviates substantially from the explicit mechanism of Wennberg *et al.* (2018) and MCM (see Figure S14). These conditions are not of general atmospheric relevance, but may occur in chamber

experiments; for such applications, we recommend the use of a mechanism that resolves the full system of allylic and peroxy radicals (Figure 1)."

*Because simulated [OH] varies by an order of magnitude (e.g. Fig. 5), probably should give corresponding [OH] for the stated lifetime.*

We have added a parenthetical clarification to the relevant sentence: " $\tau_{\text{OH}} = 1.1 \text{ h}$  for  $[\text{OH}] = 2.5 \times 10^6 \text{ molecules cm}^{-3}$  at  $T = 298 \text{ K}$ ".

*I think "Heinz Becker" should simply be "Becker" (i.e. his first name is Karl-Heinz). Similarly in the reference list "Becker, K. H." rather than "Heinz Becker, K."*

This copyediting error has been fixed as suggested.

*I believe inclusion of Archibald et al. (2010) reference in this set of references is incorrect, because that study specifically did not consider hypothetical OH recycling mechanisms. In contrast, it systematically considered a series of explicit HO<sub>x</sub> recycling mechanisms based on reported experimental and theoretical data, and was one of the first (or possibly the first) to support and demonstrate the potential significance of the reversible O<sub>2</sub> addition peroxy radical isomerisation chemistry reported by Peeters et al. (2009), and subsequently characterized in detail by Wennberg and coworkers. The historical overview therefore needs some adjustment, and should also give more recognition to Peeters and co-workers for their pivotal role in moving the understanding of isoprene chemistry forward.*

Condensing the expansive and convoluted history of research on isoprene oxidation mechanisms into a brief overview was a challenge, and we thank the reviewer for pointing out this oversight. We have removed the reference to Archibald et al. (2010) from the sentence describing hypothetical OH-recycling mechanisms, and have replaced the subsequent sentence ("These were later replaced with mechanistic OH-recycling pathways, including isoprene epoxydiol (IEPOX) formation (Paulot et al., 2009b) and H-shift chemistry (Peeters et al., 2009; Asatryan et al., 2010; Crouse et al., 2011).") as follows: "These were later replaced with mechanistic OH-recycling pathways, including isoprene epoxydiol (IEPOX) formation (Paulot et al., 2009b), radical propagation in reactions of HO<sub>2</sub> with acylperoxy radicals (Hasson et al., 2004; Jenkin et al., 2007; Dillon and Crowley, 2008), and H-shift isomerizations of the initial isoprene-hydroxy-peroxy radicals (Peeters et al., 2009). Incorporation of these mechanistic OH-recycling pathways into models showed the latter pathway to be most important for sustaining elevated OH concentrations under low-NO conditions (Archibald et al., 2010), and subsequent studies have identified and characterized additional OH-regenerating H-shift reactions throughout the isoprene oxidation mechanism (Peeters et al., 2010; Crouse et al., 2012; Crouse et al., 2013; Peeters et al., 2014; Jørgensen et al., 2016; Wang et al., 2018; Møller et al., 2019)."

We have also expanded the sentence in the subsequent section (2.1) describing the dynamic system of hydroxy-isoprene-allylic and hydroxy-isoprene-peroxy (ISOPOO) radicals to

reflect the role of Peeters and coworkers in elucidating this chemistry. The sentence "Addition of O<sub>2</sub> to allylic radicals under ambient conditions is in fact a reversible process, resulting in a dynamic system with differing initial (kinetic) and equilibrium radical distributions (Teng *et al.*, 2017)" now reads "Addition of O<sub>2</sub> to allylic radicals under ambient conditions is in fact a reversible process, resulting in a dynamic system with differing initial (kinetic) and equilibrium radical distributions, **as first postulated by Peeters *et al.* (2009) and demonstrated experimentally by Teng *et al.* (2017).**"

*Page 8, line 24: In relation to HO<sub>x</sub> production and recycling, the following statement is made about RCIM: "Assuming that photolysis is the dominant fate of the conjugated hydroperoxy-aldehydes (HPALDs) that make up 60% of the stable products, HO<sub>x</sub> production can increase . . ." If I understand pp 3352/53 of Wennberg *et al.* (2018) correctly, the conjugated HPALDs actually only account for 25 % of the products following 1,6 H isomerization; with 15 % unconjugated HPALDs and the remainder other products (e.g. di-HPCARBs). This seems quite different from the stated 60 %. Looking at Fig. 6, it looks like the conjugated species make up 60 % of the total HPALDs, but are 24 % (i.e. 60 % of 40 %) of the full suite of products (with 16 % being the unconjugated species). If this is correct, I presume that the statement on Page 8, line 5 should specify "60% of the HPALDs" rather than "60% of the stable products".*

This sentence was indeed written incorrectly, and we thank the reviewer for their careful attention. The total HO<sub>x</sub> production of 3.0 equivalents was meant to represent an upper bound if all HPALDs photolyze. To reflect this, the relevant sentence has been rewritten as follows: "**An upper limit of 3.0 equivalents of HO<sub>x</sub> production (2.2 OH + 0.75 HO<sub>2</sub> + 0.04 RO<sub>2</sub>) can be achieved in the second oxidative generation if photolysis is also the dominant fate of the HPALDs that make up the remaining 40% of the stable products.**"

*S4 caption – I think "fun" should be "run".*

This typographic error has been fixed as suggested.

*S19 caption – I think "Jenkin *et al.* 2015" here is incorrect.*

This copyediting error has been fixed as suggested.

## REVIEWER 2

*More explanation about the analysis of the fixed radical box modelling is necessary. It is understood that the model is run until complete conversion to CO<sub>2</sub> but it is not explained how the concentration for a particular species is calculated; is it the maximum value achieved by a species, the average concentration over a period of time or another metric?*

The fixed-radical box modeling is not used to compute concentrations, but only to quantify product yields from isoprene oxidation by OH. To clarify this, the following sentence has been

added to the "Fixed-radical box modeling" paragraph of Section 2.2: "Product yields are calculated by dividing the total molar production over the entirety of the simulation of each compound of interest by the amount of isoprene oxidized."

*It appears the main aim of the paper is to compare the effect of the new isoprene mechanism with older mechanisms. Therefore, it is felt that Figure 7, which compares global model results of the new isoprene mechanism with a no-isoprene scenario, is much less relevant than Figure S17 in the SI which compares global model results between the new mechanism and the standard GEOS-Chem vn11.02 mechanism. The general effect of isoprene on NO<sub>x</sub>, O<sub>3</sub> and OH is well known in the field. Fig S17 should replace current Figure 7 and the discussion in section 4 should focus more on the differences in global model output between vn11.02 and RCIM rather than RCIM vs. no isoprene. Furthermore, the no-isoprene scenarios plots in Figure 5 should be removed for clarity and more attention paid to the differences between the various mechanisms' outputs.*

Our aim in this manuscript was not primarily to compare RCIM with older mechanisms, but rather to characterize RCIM as a standalone component of box and global models, and to demonstrate the effects of isoprene oxidation (as simulated with RCIM) on regional and global budgets of oxidants, NO<sub>x</sub>, organic products, and SOA. While the general effects of isoprene on NO<sub>x</sub>, O<sub>3</sub> and OH may be well known in the field, recent changes to our understanding of isoprene oxidative chemistry have forced us to revise some of this knowledge, which merits a new assessment as presented here. We therefore chose to focus primarily on the absolute outcomes following implementation of RCIM into GEOS-Chem, rather than relative changes from the past mechanism. The GEOS-Chem v11-02c mechanism has no intrinsic geophysical value; it represents a snapshot of our chemical understanding of isoprene oxidation at a single point in time, and as such, direct comparisons between the mechanisms will soon be irrelevant when the GEOS-Chem mechanism is updated.

For these reasons, we believe the RCIM-to-no-isoprene maps are better suited for the main manuscript. We still see value in including maps and tables of RCIM-to-v11 differences as a reference, e.g. for previous studies that have used the v11 mechanism for model-measurement comparisons. We also describe the RCIM-to-v11 differences in each subsection of Sections 4 and 5 in the main manuscript. To provide additional information on the differences in global model output between v11 and RCIM as requested by the reviewer, we have added regional product yield statistics from GEOS-Chem v11 simulations to Table S3 in the Supplement, and have added a new table (S6) to the Supplement with inter-mechanism comparisons of global and regional mixing ratios of compounds of interest. We have removed the column from Table S2 that contained similar (but less detailed) information. We hope that these modifications will provide the additional detail and attention to mechanism output differences requested by the reviewer, while maintaining the focus on the RCIM output alone in the main manuscript.

*It would be beneficial to see how the model output using RCIM and vn11.02 compare to observational data. In particular the significant predicted changes to OH, NO<sub>x</sub>, CO and HCHO*

*over the Amazon and the CO change over much of the southern hemisphere should be compared to observational data if one is to have confidence in the use of RCIM.*

Detailed comparisons to observational data are beyond the scope of this work, and rely heavily on the spatiotemporal distribution of isoprene emissions, a major source of uncertainty on regional scales (see, e.g., Kaiser *et al.*, 2018, and Barkley *et al.*, 2013; we particularly avoid comparisons with formaldehyde observations for this reason, as isoprene emissions are often inferred from formaldehyde retrievals). Because RCIM is built up from chamber experiments and theoretical studies as detailed in Wennberg *et al.* (2018), it provides an independent source of mechanistic detail that should, in theory, not require additional constraint from field observations. However, we agree that some corroboration of the major changes shown in this work with ambient measurements is necessary if future users of RCIM are to have confidence in the mechanism. For this reason, we have included brief comparisons to previous model-measurement studies throughout the text as relevant (e.g., in the original manuscript, p10 L8-11 for ozone in the Southeast US, p11 L28-30 for glyoxal-formaldehyde ratios, p12 L27-30 for MVK/MACR, and p14 L1-3 for isoprene nitrate lifetime).

Observational constraints and prior model-measurement comparison studies have focused largely on the Southeast United States, and our discussion in this manuscript therefore focuses primarily on this region, but as the reviewer rightly points out, many of the largest differences between RCIM and GEOS-Chem v11-02c can be found over the Amazon Basin and in the Southern Hemisphere. While a detailed comparison with observations over the Amazon remains outside the purview of this study, we have added the following passages to relevant sections describing outcomes that exhibit sharp changes over the Amazon:

[to Section 4.1, "Effects on HO<sub>x</sub>"]: "RCIM increases the simulated annual mean OH concentration over the Amazon by +170% relative to GEOS-Chem v11-02c, and that of HO<sub>2</sub> by +30%, both in better agreement with field observations in the region (Barkley *et al.*, 2011)."

[to Section 4.2, "Effects on NO<sub>x</sub>"]: "For example, global simulations with RCIM result in a 17% increase in annual mean surface NO<sub>x</sub> mixing ratios relative to the GEOS-Chem mechanism over the Amazon Basin (see Figure S17 and Table S6), a region where surface NO<sub>x</sub> is typically underestimated in GEOS-Chem (Barkley *et al.*, 2011; Liu *et al.*, 2016)."

[to Section 5.1, "Oxygenated VOCs and CO", CO subsection]: "Distributional changes from the GEOS-Chem v11-02c mechanism include 9% higher CO concentrations over the Amazon (due to faster in situ isoprene oxidation from higher OH) and a more diffuse increase of ~2% in CO concentrations throughout the Southern Hemisphere (see Figure S24), where GEOS-Chem tends to underestimate remote surface, column, and upper-tropospheric CO (Zeng *et al.*, 2015; Huang *et al.*, 2016; Fisher *et al.*, 2017)."

*The SOA yield is predicted to be significantly higher than previous models. The contribution to SOA from various species is explained. However, little detail is provided regarding the estimates of SOA production from each species aside from IEPOX. Specifically, the estimates of*

SOA from HMML, non-IEPOX non-IDHPE species, nitrates, glyoxal and the tetrafunctionalised species are not explained. The decision to treat the tetrafunctionalised species as LVOCs within the GEOS-Chem framework also warrants further discussion as the species span a wide range of volatilities.

Substantial updates to the complex SOA formation scheme in GEOS-Chem are beyond the scope of this work, and will be the subject of a future study with more detailed treatment of reactive uptake parameterizations (e.g. Jo *et al.*, 2019), incorporation of additional reactive and depositional particle sinks (e.g. Hodzic *et al.*, 2016), and comparisons to field measurements (e.g. Pai *et al.*, 2019). For this reason, we chose to focus primarily on the production of gas-phase SOA precursors in Section 5.3 of the present manuscript, and we direct the reader to Marais *et al.* (2016) for more detail on the SOA uptake parameterizations of each individual compound in Sections 2.1 and 5.3. We describe the gas-phase production of HMML, non-IEPOX non-IDHPE species, and the tetrafunctional species in detail in Section 5.3, and in the same section briefly describe the SOA-relevant production of glyoxal (for which more detail can be found in Section 5.1) and organonitrates (the subject of Section 5.2). We agree that the uniform SOA uptake treatment of the tetrafunctional species as identical to the "LVOC" species already contained in GEOS-Chem is overly simplistic. The uptake parameterization will need to be amended as further constraints become available, and for immediate implementation in GEOS-Chem, it should be reduced to bring SOA formation in line with previous model-measurement comparisons. To highlight these points, we have a number of clauses and sentences to the C<sub>5</sub> tetrafunctional compound subsection of Section 5.3:

... "MCM and GEOS-Chem v11-02c predict similar yields of C<sub>5</sub> tetrafunctional species, but the relative contributions of individual species vary substantially between mechanisms (See Figures S22-23), and GEOS-Chem v11-02c only considered SOA formation from two such species (dihydroxy-dinitrates and "LVOC" produced in the reaction of ISOP<sub>2</sub>OOH with OH), resulting in 4 Tg a<sup>-1</sup> iSOA from C<sub>5</sub> tetrafunctional compounds. Because the rates of gas-phase oxidation, deposition, and aerosol uptake for these compounds are all poorly constrained, their contribution to iSOA remains highly uncertain, and future studies will need to evaluate the volatilities, solubilities, and particle-phase reactivities of the individual tetrafunctional species." ... "This total carries high uncertainty, due both to the SOA uptake parameterization and the lack of constraints on other loss pathways of the C<sub>5</sub> tetrafunctional compounds, but is similar to a recent estimate by Stadtler *et al.* (2018) and highlights the importance of further investigations of this iSOA formation pathway. Until such studies are performed, we recommend reducing the LVOC uptake coefficient applied to the tetrafunctional species by a factor of ten in GEOS-Chem implementations, to bring iSOA production from this pathway in line with previous model-measurement comparisons (Marais *et al.*, 2016; Pai *et al.*, 2019)."

## MINOR ADDITIONAL CHANGES

Several small changes have been made throughout the manuscript for clarity, detailed below with page and line numbers corresponding to the discussion manuscript:

[P5L6] “NO<sub>2</sub>/NO molar ratio of 5,”

[P5L17] “NO emissions are constant for a given simulation and are varied between simulations to diagnose the sensitivity of the isoprene oxidation cascade to NO<sub>x</sub>; results are presented as a function of the daytime NO<sub>x</sub> concentration.”

[P6L18] “Nighttime oxidation by NO<sub>3</sub> is particularly lower than previously reported in the literature (5-7% globally, Table 1), which largely reflects the amount of isoprene remaining at sunset. More efficient recycling of OH in RCIM would result in less isoprene at sunset.”

[P8L18] “an increase in mean diurnal daytime temperature of 10 °C causes up to a doubling in daytime OH concentrations”

[P10L20] “The final remaining 13% forms isoprene SOA, which represents a terminal sink in GEOS-Chem is assumed in GEOS-Chem to have no further chemical reactivity (Marais et al., 2016)”

[P11L12] “Fixed-radical box model simulations with RCIM”

[P11L19] “the overall global molar yield of formaldehyde from isoprene, which we estimate to be 111% (22% per carbon, a 4% increase from GEOS-Chem v11-02c). The yield is lower than in the box model simulations of Figure 10 because of deposition and aerosol uptake of isoprene oxidation intermediates.”

[P16L3] “RCIM results in similar production of HMML to as in MCM”

[P16L22] “The organonitrate iSOA formation simulated in GEOS-Chem is therefore likely an upper limit on the actual source of aerosol mass from organonitrates.”

[P16L27] “production of iSOA from glyoxal is 10% of that from IEPOX, which matches the decreased glyoxal yield between the two mechanisms in the region. Locally, however, glyoxal can still be an important contributor”

[P17L23] “ozone, CO, and formaldehyde concentrations between the two mechanisms”

[P18L7] “RCIM estimates a higher fraction of isoprene reacting with OH globally (88%) than past mechanisms. Of the fraction that reacts with OH to form The resulting hydroxy-peroxy radicals (ISOPPOO) react, the dominant atmospheric fate is reaction with HO<sub>2</sub> (41%), NO (28%), and RO<sub>2</sub> (9%), or, while over 20% of ISOPPOO radicals undergo H-shifts to regenerate HO<sub>x</sub> (22%).”

[P18L21] “76% of which proceeds via CO and including 44% via formaldehyde”

[p18L30] “This 13% SOA yield per carbon (25% yield by mass)”

The caption of Figure 3 was revised for clarity: “daytime mean NO<sub>x</sub> concentration and temperature”

The caption of Figure 4 was revised for clarity: “Percent of isoprene and the first-generation reacting with O<sub>3</sub> and NO<sub>3</sub>, and percent of the products from the reaction of isoprene with OH (ISOPOO hydroxy-peroxy radicals) (ISOPOO) reacting via each pathway.

The caption of Figure 6 was revised for clarity: “stable non-radical (closed-shell) products are shown in blue”

The caption of Figure 8 was revised for clarity: “(c) contributions to isoprene-derived SOA production.”

The caption of Figure 10 was revised for clarity: “Percent yields of organic products from isoprene + OH oxidation as a function of NO and HO<sub>2</sub> ... Contours are evenly spaced on a linear scale between the percent bounds listed minimum values (in white) and maximum values (in black) located on each plot.”

The citation for Wolfe et al. (2016) referred to the incorrect 2016 paper by Glenn Wolfe; the relevant entry in the reference list has been updated.

## REFERENCES

Alvarado, L. M. A., Richter, A., Vrekoussis, M., Wittrock, F., Hilboll, A., Schreier, S. F., and Burrows, J. P.: An improved glyoxal retrieval from OMI measurements, *Atmos. MEas. Tech.*, 7, 4133–4150, DOI:10.5194/amt-7-4133-2014, 2014.

Archibald, A. T., Cooke, M. C., Utembe, S. R., Shallcross, D. E., Derwent, R. G., and Jenkin, M. E.: Impacts of mechanistic changes on HO<sub>x</sub> formation and recycling in the oxidation of isoprene, *Atmos. Chem. Phys.*, 10, 8097–8118, 2010.

Asatryan, R., Silva, G. d., and Bozzelli, J. W.: Quantum chemical study of the acrolein (CH<sub>2</sub>CHCHO) + OH + O<sub>2</sub> reactions, *J. Phys. Chem. A*, 114, 8302–8311, DOI:10.1021/jp104828a, 2010.

Barkley, M. P., et al., Can a “state of the art” chemistry transport model simulate Amazonian tropospheric chemistry? *J. Geophys. Res.*, 116, D16302, doi:10.1029/2011JD015893, 2011.

Barkley, M. P., et al. "Top-down isoprene emissions over tropical South America inferred from SCIAMACHY and OMI formaldehyde columns," *J. Geophys. Res. - Atmos.*, 118, 12, 6849–6868, DOI: 10.1002/jgrd.50552, 2013.

Bates, K. H., Crouse, J. D., St Clair, J. M., Bennett, N. B., Nguyen, T. B., Seinfeld, J. H., Stoltz, B. M., and Wennberg, P. O.: Gas phase production and loss of isoprene epoxydiols, *J. Phys. Chem. A*, 118, 1237–46, DOI:10.1021/jp4107958, 2014.

Chan Miller, C., Gonzalez Abad, G., Wang, H., Liu, X., Kurosu, T., Jacob, D. J., and Chance, K.: Glyoxal retrieval from the Ozone Monitoring Instrument, *Atmos. Meas. Tech.*, 7, 3891–3907, DOI:10.5194/amt-7-3891-2014, 2014.

Chan Miller, C., Jacob, D. J., González Abad, G., and Chance, K.: Hotspot of glyoxal over the Pearl River delta seen from the OMI satellite instrument: implications for emissions of aromatic hydrocarbons, *Atmos. Chem. Phys.*, 16, 4631–4639, DOI:10.5194/acp-16-4631-2016, 2016.

Chan Miller, C., Jacob, D. J., Marais, E. A., Yu, K., Travis, K. R., Kim, P. S., Fisher, J. A., Zhu, L., Wolfe, G. M., Hanisco, T. F., Keutsch, F. N., Kaiser, J., Min, K.-E., Brown, S. S., Washenfelder, R. A., González Abad, G., and Chance, K.: Glyoxal yield from isoprene oxidation and relation to formaldehyde: chemical mechanism, constraints from SENEX aircraft observations, and interpretation of OMI satellite data, *Atmos. Chem. Phys.*, 17, 8725–8738, DOI:10.5194/acp-17-8725-2017, 2017.

Crouse, J. D., Paulot, F., Kjaergaard, H. G., and Wennberg, P. O.: Peroxy radical isomerization in the oxidation of isoprene, *Phys. Chem. Chem. Phys.*, 13, 13 607–13 613, 2011.

Crouse, J. D., Knap, H. C., Ørnsø, K. B., Jørgensen, S., Paulot, F., Kjaergaard, H. G., and Wennberg, P. O.: Atmospheric fate of methacrolein. 1. Peroxy radical isomerization following addition of OH and O<sub>2</sub>, *J. Phys. Chem. A*, 116, 5756–5762, 2012.

Crouse, J. D., Nielsen, L. B., Jørgensen, S., Kjaergaard, H. G., and Wennberg, P. O.: Autoxidation of organic compounds in the atmosphere, *J. Phys. Chem. Lett.*, 4, 3513–3520, 2013.

Dillon, T. J. and Crowley, J. N.: Direct detection of OH formation in the reactions of HO<sub>2</sub> with CH<sub>3</sub>C(O)O<sub>2</sub> and other substituted peroxy radicals, *Atmos. Chem. Phys.*, 8, 4877–4889, DOI:10.5194/acp-8-4877-2008, 2008.

Fisher, J. A., Murray, L. T., Jones, D. B. A., and Deutscher, N. M.: Improved method for linear carbon monoxide simulation and source attribution in atmospheric chemistry models illustrated using GEOS-Chem v9, *Geosci. Model Dev.*, 10, 4129–4144, DOI:10.5194/gmd10-4129-2017, 2017.

Fu, T.-M., Jacob, D. J., Wittrock, F., Burrows, J. P., Vrekoussis, M., and Henze, D. K.: Global budgets of atmospheric glyoxal and methylglyoxal, and implications for formation of secondary organic aerosols, *J. Geophys. Res. - Atmos.*, 113, DOI:10.1029/2007JD009505, 2008.

Hasson, A. S., Tyndall, G. S., and Orlando, J. J.: A product yield study of the reaction of HO<sub>2</sub> radicals with ethyl peroxy (C<sub>2</sub>H<sub>5</sub>O<sub>2</sub>), acetyl peroxy (CH<sub>3</sub>C(O)O<sub>2</sub>), and acetonyl peroxy (CH<sub>3</sub>C(O)CH<sub>2</sub>O<sub>2</sub>) radicals, *J. Phys. Chem. A*, 108, 5979–5989, DOI:10.1021/jp048873t, 2004.

Hodzic, A., Kasibhatla, P. S., Jo, D. S., Cappa, C. D., Jimenez, J. L., Madronich, S., and Park, R. J.: Rethinking the global secondary organic aerosol (SOA) budget: Stronger production, faster removal, shorter lifetime, *Atmos. Chem. Phys.*, 16, 7917–7941, DOI:10.5194/acp-16-7917-2016, 2016.

Huang, L., Jiang, J. H., Murray, L. T., Damon, M. R., Su, H., and Livesey, N. J.: Evaluation of UTLS carbon monoxide simulations in GMI and GEOS-Chem chemical transport models using Aura MLS observations, *Atmos. Chem. Phys.*, 16, 5641–5663, DOI:10.5194/acp16-5641-2016, 2016.

Jenkin, M. E., Hurley, M. D., and Wallington, T. J.: Investigation of the radical product channel of the CH<sub>3</sub>C(O)O<sub>2</sub> + HO<sub>2</sub> reaction in the gas phase, *Phys. Chem. Chem. Phys.*, 9, 3149–3162, DOI:10.1039/B702757E, 2007.

Jenkin, M. E., Young, J. C., and Rickard, A. R.: The MCM v3.3.1 degradation scheme for isoprene, *Atmos. Chem. Phys.*, 15, 11 433–11 459, DOI:10.5194/acp-15-11433-2015, 2015.

Jo, D. S., Hodzic, A., Emmons, L. K., Marais, E. A., Peng, Z., Nault, B. A., Hu, W., Campuzano-Jost, P., and Jimenez, J. L.: A simplified parameterization of isoprene-epoxydiol-derived secondary organic aerosol (IEPOX-SOA) for global chemistry and climate models, *Geosci. Model Dev. Discuss.*, DOI:10.5194/gmd-2019-9, in review, 2019.

Jørgensen, S., Knap, H. C., Otkjær, R. V., Jensen, A. M., Kjeldsen, M. L. H., Wennberg, P. O., and Kjaergaard, H. G.: Rapid hydrogen shift scrambling in hydroperoxy-substituted organic peroxy radicals, *J. Phys. Chem. A*, 120, 266–275, DOI:10.1021/acs.jpca.5b06768, 2016.

Kaiser, J., Wolfe, G. M., Min, K. E., Brown, S. S., Miller, C. C., Jacob, D. J., deGouw, J. A., Graus, M., Hanisco, T. F., Holloway, J., Peischl, J., Pollack, I. B., Ryerson, T. B., Warneke, C., Washenfelder, R. A., and Keutsch, F. N.: Reassessing the ratio of glyoxal to formaldehyde as an indicator of hydrocarbon precursor speciation, *Atmos. Chem. Phys.*, 15, 7571–7583, DOI:10.5194/acp-15-7571-2015, 2015.

Kaiser, J., Jacob, D. J., Zhu, L., Travis, K. R., Fisher, J. A., González Abad, G., Zhang, L., Zhang, X., Fried, A., Crouse, J. D., St. Clair, J. M., and Wisthaler, A.: High-resolution inversion of OMI formaldehyde columns to quantify isoprene emission on ecosystem-relevant scales: application

to the southeast US, *Atmos. Chem. Phys.*, **18**, 5483–5497, DOI:10.5194/acp-18-5483-2018, 2018.

Li, C., Balluz, L. S., Vaidyanathan, A., Wen, X.-J., Hao, Y., and Qualters, J. R.: Long-term exposure to ozone and life expectancy in the United States, 2002 to 2008, *Medicine*, **95**, e2474, DOI:10.1097/MD.0000000000002474, 2016.

Liu, J., D'Ambro, E. L., Lee, B. H., Lopez-Hilfiker, F. D., Zaveri, R. A., Rivera-Rios, J. C., Keutsch, F. N., Iyer, S., Kurten, T., Zhang, Z., Gold, A., Surratt, J. D., Shilling, J. E., and Thornton, J. A.: Efficient isoprene secondary organic aerosol formation from a non-IEPOX pathway, *Environ. Sci. Technol.*, **50**, 9872–9880, DOI:10.1021/acs.est.6b01872, 2016.

Marais, E. A., Jacob, D. J., Jimenez, J. L., Campuzano-Jost, P., Day, D. A., Hu, W., Krechmer, J., Zhu, L., Kim, P. S., Miller, C. C., Fisher, J. A., Travis, K., Yu, K., Hanisco, T. F., Wolfe, G. M., Arkinson, H. L., Pye, H. O. T., Froyd, K. D., Liao, J., and McNeill, V. F.: Aqueous-phase mechanism for secondary organic aerosol formation from isoprene: application to the southeast United States and co-benefit of SO<sub>2</sub> emission controls, *Atmos. Chem. Phys.*, **16**, 1603–1618, DOI:10.5194/acp-16-1603-2016, 2016.

Møller, K. H., Bates, K. H., and Kjaergaard, H. G.: The importance of peroxy radical hydrogen-shift reactions in atmospheric isoprene oxidation, *J. Phys. Chem. A*, **123**, 920–932, DOI:10.1021/acs.jpca.8b10432, 2019.

Pai, S. J., Heald, C. L., Pierce, J. R., Farina, S. C., Marais, E. A., Jimenez, J. L., Campuzano-Jost, P., Nault, B. A., Middlebrook, A. M., Coe, H., Shilling, J. E., Bahreini, R., Dingle, J. H., and Vu, K.: An evaluation of global organic aerosol schemes using airborne observations, *Atmos. Chem. Phys. Discuss.*, DOI:10.5194/acp-2019-331, 2019.

Paulot, F., Crouse, J. D., Kjaergaard, H. G., Kurten, A., St Clair, J., Seinfeld, J. H., and Wennberg, P. O.: Unexpected epoxide formation in the gas-phase photooxidation of isoprene, *Science*, **325**, 730–3, DOI:10.1126/science.1172910, 2009b.

Peeters, J. and Muller, J. F.: HO(x) radical regeneration in isoprene oxidation via peroxy radical isomerisations. II: Experimental evidence and global impact, *Phys. Chem. Chem. Phys.*, **12**, 14 227–35, DOI:10.1039/c0cp00811g, 2010.

Peeters, J., Nguyen, T. L., and Vereecken, L.: HOx radical regeneration in the oxidation of isoprene, *Phys. Chem. Chem. Phys.*, **11**, 5935–9, DOI:10.1039/b908511d, 2009.

Peeters, J., Muller, J. F., Stavrou, T., and Nguyen, V. S.: Hydroxyl radical recycling in isoprene oxidation driven by hydrogen bonding and hydrogen tunneling: The upgraded LIM1 mechanism, *J. Phys. Chem. A*, **118**, 8625–8643, DOI:10.1021/jp5033146, 2014.

Ruppert, L. and Becker, K.-H.: A product study of the OH radical-initiated oxidation of isoprene: formation of C5-unsaturated diols, *Atmos. Environ.*, 34, 1529–1542, DOI:10.1016/S1352-2310(99)00408-2, 2000.

Stadtler, S., Kühn, T., Schröder, S., Taraborrelli, D., Schultz, M. G., and Kokkola, H.: Isoprene-derived secondary organic aerosol in the global aerosol-chemistry-climate model ECHAM6.3.0-HAM2.3-MOZ1.0, *Geosci. Model Dev.*, 11, 3235–3260, DOI:10.5194/gmd-11-3235-2018, 2018.

Teng, A. P., Crouse, J. D., and Wennberg, P. O.: Isoprene Peroxy Radical Dynamics, *J. Am. Chem. Soc.*, 139, 5367–5377, 2017.

Vrekoussis, M., Wittrock, F., Richter, A., and Burrows, J. P.: Temporal and spatial variability of glyoxal as observed from space, *Atmosph. Chem. Phys.*, 9, 4485–4504, DOI:10.5194/acp-9-4485-2009, 2009.

Wang, S., Riva, M., Yan, C., Ehn, M., and Wang, L.: Primary formation of highly oxidized multifunctional products in the OH-initiated oxidation of isoprene: A combined theoretical and experimental study, *Environ. Sci. Technol.*, 52, 12 255–12 264, DOI:10.1021/acs.est.8b02783, 2018.

Wennberg, P. O., Bates, K. H., Crouse, J. D., Dodson, L. G., McVay, R. C., Mertens, L. A., Nguyen, T. B., Praske, E., Schwantes, R. H., Smarte, M. D., St Clair, J. M., Teng, A. P., Zhang, X., and Seinfeld, J. H.: Gas-phase reactions of isoprene and its major oxidation products, *Chem. Rev.*, 118, 3337–3390, DOI:10.1021/acs.chemrev.7b00439, 2018.

Wolfe, G. M., et al. Photolysis, OH reactivity and ozone reactivity of a proxy for isoprene-derived hydroperoxyenals (HPALDs), *Phys. Chem. Chem. Phys.*, 14 (20), 7276-86, 2012.

Zeng, G., Williams, J. E., Fisher, J. A., Emmons, L. K., Jones, N. B., Morgenstern, O., Robinson, J., Smale, D., Paton-Walsh, C., and Griffith, D. W. T.: Multi-model simulation of CO and HCHO in the Southern Hemisphere: Comparison with observations and impact of biogenic emissions, *Atmos. Chem. Phys.*, 15, 7217–7245, DOI:10.5194/acp-15-7217-2015, 2015.

# A new model mechanism for atmospheric oxidation of isoprene: global effects on oxidants, nitrogen oxides, organic products, and secondary organic aerosol

Kelvin H. Bates<sup>1</sup> and Daniel J. Jacob<sup>2</sup>

<sup>1</sup>Faculty of Arts and Sciences, Harvard University, Cambridge, MA 02138, USA

<sup>2</sup>School of Engineering and Applied Sciences, Harvard University, Cambridge, MA 02138, USA

**Correspondence:** Kelvin H. Bates (kelvin\_bates@fas.harvard.edu)

## Abstract.

Atmospheric oxidation of isoprene, the most abundantly emitted non-methane hydrocarbon, affects the abundances of ozone ( $O_3$ ), the hydroxyl radical (OH), nitrogen oxide radicals ( $NO_x$ ), carbon monoxide (CO), oxygenated and nitrated organic compounds, and secondary organic aerosol (SOA). We analyze these effects in box models and in the global GEOS-Chem chemical transport model using the new Reduced Caltech Isoprene Mechanism (RCIM) condensed from a recently developed explicit isoprene oxidation mechanism. We find many similarities with previous global models of isoprene chemistry along with a number of important differences. Proper accounting of the isomer distribution of peroxy radicals following the addition of OH and  $O_2$  to isoprene influences the subsequent distribution of products, decreasing in particular the yield of methacrolein, and increasing the capacity of intramolecular hydrogen shifts to promptly regenerate OH. Hydrogen shift reactions throughout the mechanism lead to increased OH recycling, resulting in less depletion of OH under low-NO conditions than in previous mechanisms. Higher organonitrate yields and faster tertiary nitrate hydrolysis lead to more efficient  $NO_x$  removal by isoprene and conversion to inorganic nitrate. Only 20% of isoprene-derived organonitrates (excluding peroxyacyl nitrates) are chemically recycled to  $NO_x$ . The global yield of formaldehyde from isoprene is 22% per carbon and less sensitive to NO than in previous mechanisms. The global molar yield of glyoxal is 2%, much lower than in previous mechanisms because of deposition and aerosol uptake of glyoxal precursors. Global production of isoprene SOA is about one third each from isoprene epoxydiols (IEPOX), organonitrates, and tetrafunctional compounds. We find a SOA yield from isoprene of 13% per carbon, much higher than commonly assumed in models, and likely offset by SOA chemical loss. We use the results of our simulations to further condense RCIM into a Mini-Caltech Isoprene Mechanism (Mini-CIM) for less expensive implementation in atmospheric models, with a total size (108 species, 345 reactions) comparable to currently used mechanisms.

## 20 1 Introduction

Isoprene (2-methyl-1,3-butadiene), the dominant hydrocarbon emitted to the atmosphere by plants, plays a central role in tropospheric chemistry. Its global emission is estimated to be  $\sim 500 \text{ Tg a}^{-1}$ , comparable to that of methane (Guenther et al., 2012). Its atmospheric lifetime is only  $\sim 1 \text{ h}$  against oxidation by the hydroxyl radical (OH), the main tropospheric oxidant

( $\tau_{OH} = 1.1$  h for  $[OH] = 2.5 \times 10^6$  molecules  $\text{cm}^{-3}$  at  $T = 298$  K). The high reactivity of isoprene and the subsequent cascade of oxidation products have important implications for tropospheric ozone (Squire et al., 2015), the hydroxyl radical (Lelieveld et al., 2008), the nitrogen cycle (Paulot et al., 2013), and secondary organic aerosol (SOA) (Carlton et al., 2009). The persistence of long-lived oxidation products extends isoprene's influence to regional and global scales (Kanakidou et al., 2005; Paulot et al., 2012).

Proper representation of isoprene chemistry is of critical importance for global models of atmospheric chemistry, but the mechanism is complicated and models often use outdated information. Wennberg et al. (2018) presented a detailed review of current knowledge and compiled a comprehensive mechanism. This mechanism is far too complex for implementation in atmospheric models, but Wennberg et al. (2018) also compiled a reduced version suitable for the range of conditions found in the atmosphere. We examine here its implications for the range of effects of isoprene on atmospheric chemistry.

The isoprene oxidation cascade varies considerably depending on local atmospheric conditions. Different branches in the chemical mechanism develop depending on the reactions of the peroxy radicals ( $\text{RO}_2$ ) produced in the initial and subsequent oxidation steps. Reaction with NO produces ozone and organic nitrates, and reactions of acylperoxy radicals with  $\text{NO}_2$  produce peroxyacyl nitrates (PANs). Reactions with  $\text{HO}_2$  are typically OH-consuming via hydroperoxide formation. Intramolecular hydrogen shift (H-shift) reactions tend to propagate radical chains and regenerate OH. These different branches of  $\text{RO}_2$  chemistry also produce a large and differing ensemble of oxygenated multifunctional compounds, some of which have low volatility and/or aqueous-phase chemistry leading to SOA formation.

Isoprene oxidation mechanisms in atmospheric models have evolved considerably over the past decades. Early mechanisms focused on high-NO conditions representative of polluted regions and the role of isoprene in driving the production of ozone and organic nitrates (Lloyd et al., 1983; Brewer et al., 1984; Trainer et al., 1987; Madronich and Calvert, 1990). These model studies led to a number of chamber experiments to test and improve the mechanisms (Atkinson et al., 1989; Tuazon and Atkinson, 1990; Paulson et al., 1992; Paulson and Seinfeld, 1992; Grosjean et al., 1993; Miyoshi et al., 1994; Kwok and Atkinson, 1995; Stevens et al., 1999; Ruppert and Becker, 2000) along with field observations of isoprene chemistry (Biesenthal and Shepson, 1997; Starn et al., 1998; Roberts et al., 1998; Wiedinmyer et al., 2001). Improved understanding of the chemistry under low-NO conditions and growing interest in formation of organic aerosol led to the development of increasingly complex mechanisms (Carter, 1996; Stockwell et al., 1997; Pöschl et al., 2000; Geiger et al., 2003; Aumont et al., 2005). The regularly updated Master Chemical Mechanism (MCM) presents a nearly explicit compilation of isoprene chemistry (Jenkin et al., 1997; Saunders et al., 2003; Jenkin et al., 2015). Various versions of these mechanisms have been incorporated into atmospheric models (Fan and Zhang, 2004; Pfister et al., 2008; Taraborrelli et al., 2009; Archibald et al., 2010; Mao et al., 2013; Squire et al., 2015; Chan Miller et al., 2017; Müller et al., 2018), with no coalescence toward a unified mechanism across models.

The effect of isoprene on OH concentrations has elicited much controversy. Early mechanisms exhibited near-complete titration of OH by isoprene under low-NO conditions (Jacob and Wofsy, 1988). However, this was contradicted in the early 2000s by observations of elevated OH concentrations in tropical forests (Carslaw et al., 2001; Lelieveld et al., 2008; Martinez et al., 2010; Pugh et al., 2010; Whalley et al., 2011; Stone et al., 2011). Models attempted to correct for this behavior by invoking hypothetical OH-recycling mechanisms in their low-NO oxidation schemes (Butler et al., 2008; Taraborrelli et al., 2009; Ku-

bistin et al., 2010). These were later replaced with mechanistic OH-recycling pathways, including isoprene epoxydiol (IEPOX) formation (Paulot et al., 2009b), radical propagation in reactions of HO<sub>2</sub> with acylperoxy radicals (Hasson et al., 2004; Jenkin et al., 2007; Dillon and Crowley, 2008), and H-shift isomerizations of the initial isoprene-hydroxy-peroxy radicals (Peeters et al., 2009). Incorporation of these mechanistic OH-recycling pathways into models showed the latter pathway to be most important for sustaining elevated OH concentrations under low-NO conditions (Archibald et al., 2010), and subsequent studies have identified and characterized additional OH-regenerating H-shift reactions throughout the isoprene oxidation mechanism (Peeters and Muller, 2010; Crouse et al., 2012, 2013; Peeters et al., 2014; Jørgensen et al., 2016; Wang et al., 2018; Møller et al., 2019).

Another focus of interest has been the role of isoprene as a sink for NO<sub>x</sub> ( $\equiv$  NO + NO<sub>2</sub>) through organonitrate formation and the subsequent fates of these organonitrates (von Kuhlmann and Lawrence, 2004; Horowitz et al., 2007; Wu et al., 2007; Paulot et al., 2012). Differences between models in organonitrate yields and recycling have large effects on simulated ozone (Fiore et al., 2012; Xie et al., 2013; Müller et al., 2014). Recent work has established that hydrolysis and deposition of isoprene-derived organonitrates can be a dominant NO<sub>x</sub> loss process in some environments (Romer et al., 2016; Fisher et al., 2016).

The role of isoprene as a SOA precursor has received increasing interest following evidence from field studies of C<sub>5</sub> compounds in ambient particles (Claeys et al., 2004; Edney et al., 2005; Kleindienst et al., 2007), which led to experimental work measuring SOA yields from isoprene oxidation (Kroll et al., 2005, 2006; Surratt et al., 2006). Further investigations of the isoprene oxidation mechanism identified specific SOA precursors such as IEPOX (Paulot et al., 2009b; Nguyen et al., 2014), oxidation products of methacryloyl peroxyoxynitrate (MPAN) (Nguyen et al., 2015a), and highly functionalized compounds with low volatility (Krechmer et al., 2015; D'Ambro et al., 2017). These SOA formation pathways are now commonly implemented in models (Marais et al., 2016; Stadtler et al., 2018).

Here we implement the condensed version of the Wennberg et al. (2018) comprehensive mechanism, which we call the Reduced Caltech isoprene mechanism (RCIM), in three types of atmospheric models – a fixed-radical box model, a diurnal-steady-state box model, and the global GEOS-Chem chemical transport model. RCIM introduces a number of components not currently included in the models, as described in Section 2. We use it to investigate the effects of isoprene chemistry on hydrogen oxide radicals (HO<sub>x</sub>  $\equiv$  OH + peroxy radicals), NO<sub>x</sub>, and ozone. We also investigate the fate of the isoprene carbon, including the yields of oxygenated organic products, CO, CO<sub>2</sub>, and SOA. In the process we compare RCIM to previous isoprene oxidation mechanisms, including MCM v3.3.1, the current GEOS-Chem standard mechanism (v11-02c), and others in the literature. Finally, we use the results of our simulations to further simplify the isoprene mechanism for computational savings in model applications.

## 2 Methods

### 2.1 Chemical mechanism

RCIM is v4.1 of the "Reduced-plus" mechanism found in the Wennberg et al. (2018) mechanism repository (DOI 10.7907/Z9S75DHB). It includes the oxidation of isoprene by OH, ozone, and NO<sub>3</sub> and condenses the ensuing oxidation cascade for the

practical range of atmospheric conditions. The mechanism includes 148 species and 412 reactions representing the complete isoprene oxidation cascade, in contrast to the 385 species and 810 reactions in the Wennberg et al. (2018) explicit mechanism, which did not seek to provide loss processes for compounds without experimental constraints and therefore did not represent a complete oxidation cascade (i.e. full conversion to CO<sub>2</sub>). RCIM was compiled concurrently with the full explicit mechanism and was designed to keep product yields of known compounds the same, with minimal simplifications beyond lumping of isomeric compounds with similar reaction pathways and removal of especially minor (<1% yield) pathways. Under atmospheric conditions, early-generation compound yields and mixing ratios in simulations with RCIM therefore closely track those of the full explicit mechanism. Major deviations occur only for later-generation compounds for which minimal experimental evidence exists to constrain reactive pathways, and for the proposed products of these reactions. For such compounds, the authors applied a self-consistent set of assumptions (Section 2 in Wennberg et al. (2018)) based on extrapolation from similar compounds and structure-activity relationships. While these assumptions were grounded in experimental evidence, they necessarily include high levels of uncertainty, which are discussed in greater detail in Section 8 of Wennberg et al. (2018).

The reader is directed to Wennberg et al. (2018) for a detailed description of RCIM. Most importantly, the mechanism treats the initial system of allylic and peroxy radicals formed following the addition of OH to isoprene dynamically, as shown in Figure 1. Older mechanisms implicitly used fixed distributions of isoprene-hydroxy-peroxy (ISOPOO) radicals, often derived from experiments performed under high-NO conditions. Addition of O<sub>2</sub> to allylic radicals under ambient conditions is in fact a reversible process, resulting in a dynamic system with differing initial (kinetic) and equilibrium radical distributions, as first postulated by Peeters et al. (2009) and demonstrated experimentally by (Teng et al., 2017). In RCIM, we simplify this ten-species, 69-reaction radical system to two species as shown in the bottom panel of Figure 1 and described in Wennberg et al. (2018). The implications of this novel treatment of the isoprene-hydroxy-peroxy radical system are manifest throughout this paper but are discussed specifically in Section 3.3.

Additional aspects of RCIM relative to older mechanisms include: new products and decreased C<sub>5</sub>-hydroperoxy-aldehyde (HPALD) yields following the 1,6-H-shifts of the Z-δ-OH-peroxy radicals shown in Figure 1 (Teng et al., 2017); more intramolecular H-shifts, including rapid peroxy-hydroperoxy shifts (Jørgensen et al., 2016; Møller et al., 2019), resulting in higher OH recycling under low-NO conditions; new parameterizations of nitrate yields from RO<sub>2</sub> + NO reactions, including pressure and temperature dependence; explicit treatment of highly functionalized products such as C<sub>5</sub>-dihydroxy-dihydroperoxides and other tetrafunctionalized C<sub>5</sub> compounds; and more detailed chemistry following the reactions of isoprene with NO<sub>3</sub> (Schwantes et al., 2015) and ozone (Nguyen et al., 2016).

In this paper we compare RCIM to MCM v3.3.1 (Jenkin et al., 2015) and to the current standard GEOS-Chem mechanism implemented in version 11-02c. MCM v3.3.1 (subsequently MCM for short) treats the chemistry of isoprene more explicitly than RCIM or the v11-02c mechanism. It includes 602 species and 1926 reactions. The GEOS-Chem v11-02c chemical mechanism includes 106 species and 335 reactions, and is primarily derived from chamber experiments separating the high- and low-NO oxidation schemes of isoprene (Mao et al., 2013; Paulot et al., 2009a, b) with targeted updates to nitrate yields, peroxy radical H-shift chemistry, and IEPOX chemistry (Bates et al., 2014, 2016; Travis et al., 2016; Fisher et al., 2016; Marais et al.,

2016; Chan Miller et al., 2017). The GEOS-Chem mechanism lumps the initial isoprene peroxy radicals into a single ISOPOO species.

Neither RCIM nor MCM include the loss of organic products by deposition or SOA formation. We exclude these processes from box model simulations, so as to isolate the effects of gas phase chemistry. For global GEOS-Chem simulations with RCIM, we extend the existing deposition (Nguyen et al., 2015b; Travis et al., 2016) and SOA formation (Marais et al., 2016) parameterizations from GEOS-Chem v11-02c to analogous species in the mechanism. All C<sub>5</sub> epoxides are thus treated identically to IEPOX, tetrafunctional C<sub>5</sub> nitrates are treated identically to isoprene dihydroxy-dinitrates, and tetrafunctional C<sub>5</sub> non-nitrates are treated identically to the "LVOC" low-volatility species that represents this group of SOA precursors in GEOS-Chem v11-02c. The one major change we implement relative to the standard v11-02c mechanism is to increase the aerosol uptake rate for tertiary nitrates by a factor of ten, following evidence that the hydrolysis of these nitrates proceeds rapidly in the atmosphere (Darer et al., 2011; Hu et al., 2011; Rindelaub et al., 2014; Xu et al., 2015; Rindelaub et al., 2016).

## 2.2 Simulations

All models use the same fast Rosenbrock kinetic solver implemented with the Kinetic Preprocessor tool (KPP; Damian et al., 2002; Daescu et al., 2003; Sandu et al., 2003).

**Fixed-radical box modeling:** In order to quantify product yields per unit of isoprene oxidized by OH under a given set of atmospheric conditions, a series of box model simulations are conducted with fixed concentrations of NO and HO<sub>2</sub>. This method serves to remove most nonlinearities and feedbacks inherent in the isoprene oxidation mechanism, so as to isolate the effects of the radicals on the oxidation pathways, and provides a quantitative reference of organic product yields from isoprene oxidation under fixed ambient conditions. The model is initialized with 1 ppbv of isoprene and run until complete conversion to CO<sub>2</sub>. (In the absence of deposition or SOA formation, all isoprene carbon is eventually converted to CO<sub>2</sub>). The branching pathways of isoprene oxidation products are computed assuming 0.1 pptv OH, an NO<sub>2</sub>/NO molar ratio of 5, no ozone or NO<sub>3</sub>, temperature of 298.15 K, and solar radiation for clear-sky equatorial midday with an ozone column of 350 DU. Product yields are calculated by dividing the total molar production over the entirety of the simulation of each compound of interest by the amount of isoprene oxidized. Additional sensitivity simulations with differing temperature and photolysis settings, along with simulations investigating isoprene + NO<sub>3</sub> chemistry, can be found in Sections S2 and S4 of the Supplement, respectively.

**Diurnal-steady-state box modeling:** Additional box model simulations are run with variable radical concentrations and diurnal cycles of temperature, sunlight, and isoprene emissions. These simulations follow the setup and conditions of Jenkin et al. (2015) for MCM to facilitate comparison. The box model simulates a tropical continental boundary layer with isoprene and NO emissions, ventilated by the background free troposphere with a fixed exchange rate constant corresponding to a ventilation time scale of 1 day. The free tropospheric background includes 1.8 ppmv CH<sub>4</sub>, 100 ppbv CO, 20 ppbv ozone, 300 pptv formaldehyde, and 1% H<sub>2</sub>O. Isoprene emissions vary diurnally with both temperature and sunlight, as parameterized by Guenther et al. (1995), for an average daytime emission rate of  $7.6 \times 10^6$  molecules cm<sup>-3</sup> s<sup>-1</sup> (Eerdekens et al., 2009). NO emissions are constant for a given simulation and are varied between simulations to diagnose the sensitivity of the isoprene oxidation cascade to NO<sub>x</sub>; results are presented as a function of the daytime NO<sub>x</sub> concentration. Photolysis rates follow the

diurnal pattern for clear sky at the Equator with an ozone column of 350 DU. Temperature follows a sinusoidal diurnal pattern with an amplitude of 4 °C, peaking at 13:00. Simulations are initialized for seven days, after which concentrations from the eighth day (daytime averages between 06:00 and 18:00) are used in the results reported below.

**Global modeling:** We incorporate RCIM into the GEOS-Chem global 3-D model (<http://geos-chem.org>). GEOS-Chem is driven by assimilated meteorological observations from the NASA Goddard Earth Observing System – Fast Processing (GEOS-FP) of the NASA Global Modeling and Assimilation Office (GMAO). We use UCX version 11-02c as a base, including both tropospheric and stratospheric chemistry (Eastham et al., 2014) and with tropospheric methane fixed on the basis of observations. Emissions use the standard HEMCO configuration in v11-02c (Keller et al., 2014), including isoprene emissions from the MEGAN v2.1 inventory (Guenther et al., 2012) as implemented into GEOS-Chem by Hu et al. (2015) and scaled uniformly to 535 Tg a<sup>-1</sup> (Guenther et al., 2012). Annual isoprene emissions are shown in Figure 2. We conduct simulations for 1 year (July 2014 – June 2015) following 1.5 years of initialization starting in January 2013. Baseline simulations are conducted at 2° × 2.5° horizontal resolution with 72 vertical levels and additional sensitivity simulations are conducted at 4° × 5° horizontal resolution. We find no significant differences in results between the two resolutions, consistent with a previous GEOS-Chem investigation of the effects of model resolution on isoprene chemistry (Yu et al., 2016). For regional-scale results, we use the outputs of 2° × 2.5° horizontal resolution simulations at 0 - 1 km altitude and average over 81.25 - 93.75 °W, 31 - 39 °N for the Southeast United States, 53.75 - 76.25 °W, 11 °S - 3 °N for the Amazon Basin, and 111.25 - 121.25 °E, 23 - 41 °N for East China.

### 3 Isoprene oxidation pathways

#### 3.1 Initial oxidant branching

Figure 3 (left panels) shows the contributions of OH, ozone, and NO<sub>3</sub> to the overall oxidation of isoprene using RCIM in diurnal-steady-state box model simulations and in GEOS-Chem. On a global scale, we find that 88% of isoprene is oxidized by OH, 10% by ozone, and 1.7% by NO<sub>3</sub>. These global averages mask some spatial variability, as shown in Figure 4 and Table 1; for example, NO<sub>3</sub> oxidation contributes up to 5% of isoprene loss locally in the Southeast United States, and oxidation by ozone contributes up to 15% over tropical forests.

Although the ozone and NO<sub>3</sub> oxidation pathways represent relatively minor contributions to global isoprene oxidation, they can be important for the global budgets of certain compounds. For example, a sensitivity GEOS-Chem simulation without isoprene ozonolysis results in a 51% global mean decrease in formic acid production from isoprene and a 25% decrease in hydroxymethyl-methyl- $\alpha$ -lactone, a product of methacrolein oxidation and SOA precursor (Nguyen et al., 2015a). Similarly, a GEOS-Chem simulation without isoprene + NO<sub>3</sub> results in a 39% decrease in isoprene-derived C<sub>2+</sub> organonitrate concentrations. Additional results from simulations excluding the ozone and NO<sub>3</sub> pathways can be found in Table S1.

RCIM results in a higher contribution of isoprene + OH to the total oxidation of isoprene than past estimates, as shown in Table 1, and lower contributions from ozone and NO<sub>3</sub>. We ascribe this change primarily to increased OH recycling relative to older mechanisms (see Section 4). This further explains the temperature dependence of the OH pathway contribution in

the diurnal-steady-state box model (Figure 3, top left), which is also stronger than in past mechanisms, as a result of the temperature dependence of OH-recycling H-shift reactions. Nighttime oxidation by  $\text{NO}_3$  is particularly lower than previously reported in the literature (5-7% *red*globally, Table 1), which largely reflects the amount of isoprene remaining at sunset. More efficient recycling of OH in RCIM results in less isoprene at sunset.

### 5 3.2 Fate of ISOPOO

The ISOPOO radicals produced following the reaction of isoprene with OH and addition of  $\text{O}_2$  (Figure 1) represent an important branching point in the isoprene oxidation cascade. The relative contributions of ISOPOO's reactions with NO,  $\text{HO}_2$ ,  $\text{RO}_2$ , and via unimolecular H-shifts largely set the chemical outcomes of the oxidation mechanism, including ozone formation, OH titration vs. recycling, and SOA production.

10 The top central panel of Figure 3 shows the relative contributions of each pathway as a function of  $\text{NO}_x$  and temperature in diurnal-steady-state box model simulations. At a mean temperature of 25 °C, reaction with NO dominates the ISOPOO fate at  $\text{NO}_x > 500$  pptv and reaction with  $\text{HO}_2$  dominates at lower  $\text{NO}_x$ , while H-shifts account for up to 30% at low  $\text{NO}_x$ . H-shift rates are strongly temperature-dependent (Teng et al., 2017), and reach a comparable importance to reaction with  $\text{HO}_2$  at 35 °C.

15 The global contributions of each pathway as computed by GEOS-Chem are summarized in Table 1. While reaction with  $\text{HO}_2$  represents the dominant fate of ISOPOO in the atmosphere, reaction with NO and H-shifts contribute major portions of the global total. We estimate a 50% larger flux through the H-shift pathway than in the GEOS-Chem v11-02c mechanism; this contributes to the higher OH recycling in RCIM (Section 4.1). Our estimated fraction of ISOPOO undergoing H-shifts is 25% lower than that of Peeters et al. (2014), which used faster 1,6-H-shift rates, and similar to the recent estimate of Müller et al.  
20 (2018).

Figure 4 illustrates the global distribution of the ISOPOO fate. The NO pathway dominates in polluted regions of northern midlatitudes, contributing up to 50% of ISOPOO reactivity in the Southeast United States and 90% in East China. In remote tropical forests, where low  $\text{NO}_x$  and  $\text{HO}_x$  lead to peroxy radical lifetimes in excess of 100 s, the H-shift pathway can account for up to 45% of the ISOPOO fate, and reaction with  $\text{RO}_2$  can contribute up to 20%.

### 25 3.3 ISOPOO isomer distributions

The right panels of Figure 3 show the fractional contributions of the ISOPOO isomers to total ISOPOO reactivity in the diurnal-steady-state and global simulations. The  $\delta$ -ISOPOO isomers are largely responsible for  $\text{HO}_x$  recycling via rapid unimolecular H-shifts, while the two  $\beta$  isomers lead to different subsequent product formation. Methyl vinyl ketone (MVK) is the major product of  $\beta$ -1-OH-ISOPOO + NO or  $\text{RO}_2$ , while methacrolein (MACR) is the main product from the equivalent  $\beta$ -  
30 4-OH-ISOPOO reactions. MACR leads to SOA formation via the production of hydroxymethyl-methyl- $\alpha$ -lactone (HMML) (Nguyen et al., 2015a), while MVK does not.

The  $\delta$  isomers comprise a higher fraction of total ISOPOO reactivity under low-NO conditions (up to 30% at 10 pptv  $\text{NO}_x$  and a mean diurnal temperature of 25 °C) due to the importance of the rapid 1,6 H-shifts of the Z- $\delta$  isomers. Within the

ISOPOO pool derived from OH addition to isoprene at C4 (comprising 37% of the total; see numbering in Figure 1), the  $\delta$  isomer contribution is even higher (up to 57%), due to the more rapid 1,6 H-shift of Z- $\delta$ -4-OH-ISOPOO. The  $\delta$  isomers account for <10% of ISOPOO reactivity at NO > 10 ppbv. At even higher concentrations of NO bimolecular reactivity can be sufficiently high to trap the ISOPOO isomer distribution at its kinetic limit, leading to much higher  $\delta$  isomer abundances. Here

5 **RCIM deviates substantially from the explicit mechanism of Wennberg et al. (2018) and MCM (see Figure S14). These conditions are not of general atmospheric relevance, but may occur in chamber experiments; for such applications, we recommend the use of a mechanism that resolves the full system of allylic and peroxy radicals (Figure 1).**

Table 1 and the bottom-right panel of Figure 3 show the isomers' contributions to total ISOPOO reactivity from GEOS-Chem simulations. We find that the  $\delta$  isomers contribute 21% of the total ISOPOO reactivity on a global annual average. This

10 contribution increases in areas with high ISOPOO H-shift fractions (e.g. to 30% in the Amazon), and decreases in areas with higher NO (e.g. to 17% in the Southeast United States).

In the GEOS-Chem v11-02c and older mechanisms, which treat the ISOPOO system as a single species, H-shifts deplete the whole ISOPOO pool, rather than preferentially depleting the 4-OH-ISOPOO radicals. As a result, the fraction of ISOPOO that go on to react bimolecularly, which should be enriched in 1-OH-ISOPOO, is instead assigned the same initial 1-OH:4-

15 OH ratio it would have without H-shifts. This leads to far higher contributions from the 4-OH pathway – up to 58% over the Amazon in the v11-02c mechanism.

The most prominent effect of this change is in the unique subsequent products of the 1-OH and 4-OH systems. By preferentially depleting the 4-OH-ISOPOO pool, H-shifts predominantly remove the potential for formation of MACR and the secondary  $\beta$ -hydroxynitrate, while the much slower 1,6 H-shift of 1-OH Z- $\delta$ -ISOPOO has a smaller effect on potential MVK

20 and tertiary  $\beta$ -hydroxynitrate formation from the 1-OH-ISOPOO system. In RCIM, increasing H-shift contributions thus increase the MVK/MACR and tertiary/secondary nitrate ratios, while in GEOS-Chem v11-02c and older mechanisms these ratios are unaffected by H-shift chemistry. Global simulations with the single-radical ISOPOO representation of Mao et al. (2013) and with the fixed ISOPOO distribution of Paulot et al. (2009a) (while leaving the rest of the chemistry unchanged from RCIM) result in 21% and 18% decreases in tropospheric production of MVK relative to RCIM, respectively, and 24% and 10%

25 increases in tropospheric production of MACR, approximately doubling the MVK/MACR ratio under low-NO conditions. The dynamic ISOPOO system also results in 25% higher tropospheric production of the tertiary  $\beta$ -hydroxynitrate in RCIM relative to the single-radical and fixed-distribution ISOPOO representations of Mao et al. (2013) and Paulot et al. (2009a). The rapid hydrolysis of this tertiary nitrate in turn leads to more efficient NO<sub>x</sub> removal by isoprene nitrates (see Section 5.2). Table S1 shows additional results of GEOS-Chem simulations with fixed-distribution and single-radical ISOPOO chemistry.

## 30 4 Effects on radical families and ozone

### 4.1 Effects on HO<sub>x</sub> radicals

Figure 5 shows the effects of isoprene on OH and HO<sub>2</sub> concentrations in diurnal-steady-state box model simulations with the RCIM, MCM, and v11-02c mechanisms. OH is depleted under low-NO conditions by direct reactions with isoprene and its

oxidation products. The effect reverses under high-NO<sub>x</sub> conditions when these reactions compete with the reaction of NO<sub>2</sub> with OH that is the dominant HO<sub>x</sub> sink. Isoprene chemistry enhances HO<sub>2</sub> concentrations under all conditions because of photolysis of formaldehyde and other carbonyls producing HO<sub>x</sub> radicals, and particularly under high-NO<sub>x</sub> conditions by competing with the NO<sub>2</sub> + OH reaction. OH depletion from isoprene oxidation under low-NO conditions is strongly temperature-dependent in  
5 RCIM and less pronounced than in previous mechanisms. In diurnal-steady-state simulations at < 100 pptv NO<sub>x</sub>, we find that an increase in mean *reddaytime* temperature of 10 °C causes up to a doubling in OH concentrations, and that RCIM sustains OH concentrations twice as high as MCM and three times higher than GEOS-Chem v11-02c.

Differences with MCM and GEOS-Chem v11-02c are due to updated H-shift chemistry in RCIM, which efficiently recycles HO<sub>x</sub> as shown in Figure 6. The initial H-shift of the Z- $\delta$ -4-OH-ISOPOO radical (the dominant ISOPOO H-shift pathway)  
10 is highly temperature-dependent and regenerates one equivalent of HO<sub>x</sub> (0.6 OH + 0.4 HO<sub>2</sub>) concurrently with the first generation of non-radical products. In RCIM, the C<sub>4</sub>-dihydroperoxy-carbonyl compounds (top right of Figure 6) produced in this reaction are assumed to rapidly photolyze as postulated in Wennberg et al. (2018), which produces an additional 1.2 HO<sub>x</sub> equivalents, for a total HO<sub>x</sub> regeneration of 2.2 equivalents (1.5 OH + 0.7 HO<sub>2</sub>) from the 1,6 H-shifts of Z- $\delta$ -ISOPOO isomers. Reaction with OH could possibly provide a competitive loss pathway for the C<sub>4</sub>-dihydroperoxy-carbonyl compounds, which  
15 would result in lower net HO<sub>x</sub> production. An upper limit of 3.0 equivalents of HO<sub>x</sub> production (2.2 OH + 0.75 HO<sub>2</sub> + 0.04 RO<sub>2</sub>) can be achieved in the second oxidative generation if photolysis is also the dominant fate of the HPALDs that make up the remaining 40% of the stable products. Such a regeneration of HO<sub>x</sub> is necessary to reconcile models and measurements in low-NO conditions (Fuchs et al., 2013; Kaser et al., 2015; Feiner et al., 2016; Kaiser et al., 2016; Mao et al., 2018).

Figure 7 and Table 2 show the effects of isoprene oxidation as simulated in GEOS-Chem. The global annual mean tro-  
20 pospheric concentration of OH decreases by 11% and that of HO<sub>2</sub> increases by 6.5%. OH decreases are largest in tropical continental boundary layers, but diffuse effects extend throughout the global troposphere due to the influence of longer-lived isoprene oxidation products, in particular CO. Thus the globally integrated effects in the upper troposphere (5-10 km) are comparable to those in the boundary layer (0-1 km). We calculate that isoprene chemistry causes a 12% increase in the tropospheric lifetime of methane with respect to oxidation by OH, thus enhancing the climatological effects of an already potent greenhouse  
25 gas.

As in the diurnal-steady-state simulations, the titration of OH by isoprene oxidation under low-NO conditions is substantially weaker in global simulations with RCIM than with the GEOS-Chem v11-02c mechanism. Whereas isoprene oxidation in the v11-02c mechanism causes reductions in annual mean OH of ~90% over the Amazon and Congo basins, RCIM exhibits only ~70% reductions. RCIM increases the simulated annual mean OH concentration over the Amazon by +170% relative to  
30 GEOS-Chem v11-02c, and that of HO<sub>2</sub> by +30%, both in better agreement with field observations in the region (Barkley et al., 2011). Again, this change is largely due to increased HO<sub>x</sub> production from the H-shifts of ISOPOO in RCIM. For additional comparison to the MCM and GEOS-Chem mechanisms, see Section S5.2 of the Supplement.

## 4.2 Effects on NO<sub>x</sub>

Table 2 and Figure 7 summarize the effects of RCIM isoprene chemistry on tropospheric NO<sub>x</sub>. These effects largely involve the formation and fate of PANs and other organonitrates, and changes in NO<sub>x</sub> lifetime due to changes in HO<sub>x</sub>. On a global annual average, isoprene chemistry depletes tropospheric NO<sub>x</sub> by 4.2%. NO<sub>x</sub> depletion reaches 50% in tropical continental regions where high VOC/NO<sub>x</sub> ratios promote NO<sub>x</sub> titration by organonitrate formation. NO<sub>x</sub> increases by up to 10% in remote regions such as the oceanic free troposphere due to release of NO<sub>x</sub> from transported PANs and other organonitrates. The fate of organonitrates including the fraction recycled as NO<sub>x</sub> will be discussed in more detail in Section 5.2.

The effects described above have been shown in past models (von Kuhlmann and Lawrence, 2004; Ito et al., 2009; Fischer et al., 2014; Jenkin et al., 2015), which calculated similar magnitudes for the overall contribution of isoprene to NO<sub>x</sub> and nitrate budgets. One significant difference that we find in comparison with the GEOS-Chem v11-02c mechanism is the composition of the organonitrate pool and its effects on NO<sub>x</sub> transport and removal. For example, due to higher formation of tertiary nitrates and their increased hydrolysis rate in RCIM, we estimate tropospheric NO<sub>x</sub> loss to hydrolysis of nitrates to be 4.9 TgN a<sup>-1</sup>, compared to only 1.8 TgN a<sup>-1</sup> with the GEOS-Chem v11-02c mechanism. This increased NO<sub>x</sub> loss rate in RCIM is offset by smaller overall organonitrate production and a substantial reduction in the formation of MPAN in low-NO conditions. Thus, the two mechanisms simulate a nearly identical tropospheric NO<sub>x</sub> burden, but with distributional differences. **For example, global simulations with RCIM result in a 17% increase in annual mean surface NO<sub>x</sub> mixing ratios relative to the GEOS-Chem mechanism over the Amazon Basin (see Figure S17 and Table S6), a region where surface NO<sub>x</sub> is typically underestimated in GEOS-Chem (Barkley et al., 2011; Liu et al., 2016).**

## 4.3 Effects on ozone

The bottom panel of Figure 5 shows the effect of isoprene oxidation on ozone in diurnal-steady-state box model simulations. Isoprene has little effect under low-NO conditions but stimulates ozone production at higher NO due to increased peroxy radical concentrations, accelerating cycling of NO to NO<sub>2</sub>. At very high NO, ozone production becomes VOC-limited and the effect of isoprene becomes very large. These dependences are relatively invariant with temperature and similar to those seen in MCM and GEOS-Chem v11-02c.

Figure 7 and Table 2 summarize the effect of isoprene chemistry on ozone as simulated in GEOS-Chem. While isoprene oxidation decreases boundary layer ozone over the Amazon by 22% (3.4 ppbv), mainly because of NO<sub>x</sub> depletion, it causes an overall increase in the annual average tropospheric ozone burden of 4.2% (1.9 ppbv), and local increases of up to 6 ppbv in China where ozone production is often VOC-limited (Jin and Holloway, 2015). The release of NO<sub>x</sub> from isoprene-derived organonitrates extends these effects to the free troposphere, with stronger ozone enhancement in the Northern Hemisphere where NO is higher. These results are consistent with past studies diagnosing the influence of isoprene and its oxidation mechanism on ozone (Wang and Shallcross, 2000; von Kuhlmann and Lawrence, 2004; Squire et al., 2015), and investigating the effects of changing isoprene emissions (Sanderson et al., 2003; Wiedinmyer et al., 2006; Ganzeveld et al., 2010; Wu et al., 2012; Pacifico et al., 2012; Squire et al., 2014).

However, certain new aspects of RCIM cause slight distributional changes in the effects of isoprene on ozone relative to past mechanisms. RCIM's higher first-generation nitrate yields and faster tertiary nitrate hydrolysis relative to the GEOS-Chem v11-02c mechanism lead to reduced ozone formation from the ISOPOO + NO pathway. In the Southeast United States, where past mechanisms have tended to overestimate surface ozone (Murazaki and Hess, 2006; Yu et al., 2007; Lin et al., 2008; Fiore et al., 2009; Yu et al., 2010; Rasmussen et al., 2012; Travis et al., 2016), RCIM results in a 1.5% decrease in annual mean boundary layer ozone relative to the GEOS-Chem v11-02c mechanism. Reduced NO<sub>x</sub> transport in RCIM and reduced MPAN formation under low-NO conditions also results in higher sustained ozone over the Amazon (+3 ppbv) and lower ozone in the remote Southern Hemisphere (-1.5 ppbv) than the GEOS-Chem v11-02c mechanism. For more detailed comparisons with MCM and GEOS-Chem v11-02c, see Section S5.2 of the Supplement.

## 10 5 Isoprene oxidation products

RCIM is carbon-conserving and can be used to track the fate of isoprene-derived carbon. Figure 8a shows global mean results for the fate of isoprene carbon in GEOS-Chem. 50% of isoprene carbon is oxidized fully to CO<sub>2</sub> in the gas phase, in good agreement with the value of 52% calculated by Safieddine et al. (2017) for all non-methane VOCs. 37% is lost to wet and dry deposition of organic oxidation products before full conversion to CO<sub>2</sub>. This falls between previous estimates of 32% (Müller et al., 2018) and 44% (Safieddine et al., 2017) for all oxidized non-methane VOCs. The **remaining** 13% forms isoprene SOA, which **is assumed in GEOS-Chem to have no further chemical reactivity** (Marais et al., 2016).

The following subsections describe the fate of isoprene-derived carbon and its organic products in greater detail: oxygenated gas-phase VOCs for which observations are available (Section 5.1), organonitrates (Section 5.2), and SOA precursors (Section 5.3). Figure 9 shows the annual average spatial distributions of important isoprene oxidation products in GEOS-Chem. Figure 10 shows molar yields of individual products from OH-initiated oxidation as a function of NO and HO<sub>2</sub> in fixed-radical box model simulations. Figure 11 shows daytime mean concentrations of major classes of isoprene products as a function of NO<sub>x</sub> and temperature in diurnal-steady-state simulations. Additional details on the organic products of isoprene oxidation are provided in the Supplement, including simulated global and regional molar yields (Table S3), the contributions of specific oxidation pathways to global production (Tables S1 and S2), sensitivities of yields to light and temperature (Section S2), molar yields from NO<sub>3</sub>-initiated oxidation (Section S4), and comparisons to MCM and GEOS-Chem v11-02c (Section S5).

### 5.1 Oxygenated VOCs and CO

**CO:** We find the molar yield of carbon monoxide from isoprene oxidation to be 190% globally, or 38% per carbon. Of the 50% of isoprene carbon oxidized fully to CO<sub>2</sub>, 76% proceeds via CO (Figure 8a). The global CO source from isoprene oxidation is 415 Tg a<sup>-1</sup>, which in GEOS-Chem represents 17% of the total atmospheric CO source (including 36% from methane, 8% from the oxidation of other VOCs, and 39% from direct emissions). Isoprene oxidation generates up to 100 ppbv of CO locally over tropical forests. Our simulated global molar CO yield from isoprene is slightly higher than the range of 100-170% from previous estimates (Miyoshi et al., 1994; Bergamaschi et al., 2000; Duncan et al., 2007; Pfister et al., 2008), but only a small

increase from the 180% molar yield with the GEOS-Chem v11-02c mechanism. **Distributional changes from the GEOS-Chem v11-02c mechanism include 9% higher CO concentrations over the Amazon (due to faster *in situ* isoprene oxidation from higher OH) and a more diffuse increase of ~2% in CO concentrations throughout the Southern Hemisphere (see Figure S24), where GEOS-Chem tends to underestimate remote surface, column, and upper-tropospheric CO (Zeng et al., 2015; Huang et al., 2016; Fisher et al., 2017).**

**Formaldehyde:** Formaldehyde is measurable by satellites and has been used in this manner to infer isoprene emissions based on estimated formaldehyde yields from isoprene (Palmer et al., 2003; Marais et al., 2012; Barkley et al., 2013; Kaiser et al., 2018). Marvin et al. (2017) and Wolfe et al. (2016) found from field observations that most current mechanisms underestimate formaldehyde yields from isoprene. Fixed-radical box model **simulations** with RCIM show 140-190% molar yields (28-38% per-carbon yields) of formaldehyde in the complete gas-phase oxidation of isoprene by OH under atmospherically relevant NO and HO<sub>2</sub> concentrations, with increasing yields at higher NO. The variation with NO is less steep than in past mechanisms, exhibiting higher formaldehyde production under low-NO conditions, much of it from the rapid (and unconstrained) photolysis of C<sub>4</sub>-dihydroperoxy-carbonyls produced by H-shift chemistry (top-right corner of Figure 6), and lower production under high-NO conditions (see Figures S20 and S24 in the Supplement). While this difference has regional impacts, e.g. increasing the mean annual boundary layer formaldehyde burden by 50% over the Amazon from GEOS-Chem v11-02c, it does not substantially change the overall global molar yield of formaldehyde from isoprene, which we estimate to be 111% (22% per carbon, a 4% increase from GEOS-Chem v11-02c). **The yield is lower than in the box model simulations of Figure 10 because of deposition and aerosol uptake of isoprene oxidation intermediates.** We find that isoprene contributes 18% of the global formaldehyde burden (Table 2), in line with previous estimates (Pfister et al., 2008).

**Glyoxal:** Glyoxal (C<sub>2</sub>H<sub>2</sub>O<sub>2</sub>) is also measured by satellites (Vrekoussis et al., 2009; Alvarado et al., 2014; Chan Miller et al., 2014), and different yields relative to formaldehyde can discriminate between emissions of different VOCs (Chan Miller et al., 2016). Past mechanisms have provided differing estimates on which isoprene oxidation pathways produce the most glyoxal (Li et al., 2016), and comparisons with field measurements show that glyoxal production is higher under low-NO conditions than most mechanisms predict (Li et al., 2016; Chan Miller et al., 2017). Our diurnal steady-state box model simulations show that the RCIM glyoxal/formaldehyde ratio remains in the 2-3% range over the ensemble of atmospheric conditions (see Figure S21), in line with field observations for isoprene-dominated environments (Kaiser et al., 2015; Chan Miller et al., 2017).

**RCIM yields of glyoxal from isoprene peak at 10% under low-NO conditions (Figure 10), while glyoxal yields in MCM are highest under high-NO conditions, and yields in the GEOS-Chem v11-02c mechanism are even higher than RCIM under low-NO conditions (Figures S18-S19). Mechanistically, these differences primarily reflect changes in the contributions from two low-NO pathways in RCIM relative to MCM and v11-02c: the products of Z- $\delta$ -ISOPOO H-shifts, and the reactions of IEPOX-derived peroxy radicals with HO<sub>2</sub>. While both MCM and RCIM include moderate yields of glyoxal (largely via hydroperoxyethanal) from the C<sub>4</sub>-dihydroperoxy-carbonyl products of Z- $\delta$ -ISOPOO H-shifts, GEOS-Chem v11-02c incorporates much higher second-generation glyoxal yields from these H-shift pathways (primarily via HPALD and dihydroperoxydicarbonyl compounds), consistent with field observations (Chan Miller et al., 2017). For the reactions of IEPOX-derived peroxy radicals with HO<sub>2</sub>, both RCIM and GEOS-Chem v11-02c include moderate yields of glyoxal presumed to form in the**

radical-propagating reaction channel ( $\text{RO}_2 + \text{HO}_2 \rightarrow \text{RO} + \text{OH} + \text{O}_2$ ), as suggested in Bates et al. (2014) and implemented in Wennberg et al. (2018), while MCM includes no glyoxal formation under low-NO conditions from IEPOX-derived peroxy radicals. Both the atmospheric fates of  $\text{C}_4$ -dihydroperoxy-carbonyl compounds and the radical-propagating channels of non-acyl  $\text{RO}_2 + \text{HO}_2$  reactions are poorly constrained (Wennberg et al., 2018), and the glyoxal yields from these pathways therefore remain uncertain.

We find in GEOS-Chem that many glyoxal precursors (IEPOX, nitrates, and tetrafunctional  $\text{C}_5$  compounds) are lost to aerosol or deposition before they can react in the gas phase, depressing the glyoxal yield relative to the box model simulations where aerosol/deposition effects are not included. This results in a global glyoxal yield from isoprene of 2% in GEOS-Chem with RCIM, only half that reported recently by Müller et al. (2018) and even lower than in some past simulations (Fu et al., 2008; Myriokefalitakis et al., 2008; Taraborrelli et al., 2009). We find a reduction in global tropospheric glyoxal loading of 60% relative to the GEOS-Chem v11-02c mechanism. However, Chan Miller et al. (2017) found good agreement between glyoxal simulated by GEOS-Chem v11-02c and aircraft observations in the Southeast United States. This suggests that RCIM may underestimate glyoxal yields from isoprene.

**Organic acids:** In GEOS-Chem simulations with RCIM, isoprene contributes  $21 \text{ Tg a}^{-1}$  of formic acid (a 5.8% molar yield) and  $25 \text{ Tg a}^{-1}$  of acetic acid (a 5.5% molar yield) globally. Over half of this formic acid comes from the initial reaction of isoprene with ozone, either directly from the stabilized  $\text{C}_1$  Criegee intermediate (Nguyen et al., 2016) or secondarily through the reaction of hydroxymethyl hydroperoxide with OH (Allen et al., 2018), while the rest is formed in the ozonolysis of MVK and MACR or the reactions of MVK-derived enols and nitrates with OH. Acetic acid is produced in the reactions of  $\text{HO}_2$  and  $\text{RO}_2$  with the acylperoxy radical, a fragmentation product from many oxidation pathways. These overall yields are similar to past estimates of isoprene's contribution to organic acid budgets (Millet et al., 2015; Müller et al., 2018).

**Hydroperoxides:** Organic hydroperoxides serve as a  $\text{HO}_x$  reservoir in the gas phase, can contribute to the oxidation of  $\text{SO}_2$  to sulfate in aerosol and cloud water (Lind et al., 1987; Zhou and Lee, 1992), and are harmful to plants and human cells (Hewitt et al., 1990; Williams et al., 1983; Runge-Morris et al., 1989; Pöchl and Shiraiwa, 2015). We simulate an overall molar yield of hydroperoxides from isoprene in excess of 50% globally (Table S3). As shown in Figure 11, the majority of this production (67%) consists of the first-generation hydroxy-hydroperoxide (ISOPOOH), with additional contributions from highly functionalized  $\text{C}_4$  and  $\text{C}_5$  compounds and from hydroperoxyacetone. Many of these are later-generation products of the initial ISOPOO + NO pathway, either through subsequent H-shifts or subsequent  $\text{RO}_2 + \text{HO}_2$  reactions; as a result, even in East China, where reaction with NO dominates the  $\text{RO}_2$  fate, the molar yield of hydroperoxides from isoprene oxidation still reaches 25%.

**MVK and MACR:** MVK and MACR are formed in the first generation of isoprene oxidation via multiple pathways, with high production branching ratios from isoprene ozonolysis, H-shifts of  $\beta$ -ISOPOO isomers, and the reactions of ISOPOO with NO and  $\text{RO}_2$ . In the GEOS-Chem simulation with RCIM we find 28% and 16% global mean molar yields for MVK and MACR respectively. This represents a pronounced decrease in the relative yield of MACR compared to past mechanisms, largely caused by the dynamic representation of the ISOPOO isomer distribution in RCIM and resulting titration of methacrolein-forming 4-OH-ISOPOO via rapid H-shift (see Section 3.3). The decreased relative importance of isoprene ozonolysis in RCIM,

which generates 26% of global MACR, also contributes. This causes a sharp increase of up to 50% from past mechanisms in the simulated MVK/MACR ratio in diurnal-steady-state simulations to a range of 1.6-2.6 depending on  $\text{NO}_x$  (see Figures S20 and S21 in the Supplement), in better agreement with observations (Greenberg et al., 1999; Karl et al., 2009; Wolfe et al., 2016). (MVK+MACR)/isoprene and (MVK+MACR+ISOPOOH)/isoprene ratios, which are used as proxies for OH and photochemical age (Kuhn et al., 2007; Karl et al., 2009), remain considerably more consistent across mechanisms.

## 5.2 Organonitrates

RCIM includes important updates to the formation and fates of organonitrates through pressure- and temperature-dependent parameterizations of nitrate branching ratios and a new structure-activity relationship for calculating the formation of nitrates from multifunctional peroxy radicals without measured yields (Wennberg et al., 2018). We also implement faster particle-phase hydrolysis of the 1-OH,2-ONO<sub>2</sub> isoprene hydroxynitrate (Darer et al., 2011; Hu et al., 2011; Rindelaub et al., 2014; Xu et al., 2015; Rindelaub et al., 2016), which decreases its ability to transport and recycle  $\text{NO}_x$ . Finally, the dynamic representation of the ISOPOO isomers causes lower production of methacrolein-derived nitrates, including MPAN, and higher production of the hydrolysis-prone tertiary hydroxynitrate than previous mechanisms, as discussed in Section 3.3.

The effects of these updates are shown in Table 2 and Figures 9-11. Isoprene is found to contribute 20% of the tropospheric burden of peroxyacyl nitrates and 28% of non-peroxyacyl nitrates, with higher contributions in the Southern Hemisphere and local contributions up to 80% in regions of concurrent isoprene and  $\text{NO}_x$  emissions. Among isoprene-derived PANs, peroxyacetyl nitrate (PAN) dominates; we estimate that 19% of global PAN is derived from isoprene. This represents a considerably smaller fraction than in the v11-02c mechanism (44%) and in Fischer et al. (2014) (37%), due primarily to lower yields of precursors; methylglyoxal yields are reduced due to higher losses of intermediates to deposition and SOA, and acetaldehyde is not produced from isoprene in RCIM. We simulate PAN/MPAN ratios between 10 and 20, similar to MCM and to observed ratios (Roberts et al., 2002; Cleary et al., 2007; Roberts et al., 2007; Jenkin et al., 2015). This is in contrast to the GEOS-Chem v11-02c mechanism, which found a large contribution from MPAN due to high methacrolein yields and a high formation rate taken from Lin et al. (2013) (see Figure S23); the rate has since been revised down in GEOS-Chem v12.

GEOS-Chem with RCIM shows substantial daytime contributions from a number of non-PAN organonitrates (Figure 11), including first-generation C<sub>5</sub> hydroxynitrates as well as later-generation C<sub>4</sub> nitrates, C<sub>5</sub> tetrafunctionalized nitrates, and propanone nitrate, similar to those in GEOS-Chem v11-02c (Fisher et al., 2016) and MCM (see Section S5.3 of the Supplement). We simulate higher yields of first-generation hydroxynitrates than GEOS-Chem v11-02c but lower later-generation yields, leading to an overall 14% decrease in non-PAN organonitrate production in RCIM. Nitrates derived from  $\text{NO}_3$ -initiated oxidation contribute substantially to nighttime burdens, but their relatively short lifetimes against photolysis and oxidation by OH mean they are rapidly lost in the day; for more on isoprene- $\text{NO}_3$  chemistry, see Section S4 of the Supplement.

In global simulations, as described in Section 4.2, the rapid hydrolysis of tertiary nitrates is an important sink of  $\text{NO}_x$ . Figure 8b shows the global fate of non-PAN isoprene-derived organonitrates in GEOS-Chem with RCIM. We find that only 20% of these organonitrates recycle  $\text{NO}_x$  via gas-phase oxidation, while 6% undergo deposition and 74% hydrolyze to inorganic nitrate. Organonitrate hydrolysis constitutes a  $\text{NO}_x$  sink of 4.9 TgN a<sup>-1</sup> globally, or 10% of total  $\text{NO}_x$  loss. Including organon-

itrate deposition and hydrogen abstraction from isoprene-derived VOCs by  $\text{NO}_3$  to form  $\text{HNO}_3$ , the overall contribution of isoprene to global  $\text{NO}_x$  loss reaches 15%. The increased hydrolysis rate also causes a 14% reduction in the production of  $\text{C}_5$  tetrafunctional compounds which may contribute to SOA (see Table S2) because their organonitrate precursors are lost to hydrolysis.

5 Over the Southeast United States, where isoprene nitrate chemistry has been extensively observed (Lee et al., 2016; Romer et al., 2016), we simulate that loss to hydrolysis is the fate of 69% of isoprene-derived nitrates annually, comprising 45% of the total regional  $\text{NO}_x$  sink, while deposition and gas-phase  $\text{NO}_x$  recycling contribute 9% and 22% respectively. Fisher et al. (2016) estimated a similar fraction of  $\text{NO}_x$  recycling from isoprene nitrates of 23% over the Southeast United States in summer, with a larger contribution from deposition (18%) and a smaller fraction lost to hydrolysis (59%). The average lifetime  
10 of isoprene-derived nitrates in the region is 3.6 h in RCIM, more consistent with the observational estimate of 2-4 hours (Romer et al., 2016; Lee et al., 2016) than the simulated lifetimes of 0.48 days with GEOS-Chem v11-02c and 0.58 days in Horowitz et al. (2007).

### 5.3 SOA and its precursors

Figures 10-11 show the yields of major precursors of isoprene-derived SOA (iSOA) in RCIM, including IEPOX, highly func-  
15 tionalized  $\text{C}_5$  compounds, HMML, other epoxides, and organonitrates, all of which are discussed in greater detail below. We find a global isoprene-derived SOA (iSOA) production of  $61 \text{ TgC a}^{-1}$  (13% yield per carbon, Figure 8a) in GEOS-Chem using RCIM. IEPOX, tetrafunctional  $\text{C}_5$  compounds, and organonitrates each contribute  $\sim 30\%$  to this total (Figure 8c). If we simply consider the individual molecular weights of the iSOA precursors, we obtain a global iSOA source of  $136 \text{ Tg SOA a}^{-1}$ , corresponding to a mass yield of 25% from isoprene, and an organic mass to organic carbon (OM/OC) ratio of 2.2 for iSOA,  
20 consistent with observations for highly oxidized SOA (Aiken et al., 2008). We assume this ratio in what follows, recognizing that subsequent aerosol-phase reactions not described here would modify it.

The 25% mass yield of SOA from isoprene simulated with RCIM is considerably higher than values commonly used in global models, e.g. the range of 0.9-6.8% in the models discussed in Carlton et al. (2009). The standard GEOS-Chem model has two options for simulating iSOA: either a fixed mass yield of 3% (Kim et al., 2015) or an explicit representation coupled  
25 to the gas-phase mechanism (Marais et al., 2016). Marais et al. (2016) find from that explicit representation a 3.3% mass yield over the Southeast US in summer, with glyoxal and IEPOX dominating the formation in the high-NO and low-NO regimes respectively. In contrast, RCIM has a low yield of glyoxal from isoprene, as discussed above, and far larger contributions from other iSOA precursors. The Marais et al. (2016) GEOS-Chem mechanism has limited representation of iSOA formation from tetrafunctional  $\text{C}_5$  compounds and organic nitrates.

30 The  $\sim 3\%$  mass yield of SOA from isoprene in GEOS-Chem was previously found to successfully account for organic aerosol observations over the US (Kim et al., 2015; Marais et al., 2016, 2017). A 25% mass yield would lead to a severe overestimate. However, these and other SOA observations in isoprene-dominated environments tend to be in high-NO conditions, where yields from IEPOX and tetrafunctionals are low (Figure 11). Organonitrates dominate iSOA formation in RCIM under high-NO conditions but hydrolyze rapidly in the aerosol phase, and the organic moiety could further react and volatilize.

Recent work suggests that increased SOA yields from isoprene may be appropriate in global simulations, likely to be partially balanced by iSOA chemical sinks in order to reconcile with SOA observations. Global models tend to underestimate the atmospheric burden of organic aerosol (Volkamer et al., 2006; de Gouw and Jimenez, 2009; Tsigaridis et al., 2014). Chamber studies isolating specific isoprene oxidation pathways have measured SOA mass yields in excess of 15% (Liu et al., 2016; Schwantes et al., 2019), while top-down (Hallquist et al., 2009; Heald et al., 2010; Spracklen et al., 2011) and mass-balance (Goldstein and Galbally, 2007) assessments of global SOA production consistently arrive at higher estimates than the models. Stadler et al. (2018) found better agreement with the top-down assessments by implementing a new isoprene mechanism (including the major tetrafunctional C<sub>5</sub> compounds) into global simulations, resulting in a 33% global iSOA mass yield (16% per carbon). Hodzic et al. (2016) showed that discrepancies between observed SOA yields and modeled SOA budgets could be reconciled by incorporating increased rates of SOA loss to deposition, photolysis, and heterogeneous reactions, balanced by SOA sources 3.9 times higher than the GEOS-Chem standard model.

**IEPOX:** The dominant contributor to iSOA worldwide (Marais et al., 2016; Stadler et al., 2018), IEPOX is a second-generation oxidation product of isoprene via the ISOPOO + HO<sub>2</sub> reaction pathway. IEPOX can form in high yields of up to 75% from isoprene in HO<sub>2</sub>-dominated conditions (Figure 10). In remote regions, these yields are strongly temperature-dependent due to competition from ISOPOO H-shift pathways. We estimate global IEPOX production to be 185 Tg a<sup>-1</sup>, or a 20% molar yield from isoprene, similar to past estimates (Bates et al., 2014; St. Clair et al., 2015; Bates et al., 2016) and to the GEOS-Chem v11-02c mechanism (183 Tg a<sup>-1</sup>). This results in 38 Tg a<sup>-1</sup> (20 TgC a<sup>-1</sup>) of iSOA formation from IEPOX, slightly lower than a recent estimate by Stadler et al. (2018). While the uptake parameterization of Marais et al. (2016) used here varies with particle acidity and sulfate content as seen in chamber studies and field observations (Gaston et al., 2014; Nguyen et al., 2014; Liao et al., 2015), it does not include the known effects of organic coatings and aerosol phase state (Riva et al., 2016; Zhang et al., 2018), which may also be important for the uptake of other precursors.

**C<sub>5</sub> tetrafunctional species:** RCIM includes eleven distinct C<sub>5</sub> tetrafunctional compounds with unique combinations of functional groups, each of which represents a variety of isomers. The global distribution of these compounds is shown in Figure 9, while their simulated daytime concentrations in diurnal-steady-state box models are shown in Figure 11 as a function of NO<sub>x</sub>. C<sub>5</sub> dihydroxy-hydroperoxy-epoxides (IDHPE), formed in H-shift reactions following the addition of OH to ISOPOOH (D'Ambro et al., 2017), are estimated to contribute the bulk of the tetrafunctional compounds globally (54% of molar production) and under most NO<sub>x</sub> conditions. MCM and GEOS-Chem v11-02c predict similar yields of C<sub>5</sub> tetrafunctional species, but the relative contributions of individual species vary substantially between mechanisms (See Figures S22-23). GEOS-Chem v11-02c only considered SOA formation from two such species (dihydroxy-dinitrates and "LVOC" produced in the reaction of ISOPOOH with OH), **resulting in 4 Tg a<sup>-1</sup> iSOA from C<sub>5</sub> tetrafunctional compounds**. Because the rates of gas-phase oxidation, deposition, and aerosol uptake for these compounds are all poorly constrained, their contribution to iSOA remains highly uncertain, **and future studies will need to evaluate the volatilities, solubilities, and particle-phase reactivities of the individual tetrafunctional species**.

While the individual yields of these compounds from isoprene may be small, their cumulative production (4.1% molar yield from isoprene globally) and relatively low volatility make them potentially substantial contributors to iSOA, and aerosol

formation has been observed from these pathways in chamber experiments (Krechmer et al., 2015; D'Ambro et al., 2017). Quantitative descriptions of their contribution to SOA remain uncertain, but we estimate a global source of  $46 \text{ Tg a}^{-1}$  ( $18 \text{ TgC a}^{-1}$ ) of iSOA from  $\text{C}_5$  tetrafunctional species. IDHPE accounts for 51% of this total, with dihydroxy-dihydroperoxides and dihydroxy-hydroperoxy-carbonyls contributing over 10% each. This total carries high uncertainty, due both to the SOA uptake parameterization and the lack of constraints on other loss pathways of the  $\text{C}_5$  tetrafunctional compounds, but is similar to a recent estimate by Stadtler et al. (2018) and highlights the importance of further investigations of this iSOA formation pathway. **Until such studies are performed, we recommend reducing the LVOC uptake coefficient applied to the tetrafunctional species by a factor of ten in GEOS-Chem implementations, to bring iSOA production from this pathway in line with previous model-measurement comparisons (Marais et al., 2016; Pai et al., 2019).**

**HMML:** Hydroxymethyl-methyl- $\alpha$ -lactone, a product of methacrolein oxidation via MPAN, is considered a major iSOA precursor under high- $\text{NO}_x$  conditions (Nguyen et al., 2015a; Kjaergaard et al., 2012; Jiang et al., 2018). Its contribution to SOA is identified in ambient aerosol from its hydrolysis product, 2-methylglyceric acid (Edney et al., 2005; Szmigielski et al., 2007; Zhang et al., 2011). While HMML is better classified as a lactone, we include it with the epoxides in Figure 11 and Tables S1-S3, as it is thought to react similarly in aerosol (Jiang et al., 2018). Our mechanism shows only minor yields of HMML under most conditions, up to a maximum of 2% molar yield from isoprene at extremely high NO (Figure 10), but it may contribute substantially to iSOA production locally; HMML production reaches 25% that of IEPOX in the  $\text{NO}_x$ -dominated conditions of East China (Table S3). RCIM results in similar production of HMML as in MCM, but a lower yield than in GEOS-Chem v11-02c, largely due to lower MACR production and MPAN formation rates (see Section 5.2); as a result, we estimate that HMML contributes only  $0.18 \text{ Tg iSOA a}^{-1}$  ( $0.11 \text{ TgC a}^{-1}$ ) globally, much lower than the  $1.7 \text{ Tg SOA a}^{-1}$  predicted in the v11-02c mechanism. However, a recent chamber study comparing iSOA yields to RCIM showed an underprediction of iSOA formation from the HMML pathway, suggesting that this global estimate may be too low (Schwantes et al., 2019).

**Other epoxides:** A new element of RCIM is the introduction of additional organic epoxide products. These include IDHPE, discussed above;  $\text{C}_5$  carbonyl-hydroxy-epoxides (ICHE), produced from the reaction of IEPOX with OH and in the H-shifts of Z- $\delta$ -ISOPOO radicals (Bates et al., 2014; Wennberg et al., 2018); and two varieties of  $\text{C}_5$  hydroxy-nitrooxy-epoxides, formed in the morning from the reactions of isoprene +  $\text{NO}_3$  products with OH (Schwantes et al., 2015). The contributions of these epoxides relative to IEPOX in diurnal-steady-state simulations are shown in Figure 11; we find that they can comprise up to 20% of ambient epoxide concentrations under low- $\text{NO}$  conditions. In global simulations, we find that non-IEPOX, non-IDHPE epoxides contribute  $5.1 \text{ Tg a}^{-1}$  ( $2.6 \text{ TgC a}^{-1}$ ) of iSOA globally.

**Nitrates:** Multifunctional nitrates derived from both the ISOPOO + NO and isoprene +  $\text{NO}_3$  pathways are also known to contribute to iSOA (Ng et al., 2008; Lee et al., 2014; Schwantes et al., 2019). In GEOS-Chem, nitrate hydrolysis results in irreversible iSOA formation; the higher organonitrate uptake and hydrolysis rates implemented in RCIM therefore result in a high iSOA formation from organonitrates of  $49 \text{ Tg a}^{-1}$  ( $21 \text{ TgC a}^{-1}$ ).  $6.9 \text{ Tg a}^{-1}$  ( $3.0 \text{ TgC a}^{-1}$ ) of this total comes from  $\text{C}_5$  tetrafunctional compounds, and is already included in the amounts listed in that section above. Much of the rest comes from  $\text{C}_5$  difunctional compounds, which are expected to form alcohols (diols in the case of hydroxynitrates) following their

particle-phase hydrolysis, many of which may be sufficiently volatile to partition back to the gas phase. The organonitrate iSOA formation simulated in GEOS-Chem is therefore likely an upper limit.

**Other compounds:** Additional known iSOA precursors include glyoxal and methylglyoxal. As discussed previously, we find that RCIM leads to low glyoxal yields relative to previous mechanisms; this results in a small estimated contribution of glyoxal to global iSOA of  $4.2 \text{ Tg a}^{-1}$  ( $1.7 \text{ TgC a}^{-1}$ ), 36% lower than in GEOS-Chem v11-02c and 58% lower than a recent estimate by Stadtler et al. (2018). In the Southeast United States, where Marais et al. (2016) found that glyoxal contributed about half as much iSOA as IEPOX, we instead find that production of iSOA from glyoxal is 10% of that from IEPOX. Locally, however, glyoxal can still be an important contributor to iSOA; we find that it contributes 23% of iSOA in East China. The production of methylglyoxal is much higher than that of glyoxal (20% molar yield from isoprene globally), but due to its low SOA yield it contributes only  $0.01 \text{ Tg iSOA a}^{-1}$  (McNeill et al., 2012). Finally, RCIM predicts a large molar yield of semivolatile highly oxidized  $\text{C}_4$  compounds, including  $51 \text{ Tg a}^{-1}$  of dihydroxy-carbonyls,  $84 \text{ Tg a}^{-1}$  of hydroxy-dicarbonyls, and  $56 \text{ Tg a}^{-1}$  of hydroxy-hydroperoxy-carbonyls, which may also contribute to iSOA formation; as with many other elements of the isoprene SOA formation scheme, further study is required to better constrain this pathway.

## 6 Further mechanism reduction

We use the results of the simulations described above to implement further simplifications to RCIM, and compile a "Mini" isoprene mechanism (Mini-CIM) for use in chemical transport modeling where computational cost is a concern. The speciation of highly functionalized isoprene oxidation products with low individual yields in RCIM goes beyond many measurement capabilities and the needs of most atmospheric model applications. We therefore combine and remove many such products, with an aim toward maintaining the effects of isoprene on OH,  $\text{NO}_x$ , ozone, SOA precursors, readily measured organic products, and organonitrates as shown in Sections 3-5.

In Mini-CIM, we create lumped species from isoprene oxidation products that meet two criteria: (1)  $< 0.1\%$  molar yield from isoprene globally, and (2)  $< 1\%$  molar yield from isoprene in each of the Amazon, Southeast United States, and East China. These products are then lumped according to their number of carbon atoms (to conserve carbon) and similarity of lifetimes and functional groups. To maintain the effects of isoprene oxidation on  $\text{NO}_x$  transport and removal, we prioritize lumping of functional groups by nitrate content. For example, all  $\text{C}_5$  dinitrate compounds are lumped into a single species, while  $\text{C}_5$  tetrafunctional mononitrates are lumped into two categories (those with and without an aldehyde, which substantially shortens the compounds' lifetimes). In addition to lumping species that meet the low-yield criteria, we remove peroxy radicals that have recently been shown to undergo rapid H-shifts (Møller et al., 2019) and replace them with the products of those H-shifts. We further combine five pairs of isomeric species that exceed the molar yield thresholds but have identical loss rates and are predominantly produced concurrently, which means that their lumping has no effect on the species' lifetimes and minimal effect on product distributions. A detailed list of the simplifications made in the Mini mechanism can be found in the Supporting Information, along with a list of the excluded species and their global and regional molar yields (Table S7).

Global simulations with Mini-CIM exhibit only minimal differences from simulations with RCIM in the outcomes described in Sections 3-5. Table S6 shows the effects of these simplifications on the simulated global and regional production and burden of tropospheric radicals, ozone, SOA, and organic products. The tropospheric methane lifetime increases by only 0.1% from RCIM to Mini-CIM. Changes in annual average HO<sub>x</sub>, NO<sub>x</sub>, ozone, CO, and formaldehyde concentrations between the two mechanisms are all below 0.2% globally, and regional differences are only minimally larger. Changes in PANs, epoxides, and SOA are below 0.5% globally and regionally, while C<sub>2</sub>-C<sub>5</sub> nitrates and hydroperoxides exhibit similarly small global changes but some regional differences of up to 4.2% in areas with low absolute loadings.

Whereas RCIM originally compiled in Wennberg et al. (2018) includes 148 organic species and 412 reactions, the new Mini-CIM contains 108 organic species involved in 345 reactions, which is comparable to the current mechanism in GEOS-Chem v11-02c (106 organic species involved in 335 reactions). We recommend the use of Mini-CIM in atmospheric models except when more detailed speciation of highly functionalized, low-yield isoprene oxidation products is required for model-measurement comparisons. A complete listing of the species and reactions in Mini-CIM can be found in KPP format in the online repository with the original mechanisms (DOI 10.7907/Z9S75DHB).

## 7 Conclusions

We have presented a detailed analysis of the Reduced Caltech Isoprene Mechanism (RCIM), a new isoprene oxidation mechanism based on a recently developed explicit scheme (Wennberg et al., 2018), to examine its atmospheric implications for HO<sub>x</sub> and NO<sub>x</sub> radicals, ozone, organic products, and secondary organic aerosol (SOA) formation. We used for that purpose a combination of box models and the GEOS-Chem global chemical transport model, and compared RCIM to the explicit MCM v3.3.1 and to the previous v11-02c version of the GEOS-Chem isoprene mechanism.

RCIM estimates a higher fraction of isoprene reacting with OH globally (88%) than past mechanisms. The resulting hydroxy-peroxy radicals (ISOPOO) react with HO<sub>2</sub> (41%), NO (28%), and RO<sub>2</sub> (9%), or undergo H-shifts to regenerate HO<sub>x</sub> (22%). The dynamic system of ISOPOO isomers, and the differences in H-shift rates between isomers, has important consequences for subsequent product formation. We show that the depletion of 4-OH ISOPOO due to its rapid H-shift leads to higher MVK/MACR ratios, higher tertiary nitrate production, and lower MPAN production than is simulated by mechanisms that do not treat the 1-OH and 4-OH ISOPOO systems separately.

The global effects of isoprene chemistry on radical families and ozone are similar in RCIM to past mechanisms, with notable regional differences. We find that isoprene is responsible for an 11% reduction in OH averaged over the troposphere, causing a 12% increase in the tropospheric lifetime of methane. Depletion of OH under low-NO conditions is much less than in previous mechanisms because of HO<sub>x</sub> recycling from H-shift pathways. Isoprene oxidation results in a 6.5% increase in mean tropospheric HO<sub>2</sub> and a 4.2% decrease in NO<sub>x</sub>. It increases tropospheric ozone by 1.9 ppbv globally but depresses ozone by up to 3.4 ppbv over tropical forests.

Mass conservation in RCIM enables a detailed accounting of the atmospheric fate of isoprene-derived carbon and the yields of oxidation products. We find globally that 50% of isoprene is oxidized to CO<sub>2</sub> in the gas phase, 76% of which proceeds via

CO including 44% via formaldehyde. Another 37% of isoprene-derived carbon is lost to organic deposition, while 13% forms SOA. For both formaldehyde and glyoxal, RCIM results in higher yields under low-NO conditions than previous mechanisms. However, deposition and aerosol uptake of isoprene oxidation intermediates greatly depresses the glyoxal yield relative to previous mechanisms.

5 The largest changes in RCIM relative to previous mechanisms are for organonitrates and SOA. We find that isoprene contributes 20% of the tropospheric burden of peroxyacyl nitrates and 28% of non-peroxyacyl nitrates, lower than in previous mechanisms. The implementation of fast tertiary nitrate hydrolysis leads to a  $\text{NO}_x$  sink of  $4.9 \text{ TgN a}^{-1}$  globally, or 10% of total  $\text{NO}_x$  loss. Only 20% of isoprene-derived organonitrates (excluding peroxyacylnitrates) chemically recycle  $\text{NO}_x$ . We estimate the total global source of SOA from isoprene to be  $61 \text{ TgC a}^{-1}$  ( $136 \text{ Tg a}^{-1}$ ), with approximately equal contributions  
10 from IEPOX, organonitrates, and highly functionalized  $\text{C}_5$  compounds. This 13% SOA yield per carbon (25% yield by mass) is much higher than in previous global models, due primarily to our inclusion of additional precursors, but is similar to a recent estimate by Stadtler et al. (2018). Such high yields imply that SOA produced from isoprene cannot be regarded as chemically inert, and must further react in the aerosol phase to generate volatile products. This aerosol-phase chemistry is not yet included in RCIM and is a topic for further research.

15 Finally, we compiled a Mini-CIM mechanism that makes further simplifications to RCIM to decrease the computational burden of simulating isoprene chemistry. Mini-CIM has 108 species and 345 reactions, comparable in size to previous mechanisms implemented in GEOS-Chem while remaining closely consistent with the original mechanism of Wennberg et al. (2018). Global simulations with Mini-CIM exhibit minimal deviations from RCIM for atmospherically relevant applications.

*Code and data availability.* The RCIM and Mini-CIM mechanisms used here are available online (DOI 10.7907/Z9S75DHB), along with the  
20 KPP code for conducting box model simulations and the model output discussed in this manuscript. MCM (<http://mcm.leeds.ac.uk/MCM/>) and GEOS-Chem (<http://geos-chem.org>) are both available online for public use.

*Author contributions.* K. H. B. designed and carried out the simulations described herein, and prepared the manuscript with substantial assistance from D. J. J.

*Competing interests.* The authors declare that they have no conflict of interest.

25 *Acknowledgements.* K. H. B. acknowledges the support of the Harvard University Center for the Environment and the National Oceanic and Atmospheric Administration's Climate and Global Change Fellowship Programs. D. J. J. was supported by the US National Science Foundation Atmospheric Chemistry Program.

## References

- Aiken, A. C., DeCarlo, P. F., Kroll, J. H., Worsnop, D. R., Huffman, J. A., Docherty, K. S., Ulbrich, I. M., Mohr, C., Kimmel, J. R., Sueper, D., Sun, Y., Zhang, Q., Trimborn, A., Northway, M., Ziemann, P. J., Canagaratna, M. R., Onasch, T. B., Alfarra, M. R., Prevot, A. S. H., Dommen, J., Duplissy, J., Metzger, A., Baltensperger, U., and Jimenez, J. L.: O/C and OM/OC ratios of primary, secondary, and ambient organic aerosols with high-resolution time-of-flight aerosol mass spectrometry, *Environ. Sci. Technol.*, 42, 4478–4485, <https://doi.org/10.1021/es703009q>, 2008.
- Allen, H. M., Crounse, J. D., Bates, K. H., Teng, A. P., Krawiec-Thayer, M. P., Rivera-Rios, J. C., Keutsch, F. N., St. Clair, J. M., Hanisco, T. F., Möller, K. H., Kjaergaard, H. G., and Wennberg, P. O.: Kinetics and product yields of the OH initiated oxidation of hydroxymethyl hydroperoxide, *J. Phys. Chem. A*, 122, 6292–6302, <https://doi.org/10.1021/acs.jpca.8b04577>, 2018.
- Alvarado, L. M. A., Richter, A., Vrekoussis, M., Wittrock, F., Hilboll, A., Schreier, S. F., and Burrows, J. P.: An improved glyoxal retrieval from OMI measurements, *Atmos. MEas. Tech.*, 7, 4133–4150, <https://doi.org/10.5194/amt-7-4133-2014>, 2014.
- Archibald, A. T., Cooke, M. C., Utembe, S. R., Shallcross, D. E., Derwent, R. G., and Jenkin, M. E.: Impacts of mechanistic changes on HOx formation and recycling in the oxidation of isoprene, *Atmos. Chem. Phys.*, 10, 8097–8118, 2010.
- Atkinson, R., Aschmann, S. M., Tuazon, E. C., Arey, J., and Zielinska, B.: Formation of 3-Methylfuran from the gas-phase reaction of OH radicals with isoprene and the rate constant for its reaction with the OH radical, *Int. J. Chem. Kinet.*, 21, 593–604, <https://doi.org/10.1002/kin.550210709>, 1989.
- Aumont, B., Szopa, S., and Madronich, S.: Modelling the evolution of organic carbon during its gas-phase tropospheric oxidation: Development of an explicit model based on a self generating approach, *Atmos. Chem. Phys.*, 5, 2497–2517, <https://doi.org/10.5194/acp-5-2497-2005>, <http://www.atmos-chem-phys.net/5/2497/2005/>, 2005.
- Barkley, M. P., Palmer, P. I., Ganzeveld, L., Arneth, A., Hagberg, D., Karl, T., Guenther, A., Paulot, F., Wennberg, P. O., Mao, J., Kurosu, T. P., Chance, K., Müller, J.-F., De Smedt, I., Van Roozendaal, M., Chen, D., Wang, Y., and Yantosca, R. M.: Can a "state of the art" chemistry transport model simulate Amazonian tropospheric chemistry?, *J. Geophys. Res. - Atmos.*, 116, <https://doi.org/10.1029/2011JD015893>, 2011.
- Barkley, M. P., de Smedt, I., Van Roozendaal, M., Kurosu, T. P., Chance, K., Arneth, A., Hagberg, D., Guenther, A., Paulot, F., Marais, E., and Mao, J.: Top-down isoprene emissions over tropical South America inferred from SCIAMACHY and OMI formaldehyde columns, *J. Geophys. Res. - Atmos.*, 118, 6849–6868, <https://doi.org/10.1002/jgrd.50552>, 2013.
- Bates, K. H., Crounse, J. D., St. Clair, J. M., Bennett, N. B., Nguyen, T. B., Seinfeld, J. H., Stoltz, B. M., and Wennberg, P. O.: Gas phase production and loss of isoprene epoxydiols, *J. Phys. Chem. A*, 118, 1237–46, <https://doi.org/10.1021/jp4107958>, 2014.
- Bates, K. H., Nguyen, T. B., Teng, A. P., Crounse, J. D., Kjaergaard, H. G., Stoltz, B. M., Seinfeld, J. H., and Wennberg, P. O.: Production and fate of C4 dihydroxycarbonyl compounds from isoprene oxidation, *J. Phys. Chem. A*, 120, 106–117, <https://doi.org/10.1021/acs.jpca.5b10335>, 2016.
- Bergamaschi, P., Hein, R., Heimann, M., and Crutzen, P. J.: Inverse modeling of the global CO cycle: 1. Inversion of CO mixing ratios, *J. Geophys. Res. - Atmos.*, 105, 1909–1927, <https://doi.org/10.1029/1999JD900818>, 2000.
- Biesenthal, T. A. and Shepson, P. B.: Observations of anthropogenic inputs of the isoprene oxidation products methyl vinyl ketone and methacrolein to the atmosphere, *Geophys. Res. Lett.*, 24, 1375–1378, <https://doi.org/10.1029/97GL01337>, <http://dx.doi.org/10.1029/97GL01337>, 1997.

- Brewer, D. A., Oglaruso, M. A., Augustsson, T. R., and Levine, J. S.: The oxidation of isoprene in the troposphere: Mechanism and model calculations, *Atmos. Environ.*, 18, 2723 – 2744, [https://doi.org/10.1016/0004-6981\(84\)90338-X](https://doi.org/10.1016/0004-6981(84)90338-X), 1984.
- Butler, T. M., Taraborrelli, D., Brühl, C., Fischer, H., Harder, H., Martinez, M., Williams, J., Lawrence, M. G., and Lelieveld, J.: Improved simulation of isoprene oxidation chemistry with the ECHAM5/MESSy chemistry-climate model: lessons from the GABRIEL airborne field campaign, *Atmos. Chem. Phys.*, 8, 4529–4546, <https://doi.org/10.5194/acp-8-4529-2008>, <https://www.atmos-chem-phys.net/8/4529/2008/>, 2008.
- Carlton, A. G., Wiedinmyer, C., and Kroll, J. H.: A review of secondary organic aerosol (SOA) formation from isoprene, *Atmos. Chem. Phys.*, 9, 4987–5005, <https://doi.org/10.5194/acp-9-4987-2009>, <http://www.atmos-chem-phys.net/9/4987/2009/>, 2009.
- Carslaw, N., Creasey, D., Harrison, D., Heard, D., Hunter, M., Jacobs, P., Jenkin, M., Lee, J., Lewis, A., Pilling, M., Saunders, S., and Seakins, P.: OH and HO<sub>2</sub> radical chemistry in a forested region of north-western Greece, *Atmos. Environ.*, 35, 4725 – 4737, [https://doi.org/https://doi.org/10.1016/S1352-2310\(01\)00089-9](https://doi.org/https://doi.org/10.1016/S1352-2310(01)00089-9), 2001.
- Carter, W. P. L.: Condensed atmospheric photooxidation mechanisms for isoprene, *Atmos. Environ.*, 30, 4275–4290, 1996.
- Chan Miller, C., Gonzalez Abad, G., Wang, H., Liu, X., Kurosu, T., Jacob, D. J., and Chance, K.: Glyoxal retrieval from the Ozone Monitoring Instrument, *Atmos. Meas. Tech.*, 7, 3891–3907, <https://doi.org/10.5194/amt-7-3891-2014>, 2014.
- Chan Miller, C., Jacob, D. J., González Abad, G., and Chance, K.: Hotspot of glyoxal over the Pearl River delta seen from the OMI satellite instrument: implications for emissions of aromatic hydrocarbons, *Atmos. Chem. Phys.*, 16, 4631–4639, <https://doi.org/10.5194/acp-16-4631-2016>, 2016.
- Chan Miller, C., Jacob, D. J., Marais, E. A., Yu, K., Travis, K. R., Kim, P. S., Fisher, J. A., Zhu, L., Wolfe, G. M., Hanisco, T. F., Keutsch, F. N., Kaiser, J., Min, K.-E., Brown, S. S., Washenfelder, R. A., González Abad, G., and Chance, K.: Glyoxal yield from isoprene oxidation and relation to formaldehyde: chemical mechanism, constraints from SENEX aircraft observations, and interpretation of OMI satellite data, *Atmos. Chem. Phys.*, 17, 8725–8738, <https://doi.org/10.5194/acp-17-8725-2017>, 2017.
- Claeys, M., Graham, B., Vas, G., Wang, W., Vermeylen, R., Pashynska, V., Cafmeyer, J., Guyon, P., Andreae, M. O., Artaxo, P., and Maenhaut, W.: Formation of secondary organic aerosols through photooxidation of isoprene., *Science*, 303, 1173–6, <https://doi.org/10.1126/science.1092805>, <http://www.sciencemag.org/content/303/5661/1173.full.pdf>, 2004.
- Cleary, P. A., Wooldridge, P. J., Millet, D. B., McKay, M., Goldstein, A. H., and Cohen, R. C.: Observations of total peroxy nitrates and aldehydes: Measurement interpretation and inference of OH radical concentrations, *Atmos. Chem. Phys.*, 7, 1947–1960, <https://doi.org/10.5194/acp-7-1947-2007>, 2007.
- Crounse, J. D., Paulot, F., Kjaergaard, H. G., and Wennberg, P. O.: Peroxy radical isomerization in the oxidation of isoprene, *Phys. Chem. Chem. Phys.*, 13, 13 607–13 613, 2011.
- Crounse, J. D., Knap, H. C., Ørnø, K. B., Jørgensen, S., Paulot, F., Kjaergaard, H. G., and Wennberg, P. O.: Atmospheric fate of methacrolein. 1. Peroxy radical isomerization following addition of OH and O<sub>2</sub>, *J. Phys. Chem. A*, 116, 5756–5762, 2012.
- Crounse, J. D., Nielsen, L. B., Jørgensen, S., Kjaergaard, H. G., and Wennberg, P. O.: Autoxidation of organic compounds in the atmosphere, *J. Phys. Chem. Lett.*, 4, 3513–3520, 2013.
- Daescu, D., Sandu, A., and Carmichael, G.: Direct and adjoint sensitivity analysis of chemical kinetic systems with KPP: II - validation and numerical experiments, *Atmos. Environ.*, 37, 5097–5114, 2003.
- D'Ambro, E. L., Moller, K. H., Lopez-Hilfiker, F. D., Schobesberger, S., Liu, J., Shilling, J. E., Lee, B. H., Kjaergaard, H. G., and Thornton, J. A.: Isomerization of second generation isoprene peroxy radicals: Epoxide formation and implications for secondary organic aerosol yields, *Environ. Sci. Technol.*, submitted, 2017.

- Damian, V., Sandu, A., Damian, M., Potra, F., and Carmichael, G.: The Kinetic PreProcessor (KPP) - a software environment for solving chemical kinetics, *Comp. and Chem. Eng.*, 26, 1567–1579, 2002.
- Darer, A. I., Cole-Filipiak, N. C., O'Connor, A. E., and Elrod, M. J.: Formation and stability of atmospherically relevant isoprene-derived organosulfates and organonitrates, *Environ. Sci. Technol.*, 45, 1895–1902, <https://doi.org/10.1021/es103797z>, <http://dx.doi.org/10.1021/es103797z>, 2011.
- de Gouw, J. and Jimenez, J. L.: Organic aerosols in the Earth's atmosphere, *Environ. Sci. Technol.*, 43, 7614–7618, <https://doi.org/10.1021/es9006004>, 2009.
- Dillon, T. J. and Crowley, J. N.: Direct detection of OH formation in the reactions of HO<sub>2</sub> with CH<sub>3</sub>C(O)O<sub>2</sub> and other substituted peroxy radicals, *Atmos. Chem. Phys.*, 8, 4877–4889, <https://doi.org/10.5194/acp-8-4877-2008>, <http://www.atmos-chem-phys.net/8/4877/2008/>, 2008.
- Duncan, B. N., Logan, J. A., Bey, I., Megretskaja, I. A., Yantosca, R. M., Novelli, P. C., Jones, N. B., and Rinsland, C. P.: Global budget of CO, 1988-1997: Source estimates and validation with a global model, *J. Geophys. Res. - Atmos.*, 112, <https://doi.org/10.1029/2007JD008459>, 2007.
- Eastham, S. D., Weisenstein, D. K., and Barrett, S. R.: Development and evaluation of the unified tropospheric–stratospheric chemistry extension (UCX) for the global chemistry-transport model GEOS-Chem, *Atmos. Environ.*, 89, 52 – 63, <https://doi.org/https://doi.org/10.1016/j.atmosenv.2014.02.001>, 2014.
- Edney, E. O., Kleindienst, T. E., Jaoui, M., Lewandowski, M., Offenberg, J. H., Wang, W., and Claeys, M.: Formation of 2-methyl tetrols and 2-methylglyceric acid in secondary organic aerosol from laboratory irradiated isoprene/NOX/SO<sub>2</sub>/air mixtures and their detection in ambient PM<sub>2.5</sub> samples collected in the eastern United States, *Atmos. Environ.*, 39, 5281–5289, <https://doi.org/http://dx.doi.org/10.1016/j.atmosenv.2005.05.031>, <http://www.sciencedirect.com/science/article/pii/S1352231005004875>, 2005.
- Eerdekens, G., Ganzeveld, L., Vilà-Guerau de Arellano, J., Klüpfel, T., Sinha, V., Yassaa, N., Williams, J., Harder, H., Kubistin, D., Martinez, M., and Lelieveld, J.: Flux estimates of isoprene, methanol and acetone from airborne PTR-MS measurements over the tropical rainforest during the GABRIEL 2005 campaign, *Atmos. Chem. Phys.*, 9, 4207–4227, <https://doi.org/10.5194/acp-9-4207-2009>, 2009.
- Fan, J. and Zhang, R.: Atmospheric oxidation mechanism of isoprene, *Environ. Chem.*, 1, 140–149, <http://dx.doi.org/10.1071/EN04045>, 2004.
- Feiner, P. A., Brune, W. H., Miller, D. O., Zhang, L., Cohen, R. C., Romer, P. S., Goldstein, A. H., Keutsch, F. N., Skog, K. M., Wennberg, P. O., et al.: Testing atmospheric oxidation in an Alabama forest, *J. Atmos. Sci.*, 73, 4699–4710, 2016.
- Fiore, A. M., Dentener, F. J., Wild, O., Cuvelier, C., Schultz, M. G., Hess, P., Textor, C., Schulz, M., Doherty, R. M., Horowitz, L. W., MacKenzie, I. A., Sanderson, M. G., Shindell, D. T., Stevenson, D. S., Szopa, S., Van Dingenen, R., Zeng, G., Atherton, C., Bergmann, D., Bey, I., Carmichael, G., Collins, W. J., Duncan, B. N., Faluvegi, G., Folberth, G., Gauss, M., Gong, S., Hauglustaine, D., Holloway, T., Isaksen, I. S. A., Jacob, D. J., Jonson, J. E., Kaminski, J. W., Keating, T. J., Lupu, A., Marmer, E., Montanaro, V., Park, R. J., Pitari, G., Pringle, K. J., Pyle, J. A., Schroeder, S., Vivanco, M. G., Wind, P., Wojcik, G., Wu, S., and Zuber, A.: Multimodel estimates of intercontinental source-receptor relationships for ozone pollution, *J. Geophys. Res. - Atmos.*, 114, <https://doi.org/10.1029/2008JD010816>, 2009.
- Fiore, A. M., Naik, V., Spracklen, D. V., Steiner, A., Unger, N., Prather, M., Bergmann, D., Cameron-Smith, P. J., Cionni, I., Collins, W. J., Dalsøren, S., Eyring, V., Folberth, G. A., Ginoux, P., Horowitz, L. W., Josse, B., Lamarque, J.-F., MacKenzie, I. A., Nagashima, T.,

- O'Connor, F. M., Righi, M., Rumbold, S. T., Shindell, D. T., Skeie, R. B., Sudo, K., Szopa, S., Takemura, T., and Zeng, G.: Global air quality and climate, *Chem. Soc. Rev.*, 41, 6663–6683, <https://doi.org/10.1039/C2CS35095E>, 2012.
- Fischer, E. V., Jacob, D. J., Yantosca, R. M., Sulprizio, M. P., Millet, D. B., Mao, J., Paulot, F., Singh, H. B., Roiger, A., Ries, L., Talbot, R. W., Dzepina, K., and Pandey Deolal, S.: Atmospheric peroxyacetyl nitrate (PAN): a global budget and source attribution, *Atmos. Chem. Phys.*, 14, 2679–2698, <https://doi.org/10.5194/acp-14-2679-2014>, 2014.
- Fisher, J. A., Jacob, D. J., Travis, K. R., Kim, P. S., Marais, E. A., Chan Miller, C., Yu, K., Zhu, L., Yantosca, R. M., Sulprizio, M. P., et al.: Organic nitrate chemistry and its implications for nitrogen budgets in an isoprene-and monoterpene-rich atmosphere: constraints from aircraft (SEAC4RS) and ground-based (SOAS) observations in the Southeast US, *Atmos. Chem. Phys.*, 16, 5969–5991, 2016.
- Fisher, J. A., Murray, L. T., Jones, D. B. A., and Deutscher, N. M.: Improved method for linear carbon monoxide simulation and source attribution in atmospheric chemistry models illustrated using GEOS-Chem v9, *Geosci. Model Dev.*, 10, 4129–4144, <https://doi.org/10.5194/gmd-10-4129-2017>, 2017.
- Fu, T.-M., Jacob, D. J., Wittrock, F., Burrows, J. P., Vrekoussis, M., and Henze, D. K.: Global budgets of atmospheric glyoxal and methylglyoxal, and implications for formation of secondary organic aerosols, *J. Geophys. Res. - Atmos.*, 113, <https://doi.org/10.1029/2007JD009505>, 2008.
- Fuchs, H., Hofzumahaus, A., Rohrer, F., Bohn, B., Brauers, T., Dorn, H. P., Haseler, R., Holland, F., Kaminski, M., Li, X., Lu, K., Nehr, S., Tillmann, R., Wegener, R., and Wahner, A.: Experimental evidence for efficient hydroxyl radical regeneration in isoprene oxidation, *Nature Geosci.*, 6, 1023–1026, <https://doi.org/10.1038/ngeo1964> <http://www.nature.com/ngeo/journal/v6/n12/abs/ngeo1964.html#supplementary-information>, <http://dx.doi.org/10.1038/ngeo1964>, 2013.
- Ganzeveld, L., Bouwman, L., Stehfest, E., van Vuuren, D. P., Eickhout, B., and Lelieveld, J.: Impact of future land use and land cover changes on atmospheric chemistry-climate interactions, *J. Geophys. Res. - Atmos.*, 115, <https://doi.org/10.1029/2010JD014041>, 2010.
- Gaston, C. J., Riedel, T. P., Zhang, Z., Gold, A., Surratt, J. D., and Thornton, J. A.: Reactive uptake of an isoprene-derived epoxydiol to submicron aerosol particles, *Environ. Sci. Technol.*, 48, 11 178–11 186, 2014.
- Geiger, H., Barnes, I., Bejan, I., Benter, T., and Spittler, M.: The tropospheric degradation of isoprene: An updated module for the regional atmospheric chemistry mechanism, *Atmos. Environ.*, 37, 1503 – 1519, [https://doi.org/10.1016/S1352-2310\(02\)01047-6](https://doi.org/10.1016/S1352-2310(02)01047-6), 2003.
- Goldstein, A. H. and Galbally, I. E.: Known and unexplored organic constituents in the Earth's atmosphere, *Environ. Sci. Technol.*, 41, 1514–1521, <https://doi.org/10.1021/es072476p>, <http://dx.doi.org/10.1021/es072476p>, 2007.
- Greenberg, J., Guenther, A., Zimmerman, P., Baugh, W., Geron, C., Davis, K., Helmig, D., and Klinger, L.: Tethered balloon measurements of biogenic VOCs in the atmospheric boundary layer, *Atmos. Environ.*, 33, 855 – 867, [https://doi.org/https://doi.org/10.1016/S1352-2310\(98\)00302-1](https://doi.org/https://doi.org/10.1016/S1352-2310(98)00302-1), 1999.
- Grosjean, D., II, E. L. W., and Grosjean, E.: Atmospheric chemistry of isoprene and of its carbonyl products, *Environ. Sci. Technol.*, 27, 830–840, <https://doi.org/10.1021/es00042a004>, <http://dx.doi.org/10.1021/es00042a004>, 1993.
- Guenther, A., Hewitt, C. N., Erickson, D., Fall, R., Geron, C., Graedel, T., Harley, P., Klinger, L., Lerdau, M., McKay, W. A., Pierce, T., Scholes, B., Steinbrecher, R., Tallamraju, R., Taylor, J., and Zimmerman, P.: A global model of natural volatile organic compound emissions, *J. Geophys. Res. - Atmos.*, 100, 8873–8892, <https://doi.org/10.1029/94JD02950>, <http://dx.doi.org/10.1029/94JD02950>, 1995.
- Guenther, A., Jiang, X., Heald, C. L., Sakulyanontvittaya, T., Duhl, T., Emmons, L. K., and Wang, X.: The Model of Emissions of Gases and Aerosols from Nature version 2.1 (MEGAN 2.1): an extended and updated framework for modeling biogenic emissions, *Geosci. Model Dev.*, 5, 1471–1492, 2012.

- Hallquist, M., Wenger, J. C., Baltensperger, U., Rudich, Y., Simpson, D., Claeys, M., Dommen, J., Donahue, N. M., George, C., Goldstein, A. H., Hamilton, J. F., Herrmann, H., Hoffmann, T., Iinuma, Y., Jang, M., Jenkin, M. E., Jimenez, J. L., Kiendler-Scharr, A., Maenhaut, W., McFiggans, G., Mentel, T. F., Monod, A., Prévôt, A. S. H., Seinfeld, J. H., Surratt, J. D., Szmigielski, R., and Wildt, J.: The formation, properties and impact of secondary organic aerosol: current and emerging issues, *Atmos. Chem. Phys.*, 9, 5155–5236, <https://doi.org/10.5194/acp-9-5155-2009>, <http://www.atmos-chem-phys.net/9/5155/2009/>, 2009.
- 5 Hasson, A. S., Tyndall, G. S., and Orlando, J. J.: A product yield study of the reaction of HO<sub>2</sub> radicals with ethyl peroxy (C<sub>2</sub>H<sub>5</sub>O<sub>2</sub>), acetyl peroxy (CH<sub>3</sub>C(O)O<sub>2</sub>), and acetonyl peroxy (CH<sub>3</sub>C(O)CH<sub>2</sub>O<sub>2</sub>) radicals, *J. Phys. Chem. A*, 108, 5979–5989, <https://doi.org/10.1021/jp048873t>, <http://dx.doi.org/10.1021/jp048873t><http://pubs.acs.org/doi/pdfplus/10.1021/jp048873t>, 2004.
- Heald, C. L., Ridley, D. A., Kreidenweis, S. M., and Drury, E. E.: Satellite observations cap the atmospheric organic aerosol budget, *Geophys. Res. Lett.*, 37, <https://doi.org/10.1029/2010GL045095>, 2010.
- 10 Hewitt, C. N., Kok, G. L., and Fall, R.: Hydroperoxides in plants exposed to ozone mediate air pollution damage to alkene emitters, *Nature*, 344, 56–58, <https://doi.org/10.1038/344056a0>, 1990.
- Hodzic, A., Kasibhatla, P. S., Jo, D. S., Cappa, C. D., Jimenez, J. L., Madronich, S., and Park, R. J.: Rethinking the global secondary organic aerosol (SOA) budget: Stronger production, faster removal, shorter lifetime, *Atmos. Chem. Phys.*, 16, 7917–7941, <https://doi.org/10.5194/acp-16-7917-2016>, 2016.
- 15 Horowitz, L. W., Fiore, A. M., Milly, G. P., Cohen, R. C., Perring, A., Wooldridge, P. J., Hess, P. G., Emmons, L. K., and Lamarque, J.-F.: Observational constraints on the chemistry of isoprene nitrates over the eastern United States, *J. Geophys. Res. - Atmos.*, 112, <https://doi.org/10.1029/2006JD007747>, <http://dx.doi.org/10.1029/2006JD007747>, d12S08, 2007.
- Hu, K. S., Darer, A. I., and Elrod, M. J.: Thermodynamics and kinetics of the hydrolysis of atmospherically relevant organonitrates and organosulfates, *Atmos. Chem. Phys.*, 11, 8307–8320, <https://doi.org/10.5194/acp-11-8307-2011>, <http://www.atmos-chem-phys.net/11/8307/2011/>, 2011.
- 20 Hu, L., Millet, D. B., Baasandorj, M., Griffis, T. J., Turner, P., Helmig, D., Curtis, A. J., and Hueber, J.: Isoprene emissions and impacts over an ecological transition region in the U.S. Upper Midwest inferred from tall tower measurements, *J. Geophys. Res. - Atmos.*, 120, 3553–3571, <https://doi.org/10.1002/2014JD022732>, 2015.
- 25 Huang, L., Jiang, J. H., Murray, L. T., Damon, M. R., Su, H., and Livesey, N. J.: Evaluation of UTLS carbon monoxide simulations in GMI and GEOS-Chem chemical transport models using Aura MLS observations, *Atmos. Chem. Phys.*, 16, 5641–5663, <https://doi.org/10.5194/acp-16-5641-2016>, 2016.
- Ito, A., Sillman, S., and Penner, J. E.: Global chemical transport model study of ozone response to changes in chemical kinetics and biogenic volatile organic compounds emissions due to increasing temperatures: Sensitivities to isoprene nitrate chemistry and grid resolution, *J. Geophys. Res. - Atmos.*, 114, <https://doi.org/10.1029/2008jd011254>, 2009.
- 30 Jacob, D. J. and Wofsy, S. C.: Photochemistry of biogenic emissions over the Amazon forest, *J. Geophys. Res. - Atmos.*, 93, 1477–1486, <https://doi.org/10.1029/JD093iD02p01477>, <http://dx.doi.org/10.1029/JD093iD02p01477>, 1988.
- Jenkin, M. E., Saunders, S. M., and Pilling, M. J.: The tropospheric degradation of volatile organic compounds: A protocol for mechanism development, *Atmos. Environ.*, 31, 81–104, 1997.
- 35 Jenkin, M. E., Hurley, M. D., and Wallington, T. J.: Investigation of the radical product channel of the CH<sub>3</sub>C(O)O<sub>2</sub> + HO<sub>2</sub> reaction in the gas phase, *Phys. Chem. Chem. Phys.*, 9, 3149–3162, <https://doi.org/10.1039/B702757E>, <http://dx.doi.org/10.1039/B702757E>, 2007.
- Jenkin, M. E., Young, J. C., and Rickard, A. R.: The MCM v3.3.1 degradation scheme for isoprene, *Atmos. Chem. Phys.*, 15, 11 433–11 459, <https://doi.org/10.5194/acp-15-11433-2015>, <http://www.atmos-chem-phys.net/15/11433/2015/>, 2015.

- Jiang, K., Hill, D. R., and Elrod, M. J.: Assessing the potential for oligomer formation from the reactions of lactones in secondary organic aerosols, *J. Phys. Chem. A*, 122, 292–302, <https://doi.org/10.1021/acs.jpca.7b10411>, 2018.
- Jin, X. and Holloway, T.: Spatial and temporal variability of ozone sensitivity over China observed from the Ozone Monitoring Instrument, *J. Geophys. Res. - Atmos.*, 120, 7229–7246, <https://doi.org/10.1002/2015JD023250>, 2015.
- 5 Jørgensen, S., Knap, H. C., Otkjær, R. V., Jensen, A. M., Kjeldsen, M. L. H., Wennberg, P. O., and Kjaergaard, H. G.: Rapid hydrogen shift scrambling in hydroperoxy-substituted organic peroxy radicals, *J. Phys. Chem. A*, 120, 266–275, <https://doi.org/10.1021/acs.jpca.5b06768>, <http://dx.doi.org/10.1021/acs.jpca.5b06768>, 2016.
- Kaiser, J., Wolfe, G. M., Min, K. E., Brown, S. S., Miller, C. C., Jacob, D. J., deGouw, J. A., Graus, M., Hanisco, T. F., Holloway, J., Peischl, J., Pollack, I. B., Ryerson, T. B., Warneke, C., Washenfelder, R. A., and Keutsch, F. N.: Reassessing the ratio of glyoxal to formaldehyde as  
10 an indicator of hydrocarbon precursor speciation, *Atmos. Chem. Phys.*, 15, 7571–7583, <https://doi.org/10.5194/acp-15-7571-2015>, 2015.
- Kaiser, J., Skog, K. M., Baumann, K., Bertman, S. B., Brown, S. B., Brune, W. H., Crounse, J. D., de Gouw, J. A., Edgerton, E. S., Feiner, P. A., Goldstein, A. H., Koss, A., Misztal, P. K., Nguyen, T. B., Olson, K. F., St. Clair, J. M., Teng, A. P., Toma, S., Wennberg, P. O., Wild, R. J., Zhang, L., and Keutsch, F. N.: Speciation of OH reactivity above the canopy of an isoprene-dominated forest, *Atmos. Chem. Phys.*, 16, 9349–9359, <https://doi.org/10.5194/acp-16-9349-2016>, 2016.
- 15 Kaiser, J., Jacob, D. J., Zhu, L., Travis, K. R., Fisher, J. A., González Abad, G., Zhang, L., Zhang, X., Fried, A., Crounse, J. D., St. Clair, J. M., and Wisthaler, A.: High-resolution inversion of OMI formaldehyde columns to quantify isoprene emission on ecosystem-relevant scales: application to the southeast US, *Atmos. Chem. Phys.*, 18, 5483–5497, <https://doi.org/10.5194/acp-18-5483-2018>, 2018.
- Kanakidou, M., Seinfeld, J. H., Pandis, S. N., Barnes, I., Dentener, F. J., Facchini, M. C., Van Dingenen, R., Ervens, B., Nenes, A., Nielsen, C. J., Swietlicki, E., Putaud, J. P., Balkanski, Y., Fuzzi, S., Horth, J., Moortgat, G. K., Winterhalter, R., Myhre, C. E. L., Tsigaridis, K.,  
20 Vignati, E., Stephanou, E. G., and Wilson, J.: Organic aerosol and global climate modelling: A review, *Atmos. Chem. Phys.*, 5, 1053–1123, <https://doi.org/10.5194/acp-5-1053-2005>, <http://www.atmos-chem-phys.net/5/1053/2005/>, 2005.
- Karl, T., Guenther, A., Turnipseed, A., Tyndall, G., Artaxo, P., and Martin, S.: Rapid formation of isoprene photo-oxidation products observed in Amazonia, *Atmos. Chem. Phys.*, 9, 7753–7767, <https://doi.org/10.5194/acp-9-7753-2009>, <http://www.atmos-chem-phys.net/9/7753/2009/>, 2009.
- 25 Kaser, L., Karl, T., Yuan, B., Mauldin, R. L., Cantrell, C. A., Guenther, A. B., Patton, E. G., Weinheimer, A. J., Knute, C., Orlando, J., Emmons, L., Apel, E., Hornbrook, R., Shertz, S., Ullmann, K., Hall, S., Graus, M., Gouw, J., Zhou, X., and Ye, C.: Chemistry-turbulence interactions and mesoscale variability influence the cleansing efficiency of the atmosphere, *Geophys. Res. Lett.*, 42, 10,894–10,903, <https://doi.org/10.1002/2015GL066641>, 2015.
- Keller, C. A., Long, M. S., Yantosca, R. M., Da Silva, A. M., Pawson, S., and Jacob, D. J.: HEMCO v1.0: a versatile, ESMF-compliant  
30 component for calculating emissions in atmospheric models, *Geosci. Model Dev.*, 7, 1409–1417, <https://doi.org/10.5194/gmd-7-1409-2014>, 2014.
- Kim, P. S., Jacob, D. J., Fisher, J. A., Travis, K., Yu, K., Zhu, L., Yantosca, R. M., Sulprizio, M. P., Jimenez, J. L., Campuzano-Jost, P., Froyd, K. D., Liao, J., Hair, J. W., Fenn, M. A., Butler, C. F., Wagner, N. L., Gordon, T. D., Welti, A., Wennberg, P. O., Crounse, J. D., St. Clair, J. M., Teng, A. P., Millet, D. B., Schwarz, J. P., Markovic, M. Z., and Perring, A. E.: Sources, seasonality, and trends of southeast  
35 US aerosol: an integrated analysis of surface, aircraft, and satellite observations with the GEOS-Chem chemical transport model, *Atmos. Chem. Phys.*, 15, 10411–10433, <https://doi.org/10.5194/acp-15-10411-2015>, 2015.
- Kjaergaard, H. G., Knap, H. C., Ornsø, K. B., Jørgensen, S., Crounse, J. D., Paulot, F., and Wennberg, P. O.: Atmospheric fate of methacrolein. 2. Formation of lactone and implications for organic aerosol production, *J. Phys. Chem. A*, 116, 5763–5768, 2012.

- Kleindienst, T. E., Jaoui, M., Lewandowski, M., Offenberg, J. H., Lewis, C. W., Bhave, P. V., and Edney, E. O.: Estimates of the contributions of biogenic and anthropogenic hydrocarbons to secondary organic aerosol at a southeastern US location, *Atmos. Environ.*, 41, 8288–8300, <https://doi.org/http://doi.org/10.1016/j.atmosenv.2007.06.045>, <http://www.sciencedirect.com/science/article/pii/S135223100700581X>, 2007.
- 5 Krechmer, J. E., Coggon, M. M., Massoli, P., Nguyen, T. B., Crouse, J. D., Hu, W., Day, D. A., Tyndall, G. S., Henze, D. K., Rivera-Rios, J. C., Nowak, J. B., Kimmel, J. R., Mauldin, R. L., Stark, H., Jayne, J. T., Sipilä, M., Junninen, H., Clair, J. M. S., Zhang, X., Feiner, P. A., Zhang, L., Miller, D. O., Brune, W. H., Keutsch, F. N., Wennberg, P. O., Seinfeld, J. H., Worsnop, D. R., Jimenez, J. L., and Canagaratna, M. R.: Formation hydroxyhydroperoxide low-NO oxidation, *Environ. Sci. Technol.*, 49, 10330–10339, <https://doi.org/10.1021/acs.est.5b02031>, <http://dx.doi.org/10.1021/acs.est.5b02031>, 2015.
- 10 Kroll, J. H., Ng, N. L., Murphy, S. M., Flagan, R. C., and Seinfeld, J. H.: Secondary organic aerosol formation from isoprene photooxidation under high-NO<sub>x</sub> conditions, *Geophys. Res. Lett.*, 32, L18 808, <https://doi.org/10.1029/2005GL023637>, 2005.
- Kroll, J. H., Ng, N. L., Murphy, S. M., Flagan, R. C., and Seinfeld, J. H.: Secondary organic aerosol formation from isoprene photooxidation, *Environ. Sci. Technol.*, 40, 1869–1877, <https://doi.org/10.1021/es0524301>, 2006.
- Kubistin, D., Harder, H., Martinez, M., Rudolf, M., Sander, R., Bozem, H., Eerdeken, G., Fischer, H., Gurk, C., Klüpfel, T., Königstedt, R., Parchatka, U., Schiller, C. L., Stickler, A., Taraborrelli, D., Williams, J., and Lelieveld, J.: Hydroxyl radicals in the tropical troposphere over the Suriname rainforest: comparison of measurements with the box model MECCA, *Atmos. Chem. Phys.*, 10, 9705–9728, <https://doi.org/10.5194/acp-10-9705-2010>, 2010.
- 15 Kuhn, U., Andreae, M. O., Ammann, C., Araújo, A. C., Brancaleoni, E., Ciccioli, P., Dindorf, T., Frattoni, M., Gatti, L. V., Ganzeveld, L., Kruijt, B., Lelieveld, J., Lloyd, J., Meixner, F. X., Nobre, A. D., Pöschl, U., Spirig, C., Stefani, P., Thielmann, A., Valentini, R., and Kesselmeier, J.: Isoprene and monoterpene fluxes from Central Amazonian rainforest inferred from tower-based and airborne measurements, and implications on the atmospheric chemistry and the local carbon budget, *Atmos. Chem. Phys.*, 7, 2855–2879, <https://doi.org/10.5194/acp-7-2855-2007>, <http://www.atmos-chem-phys.net/7/2855/2007/>, 2007.
- 20 Kwok, E. S. C. and Atkinson, R.: Estimation of hydroxyl radical reaction rate constants for gas-phase organic compounds using a structure-reactivity relationship: An update., *Atmos. Environ.*, 29, 1685–1695, 1995.
- 25 Lee, B. H., Mohr, C., Lopez-Hilfiker, F. D., Lutz, A., Hallquist, M., Lee, L., Romer, P., Cohen, R. C., Iyer, S., Kurtén, T., et al.: Highly functionalized organic nitrates in the southeast United States: Contribution to secondary organic aerosol and reactive nitrogen budgets, *Proc. Nat'l. Acad. Sci.*, 113, 1516–1521, 2016.
- Lee, L., Teng, A. P., Wennberg, P. O., Crouse, J. D., and Cohen, R. C.: On rates and mechanisms of OH and O<sub>3</sub> reactions with isoprene-derived hydroxy nitrates, *J. Phys. Chem. A*, 2014.
- 30 Lelieveld, J., Butler, T. M., Crowley, J. N., Dillon, T. J., Fischer, H., Ganzeveld, L., Harder, H., Lawrence, M. G., Martinez, M., Taraborrelli, D., and Williams, J.: Atmospheric oxidation capacity sustained by a tropical forest, *Nature*, 452, 737–40, <https://doi.org/10.1038/nature06870>, <http://www.nature.com/nature/journal/v452/n7188/pdf/nature06870.pdf>, 2008.
- Li, C., Balluz, L. S., Vaidyanathan, A., Wen, X.-J., Hao, Y., and Qualters, J. R.: Long-term exposure to ozone and life expectancy in the United States, 2002 to 2008, *Medicine*, 95, e2474, <https://doi.org/10.1097/MD.0000000000002474>, <http://www.ncbi.nlm.nih.gov/pmc/articles/PMC4998595/>, 2016.
- 35 Liao, J., Froyd, K. D., Murphy, D. M., Keutsch, F. N., Yu, G., Wennberg, P. O., St. Clair, J. M., Crouse, J. D., Wisthaler, A., Mikoviny, T., Jimenez, J.-L., Campuzano-Jost, P., Day, D. A., Hu, W., Ryerson, T. B., Pollack, I. B., Peischl, J., Anderson, B. E., Ziemba, L. D., Blake,

- D. R., Meinardi, S., and Diskin, G.: Airborne measurements of organosulfates over the continental U.S., *J. Geophys. Res. - Atmos.*, 120, 2990–3005, 2015.
- Lin, J.-T., Youn, D., Liang, X.-Z., and Wuebbles, D. J.: Global model simulation of summertime U.S. ozone diurnal cycle and its sensitivity to PBL mixing, spatial resolution, and emissions, *Atmos. Environ.*, 42, 8470 – 8483, <https://doi.org/https://doi.org/10.1016/j.atmosenv.2008.08.012>, 2008.
- Lin, Y.-H., Zhang, H., Pye, H. O., Zhang, Z., Marth, W. J., Park, S., Arashiro, M., Cui, T., Budisulistiorini, S. H., Sexton, K. G., Vizuete, W., Xie, Y., Luecken, D. J., Piletic, I. R., Edney, E. O., Bartolotti, L. J., Gold, A., and Surratt, J. D.: Epoxide as a precursor to secondary organic aerosol formation from isoprene photooxidation in the presence of nitrogen oxides, *Proc. Nat'l. Acad. Sci.*, 110, 6718–6723, 2013.
- Lind, J. A., Lazrus, A. L., and Kok, G. L.: Aqueous phase oxidation of sulfur(IV) by hydrogen peroxide, methylhydroperoxide, and peroxyacetic acid, *J. Geophys. Res. - Atmos.*, 92, 4171–4177, <https://doi.org/10.1029/JD092iD04p04171>, 1987.
- Liu, J., D'Ambro, E. L., Lee, B. H., Lopez-Hilfiker, F. D., Zaveri, R. A., Rivera-Rios, J. C., Keutsch, F. N., Iyer, S., Kurten, T., Zhang, Z., Gold, A., Surratt, J. D., Shilling, J. E., and Thornton, J. A.: Efficient isoprene secondary organic aerosol formation from a non-IEPOX pathway, *Environ. Sci. Technol.*, 50, 9872–9880, <https://doi.org/10.1021/acs.est.6b01872>, <http://dx.doi.org/10.1021/acs.est.6b01872>, 2016.
- Lloyd, A. C., Atkinson, R., Lurmann, F., and Nitta, B.: Modeling potential ozone impacts from natural hydrocarbons - I. Development and testing of a chemical mechanism for the NO<sub>x</sub>-air photooxidations of isoprene and alpha-pinene under ambient conditions, *Atmos. Environ.*, 17, 1931–1950, 1983.
- Madronich, S. and Calvert, J. G.: Permutation reactions of organic peroxy radicals in the troposphere, *J. Geophys. Res.*, 95, 5697–5715, 1990.
- Mao, J., Paulot, F., Jacob, D. J., Cohen, R. C., Crounse, J. D., Wennberg, P. O., Keller, C. A., Hudman, R. C., Barkley, M. P., and Horowitz, L. W.: Ozone and organic nitrates over the eastern United States: Sensitivity to isoprene chemistry, *J. Geophys. Res.*, 118, 11 256–11 268, 2013.
- Mao, J., Carlton, A., Cohen, R. C., Brune, W. H., Brown, S. S., Wolfe, G. M., Jimenez, J. L., Pye, H. O. T., Lee Ng, N., Xu, L., McNeill, V. F., Tsigaridis, K., McDonald, B. C., Warneke, C., Guenther, A., Alvarado, M. J., de Gouw, J., Mickley, L. J., Leibensperger, E. M., Mathur, R., Nolte, C. G., Portmann, R. W., Unger, N., Tosca, M., and Horowitz, L. W.: Southeast Atmosphere Studies: learning from model-observation syntheses, *Atmos. Chem. Phys.*, 18, 2615–2651, <https://doi.org/10.5194/acp-18-2615-2018>, 2018.
- Marais, E. A., Jacob, D. J., Kurosu, T. P., Chance, K., Murphy, J. G., Reeves, C., Mills, G., Casadio, S., Millet, D. B., Barkley, M. P., Paulot, F., and Mao, J.: Isoprene emissions in Africa inferred from OMI observations of formaldehyde columns, *Atmos. Chem. Phys.*, 12, 6219–6235, <https://doi.org/10.5194/acp-12-6219-2012>, 2012.
- Marais, E. A., Jacob, D. J., Jimenez, J. L., Campuzano-Jost, P., Day, D. A., Hu, W., Krechmer, J., Zhu, L., Kim, P. S., Miller, C. C., Fisher, J. A., Travis, K., Yu, K., Hanisco, T. F., Wolfe, G. M., Arkinson, H. L., Pye, H. O. T., Froyd, K. D., Liao, J., and McNeill, V. F.: Aqueous-phase mechanism for secondary organic aerosol formation from isoprene: application to the southeast United States and co-benefit of SO<sub>2</sub> emission controls, *Atmos. Chem. Phys.*, 16, 1603–1618, <https://doi.org/10.5194/acp-16-1603-2016>, <http://www.atmos-chem-phys.net/16/1603/2016/>, 2016.
- Marais, E. A., Jacob, D. J., Turner, J. R., and Mickley, L. J.: Evidence of 1991-2013 decrease of biogenic secondary organic aerosol in response to SO<sub>2</sub> emission controls, *Environ. Res. Lett.*, 12, 054 018, <https://doi.org/10.1088/1748-9326/aa69c8>, 2017.
- Martinez, M., Harder, H., Kubistin, D., Rudolf, M., Bozem, H., Eerdekens, G., Fischer, H., Klüpfel, T., Gurk, C., Königstedt, R., Parchatka, U., Schiller, C. L., Sticker, A., Williams, J., and Lelieveld, J.: Hydroxyl radicals in the tropical troposphere over the Suriname rainforest: airborne measurements, *Atmos. Chem. Phys.*, 10, 3759–3773, <https://doi.org/10.5194/acp-10-3759-2010>, 2010.

- Marvin, M. R., Wolfe, G. M., Salawitch, R. J., Canty, T. P., Roberts, S. J., Travis, K. R., Aikin, K. C., de Gouw, J. A., Graus, M., Hanisco, T. F., Holloway, J. S., Hüler, G., Kaiser, J., Keutsch, F. N., Peischl, J., Pollack, I. B., Roberts, J. M., Ryerson, T. B., Veres, P. R., and Warneke, C.: Impact of evolving isoprene mechanisms on simulated formaldehyde: An inter-comparison supported by in situ observations from SENEX, *Atmos. Environ.*, 164, 325 – 336, <https://doi.org/10.1016/j.atmosenv.2017.05.049>, 2017.
- 5 McNeill, V. F., Woo, J. L., Kim, D. D., Schwier, A. N., Wannell, N. J., Sumner, A. J., and Barakat, J. M.: Aqueous-phase secondary organic aerosol and organosulfate formation in atmospheric aerosols: A modeling study, *Environ. Sci. Technol.*, 46, 8075–8081, <https://doi.org/10.1021/es3002986>, <http://www.ncbi.nlm.nih.gov/pubmed/22788757>, 2012.
- Millet, D. B., Baasandorj, M., Farmer, D. K., Thornton, J. A., Baumann, K., Brophy, P., Chaliyakunnel, S., de Gouw, J. A., Graus, M., Hu, L., Koss, A., Lee, B. H., Lopez-Hilfiker, F. D., Neuman, J. A., Paulot, F., Peischl, J., Pollack, I. B., Ryerson, T. B., Warneke, C., Williams, B. J., and Xu, J.: A large and ubiquitous source of atmospheric formic acid, *Atmos. Chem. Phys.*, 15, 6283–6304, <https://doi.org/10.5194/acp-15-6283-2015>, 2015.
- Miyoshi, A., Hatakeyama, S., and Washida, N.: OH radical-initiated photooxidation of isoprene: An estimate of global CO production, *J. Geophys. Res. - Atmos.*, 99, 18 779–18 787, <https://doi.org/10.1029/94JD01334>, <http://dx.doi.org/10.1029/94JD01334>, 1994.
- Müller, J.-F., Peeters, J., and Stavrou, T.: Fast photolysis of carbonyl nitrates from isoprene, *Atmos. Chem. Phys.*, 14, 2497–2508, <https://doi.org/10.5194/acp-14-2497-2014>, <http://www.atmos-chem-phys.net/14/2497/2014/>, 2014.
- 15 Müller, J.-F., Stavrou, T., and Peeters, J.: Chemistry and deposition in the Model of Atmospheric composition at Global and Regional scales using Inversion Techniques for Trace gas Emissions (MAGRITTEv1.0). Part A. Chemical mechanism, *Geosci. Model Dev. Discuss.*, 2018, 1–59, <https://doi.org/10.5194/gmd-2018-316>, 2018.
- Murazaki, K. and Hess, P.: How does climate change contribute to surface ozone change over the United States?, *J. Geophys. Res. - Atmos.*, 20 111, <https://doi.org/10.1029/2005JD005873>, 2006.
- Myriokefalitakis, S., Vrekoussis, M., Tsigaridis, K., Wittrock, F., Richter, A., Brühl, C., Volkamer, R., Burrows, J. P., and Kanakidou, M.: The influence of natural and anthropogenic secondary sources on the glyoxal global distribution, *Atmos. Chem. Phys.*, 8, 4965–4981, <http://www.atmos-chem-phys.net/8/4965/2008/>, 2008.
- Møller, K. H., Bates, K. H., and Kjaergaard, H. G.: The importance of peroxy radical hydrogen-shift reactions in atmospheric isoprene oxidation, *J. Phys. Chem. A*, 123, 920–932, <https://doi.org/10.1021/acs.jpca.8b10432>, 2019.
- 25 Ng, N., Kwan, A., Surratt, J., Chan, A., Chhabra, P., Sorooshian, A., Pye, H., Crounse, J., Wennberg, P., Flagan, R., et al.: Secondary organic aerosol (SOA) formation from reaction of isoprene with nitrate radicals (NO<sub>3</sub>), *Atmos. Chem. Phys.*, 8, 4117–4140, 2008.
- Nguyen, T. B., Coggon, M. M., Bates, K. H., Zhang, X., Schwantes, R. H., Schilling, K. A., Loza, C. L., Flagan, R. C., Wennberg, P. O., and Seinfeld, J. H.: Organic aerosol formation from the reactive uptake of isoprene epoxydiols (IEPOX) onto non-acidified inorganic seeds, *Atmos. Chem. Phys.*, 14, 3497–3510, 2014.
- 30 Nguyen, T. B., Bates, K. H., Crounse, J. D., Schwantes, R. H., Zhang, X., Kjaergaard, H. G., Surratt, J. D., Lin, P., Laskin, A., Seinfeld, J. H., and Wennberg, P. O.: Mechanism of the hydroxyl radical oxidation of methacryloyl peroxyxynitrate (MPAN) and its pathway toward secondary organic aerosol formation in the atmosphere, *Phys. Chem. Chem. Phys.*, 17, 17 914–17 926, <https://doi.org/10.1039/C5CP02001H>, <http://dx.doi.org/10.1039/C5CP02001H><http://pubs.rsc.org/en/content/articlepdf/2015/cp/c5cp02001h>, 2015a.
- 35 Nguyen, T. B., Crounse, J. D., Teng, A. P., St. Clair, J. M., Paulot, F., Wolfe, G. M., and Wennberg, P. O.: Rapid deposition of oxidized biogenic compounds to a temperate forest, *Proc. Nat'l. Acad. Sci.*, 112, E392–E401, 2015b.
- Nguyen, T. B., Tyndall, G. S., Crounse, J. D., Teng, A. P., Bates, K. H., Schwantes, R. H., Coggon, M. M., Zhang, L., Feiner, P., Miller, D. O., Skog, K. M., Rivera-Rios, J. C., Dorris, M., Olson, K. F., Koss, A., Wild, R. J., Brown, S. S., Goldstein, A. H., de Gouw, J. A., Brune,

- W. H., Keutsch, F. N., Seinfeld, J. H., and Wennberg, P. O.: Atmospheric fates of Criegee intermediates in the ozonolysis of isoprene, *Phys. Chem. Chem. Phys.*, 18, 10241–10254, <https://doi.org/10.1039/C6CP00053C>, <http://dx.doi.org/10.1039/C6CP00053C>, 2016.
- Pacifico, F., Folberth, G. A., Jones, C. D., Harrison, S. P., and Collins, W. J.: Sensitivity of biogenic isoprene emissions to past, present, and future environmental conditions and implications for atmospheric chemistry, *J. Geophys. Res. - Atmos.*, 117, <https://doi.org/10.1029/2012JD018276>, 2012.
- 5 Pai, S. J., Heald, C. L., Pierce, J. R., Farina, S. C., Marais, E. A., Jimenez, J. L., Campuzano-Jost, P., Nault, B. A., Middlebrook, A. M., Coe, H., Shilling, J. E., Bahreini, R., Dingle, J. H., and Vu, K.: An evaluation of global organic aerosol schemes using airborne observations, *Atmos. Chem. Phys. Discuss.*, <https://doi.org/10.5194/acp-2019-331>, 2019.
- Palmer, P. I., Jacob, D. J., Fiore, A. M., Martin, R. V., Chance, K., and Kurosu, T. P.: Mapping isoprene emissions over North America using formaldehyde column observations from space, *J. Geophys. Res. - Atmos.*, 108, <https://doi.org/10.1029/2002JD002153>, 2003.
- 10 Paulot, F., Crounse, J. D., Kjaergaard, H. G., Kroll, J. H., Seinfeld, J. H., and Wennberg, P. O.: Isoprene photooxidation: new insights into the production of acids and organic nitrates, *Atmos. Chem. Phys.*, 9, 1479–1501, 2009a.
- Paulot, F., Crounse, J. D., Kjaergaard, H. G., Kurten, A., St Clair, J., Seinfeld, J. H., and Wennberg, P. O.: Unexpected epoxide formation in the gas-phase photooxidation of isoprene, *Science*, 325, 730–3, <https://doi.org/10.1126/science.1172910>, <http://www.ncbi.nlm.nih.gov/pubmed/19661425>, 2009b.
- 15 Paulot, F., Henze, D. K., and Wennberg, P. O.: Impact of the isoprene photochemical cascade on tropical ozone, *Atmos. Chem. Phys.*, 12, 1307–1325, <https://doi.org/10.5194/acp-12-1307-2012>, <http://www.atmos-chem-phys.net/12/1307/2012/>, 2012.
- Paulot, F., Jacob, D. J., and Henze, D. K.: Sources and processes contributing to nitrogen deposition: An adjoint model analysis applied to biodiversity hotspots worldwide, *Environ. Sci. Technol.*, 47, 3226–3233, <https://doi.org/10.1021/es3027727>, 2013.
- 20 Paulson, S. E. and Seinfeld, J. H.: Development and evaluation of a photooxidation mechanism for isoprene, *J. Geophys. Res. - Atmos.*, 97, 20703–20715, <https://doi.org/10.1029/92JD01914>, <http://dx.doi.org/10.1029/92JD01914>, 1992.
- Paulson, S. E., Flagan, R. C., and Seinfeld, J. H.: Atmospheric photooxidation of isoprene part I: The hydroxyl radical and ground state atomic oxygen reactions, *Int. J. Chem. Kinetics*, 24, 79–101, <https://doi.org/10.1002/kin.550240109>, <http://dx.doi.org/10.1002/kin.550240109>, 1992.
- 25 Peeters, J. and Muller, J. F.: HO(x) radical regeneration in isoprene oxidation via peroxy radical isomerisations. II: Experimental evidence and global impact, *Phys. Chem. Chem. Phys.*, 12, 14227–35, <https://doi.org/10.1039/c0cp00811g>, <http://www.ncbi.nlm.nih.gov/pubmed/20882226>, 2010.
- Peeters, J., Nguyen, T. L., and Vereecken, L.: HOx radical regeneration in the oxidation of isoprene, *Phys. Chem. Chem. Phys.*, 11, 5935–9, <https://doi.org/10.1039/b908511d>, <http://www.ncbi.nlm.nih.gov/pubmed/19588016>, 2009.
- 30 Peeters, J., Muller, J. F., Stavrou, T., and Nguyen, V. S.: Hydroxyl radical recycling in isoprene oxidation driven by hydrogen bonding and hydrogen tunneling: The upgraded LIM1 mechanism, *J Phys. Chem. A*, 118, 8625–8643, <https://doi.org/10.1021/jp5033146>, 2014.
- Pfister, G. G., Emmons, L. K., Hess, P. G., Lamarque, J.-F., Orlando, J. J., Walters, S., Guenther, A., Palmer, P. I., and Lawrence, P. J.: Contribution of isoprene to chemical budgets: A model tracer study with the NCAR CTM MOZART-4, *J. Geophys. Res.*, 113, <https://doi.org/10.1029/2007JD008948>, 2008.
- 35 Pöchl, U. and Shiraiwa, M.: Multiphase chemistry at the atmosphere-biosphere interface influencing climate and public health in the anthropocene, *Chem. Rev.*, 115, 4440–4475, <https://doi.org/10.1021/cr500487s>, 2015.
- Pugh, T. A. M., MacKenzie, A. R., Hewitt, C. N., Langford, B., Edwards, P. M., Furneaux, K. L., Heard, D. E., Hopkins, J. R., Jones, C. E., Karunaharan, A., Lee, J., Mills, G., Misztal, P., Moller, S., Monks, P. S., and Whalley, L. K.: Simulating atmospheric com-

- position over a South-East Asian tropical rainforest: performance of a chemistry box model, *Atmos. Chem. Phys.*, 10, 279–298, <https://doi.org/10.5194/acp-10-279-2010>, 2010.
- Pöschl, U., von Kuhlmann, R., Poisson, N., and Crutzen, P. J.: Development and intercomparison of condensed isoprene oxidation mechanisms for global atmospheric modeling, *J. Atmos. Chem.*, 37, 29–52, <https://doi.org/10.1023/A:1006391009798>, <http://dx.doi.org/10.1023/A:1006391009798>, 2000.
- 5 Rasmussen, D., Fiore, A., Naik, V., Horowitz, L., McGinnis, S., and Schultz, M.: Surface ozone-temperature relationships in the eastern US: A monthly climatology for evaluating chemistry-climate models, *Atmos. Environ.*, 47, 142 – 153, <https://doi.org/https://doi.org/10.1016/j.atmosenv.2011.11.021>, 2012.
- Rindelaub, J. D., McAvey, K. M., and Shepson, P. B.: Determination of a-pinene-derived organic nitrate yields: particle phase partitioning and hydrolysis, *Atmos. Chem. Phys. Discuss.*, 14, 3301–3335, <https://doi.org/10.5194/acpd-14-3301-2014>, <http://www.atmos-chem-phys-discuss.net/14/3301/2014/>, 2014.
- 10 Rindelaub, J. D., Borca, C. H., Hostetler, M. A., Slade, J. H., Lipton, M. A., Slipchenko, L. V., and Shepson, P. B.: The acid-catalyzed hydrolysis of an  $\alpha$ -pinene-derived organic nitrate: kinetics, products, reaction mechanisms, and atmospheric impact, *Atmos. Chem. Phys.*, 16, 15 425–15 432, <https://doi.org/10.5194/acp-16-15425-2016>, 2016.
- 15 Riva, M., Bell, D. M., Hansen, A.-M. K., Drozd, G. T., Zhang, Z., Gold, A., Imre, D., Surratt, J. D., Glasius, M., and Zelenyuk, A.: Effect of organic coatings, humidity and aerosol acidity on multiphase chemistry of isoprene epoxydiols, *Environ. Sci. Technol.*, 50, 5580–5588, <https://doi.org/10.1021/acs.est.5b06050>, <http://dx.doi.org/10.1021/acs.est.5b06050>, 2016.
- Roberts, J. M., Williams, J., Baumann, K., Buhr, M. P., Goldan, P. D., Holloway, J., Hübler, G., Kuster, W. C., McKeen, S. A., Rye-son, T. B., Trainer, M., Williams, E. J., Fehsenfeld, F. C., Bertman, S. B., Nouaime, G., Seaver, C., Grodzinsky, G., Rodgers, M., and Young, V. L.: Measurements of PAN, PPN, and MPAN made during the 1994 and 1995 Nashville Intensives of the Southern Oxidant Study: Implications for regional ozone production from biogenic hydrocarbons, *J. Geophys. Res. - Atmos.*, 103, 22 473–22 490, <https://doi.org/10.1029/98JD01637>, <http://dx.doi.org/10.1029/98JD01637>, 1998.
- 20 Roberts, J. M., Flocke, F., Stroud, C. A., Hereid, D., Williams, E., Fehsenfeld, F., Brune, W., Martinez, M., and Harder, H.: Ground-based measurements of peroxy-carboxylic nitric anhydrides (PANs) during the 1999 Southern Oxidants Study Nashville Intensive, *J. Geophys. Res. - Atmos.*, 107, ACH 1–1–ACH 1–10, <https://doi.org/10.1029/2001JD000947>, 2002.
- 25 Roberts, J. M., Marchewka, M., Bertman, S. B., Sommariva, R., Warneke, C., de Gouw, J., Kuster, W., Goldan, P., Williams, E., Lerner, B. M., Murphy, P., and Fehsenfeld, F. C.: Measurements of PANs during the New England Air Quality Study 2002, *J. Geophys. Res. - Atmos.*, 112, <https://doi.org/10.1029/2007JD008667>, 2007.
- Romer, P. S., Duffey, K. C., Wooldridge, P. J., Allen, H. M., Ayres, B. R., Brown, S. S., Brune, W. H., Crouse, J. D., de Gouw, J., Draper, D. C., Feiner, P. A., Fry, J. L., Goldstein, A. H., Koss, A., Misztal, P. K., Nguyen, T. B., Olson, K., Teng, A. P., Wennberg, P. O., Wild, R. J., Zhang, L., and Cohen, R. C.: The lifetime of nitrogen oxides in an isoprene-dominated forest, *Atmos. Chem. Phys.*, 16, 7623–7637, <https://doi.org/10.5194/acp-16-7623-2016>, <http://www.atmos-chem-phys.net/16/7623/2016/>, 2016.
- 30 Runge-Morris, M., Frank, P., and Novak, R. F.: Differential effects of organic hydroperoxides and hydrogen peroxide on proteolysis in human erythrocytes, *Chem. Res. Toxicol.*, 2, 76–83, <https://doi.org/10.1021/tx00008a002>, 1989.
- 35 Ruppert, L. and Becker, K.-H.: A product study of the OH radical-initiated oxidation of isoprene: formation of C5-unsaturated diols, *Atmos. Environ.*, 34, 1529–1542, [https://doi.org/http://dx.doi.org/10.1016/S1352-2310\(99\)00408-2](https://doi.org/http://dx.doi.org/10.1016/S1352-2310(99)00408-2), <http://www.sciencedirect.com/science/article/pii/S1352231099004082>, 2000.

- Safieddine, S. A., Heald, C. L., and Henderson, B. H.: The global nonmethane reactive organic carbon budget: A modeling perspective, *Geophys. Res. Lett.*, 44, 3897–3906, <https://doi.org/10.1002/2017GL072602>, 2017.
- Sanderson, M. G., Jones, C. D., Collins, W. J., Johnson, C. E., and Derwent, R. G.: Effect of climate change on isoprene emissions and surface ozone levels, *Geophys. Res. Lett.*, 30, <https://doi.org/10.1029/2003GL017642>, 2003.
- 5 Sandu, A., Daescu, D., and Carmichael, G.: Direct and adjoint sensitivity analysis of chemical kinetic systems with KPP: I - theory and software tools, *Atmos. Environ.*, 37, 5083–5096, 2003.
- Saunders, S. M., Jenkin, M. E., Derwent, R. G., and Pilling, M. J.: Protocol for the development of the Master Chemical Mechanism, MCM v3 (Part A): tropospheric degradation of non-aromatic volatile organic compounds, *Atmos. Chem. Phys.*, 3, 161–180, 2003.
- Schwantes, R. H., Teng, A. P., Nguyen, T. B., Coggon, M. M., Crouse, J. D., Clair, J. M. S., Zhang, X., Schilling, K. A., Seinfeld, J. H., and Wennberg, P. O.: Isoprene NO<sub>3</sub> oxidation products from the RO<sub>2</sub> + HO<sub>2</sub> pathway, *J. Phys. Chem. A*, 119, 10 158–10 171, <https://doi.org/10.1021/acs.jpca.5b06355>, <http://dx.doi.org/10.1021/acs.jpca.5b06355>, 2015.
- 10 Schwantes, R. H., Charan, S. M., Bates, K. H., Huang, Y., Nguyen, T. B., Mai, H., Kong, W., Flagan, R. C., and Seinfeld, J. H.: Low-volatility compounds contribute significantly to isoprene SOA under high-NO conditions, *Atmos. Chem. Phys.*, 19, 7255–7278, <https://doi.org/10.5194/acp-19-7255-2019>, 2019.
- 15 Spracklen, D. V., Jimenez, J. L., Carslaw, K. S., Worsnop, D. R., Evans, M. J., Mann, G. W., Zhang, Q., Canagaratna, M. R., Allan, J., Coe, H., McFiggans, G., Rap, A., and Forster, P.: Aerosol mass spectrometer constraint on the global secondary organic aerosol budget, *Atmos. Chem. Phys.*, 11, 12 109–12 136, <https://doi.org/10.5194/acp-11-12109-2011>, 2011.
- Squire, O. J., Archibald, A. T., Abraham, N. L., Beerling, D. J., Hewitt, C. N., Lathièrè, J., Pike, R. C., Telford, P. J., and Pyle, J. A.: Influence of future climate and cropland expansion on isoprene emissions and tropospheric ozone, *Atmos. Chem. Phys.*, 14, 1011–1024, <https://doi.org/10.5194/acp-14-1011-2014>, 2014.
- 20 Squire, O. J., Archibald, A. T., Griffiths, P. T., Jenkin, M. E., Smith, D., and Pyle, J. A.: Influence of isoprene chemical mechanism on modeled changes in tropospheric ozone due to climate and land use over the 21st century, *Atmos. Chem. Phys.*, 15, 5123–5143, <https://doi.org/10.5194/acp-15-5123-2015>, <http://www.atmos-chem-phys.net/15/5123/2015/>, 2015.
- St. Clair, J. M., Rivera-Rios, J. C., Crouse, J. D., Knap, H. C., Bates, K. H., Teng, A. P., Jorgensen, S., Kjaergaard, H. G., Keutsch, F. N., and Wennberg, P. O.: Kinetics and products of the reaction of the first-generation isoprene hydroxy hydroperoxide (ISOPOOH) with OH, *J. Phys. Chem. A*, p. just accepted, <https://doi.org/10.1021/acs.jpca.5b06532>, 2015.
- 25 Stadler, S., Kühn, T., Schröder, S., Taraborrelli, D., Schultz, M. G., and Kokkola, H.: Isoprene-derived secondary organic aerosol in the global aerosol-chemistry-climate model ECHAM6.3.0-HAM2.3-MOZ1.0, *Geosci. Model Dev.*, 11, 3235–3260, <https://doi.org/10.5194/gmd-11-3235-2018>, 2018.
- 30 Starn, T. K., Shepson, P. B., Bertman, S. B., Riemer, D. D., Zika, R. G., and Olszyna, K.: Nighttime isoprene chemistry at an urban-impacted forest site, *J. Geophys. Res. - Atmos.*, 103, 22 437–22 447, <https://doi.org/10.1029/98JD01201>, <http://dx.doi.org/10.1029/98JD01201>, 1998.
- Stevens, P., L'Esperance, D., Chuong, B., and Martin, G.: Measurements of the kinetics of the OH-initiated oxidation of isoprene: Radical propagation in the OH + isoprene + O<sub>2</sub> + NO reaction system, *Int. J. Chem. Kinetics*, 31, 637–643, [https://doi.org/10.1002/\(SICI\)1097-4601\(1999\)31:9<637::AID-KIN5>3.0.CO;2-O](https://doi.org/10.1002/(SICI)1097-4601(1999)31:9<637::AID-KIN5>3.0.CO;2-O), [http://dx.doi.org/10.1002/\(SICI\)1097-4601\(1999\)31:9<637::AID-KIN5>3.0.CO;2-O](http://dx.doi.org/10.1002/(SICI)1097-4601(1999)31:9<637::AID-KIN5>3.0.CO;2-O), 1999.
- 35 Stockwell, W. R., Kirchner, F., Kuhn, M., and Seefeld, S.: A new mechanism for regional atmospheric chemistry modeling, *J. Geophys. Res. - Atmos.*, 102, 25 847–25 879, <https://doi.org/10.1029/97JD00849>, 1997.

- Stone, D., Evans, M. J., Edwards, P. M., Commane, R., Ingham, T., Rickard, A. R., Brookes, D. M., Hopkins, J., Leigh, R. J., Lewis, A. C., Monks, P. S., Oram, D., Reeves, C. E., Stewart, D., and Heard, D. E.: Isoprene oxidation mechanisms: measurements and modelling of OH and HO<sub>2</sub> over a South-East Asian tropical rainforest during the OP3 field campaign, *Atmos. Chem. Phys.*, 11, 6749–6771, <https://doi.org/10.5194/acp-11-6749-2011>, <http://www.atmos-chem-phys.net/11/6749/2011/http://www.atmos-chem-phys.net/11/6749/2011/acp-11-6749-2011.pdf>, 2011.
- 5 Surratt, J. D., Murphy, S. M., Kroll, J. H., Ng, N. L., Hildebrandt, L., Sorooshian, A., Szmigielski, R., Vermeylen, R., Maenhaut, W., Claeys, M., Flagan, R. C., and Seinfeld, J. H.: Chemical composition of secondary organic aerosol formed from the photooxidation of isoprene., *J. Phys. Chem. A*, 110, 9665–90, <https://doi.org/10.1021/jp061734m>, <http://pubs.acs.org/doi/pdfplus/10.1021/jp061734m>, 2006.
- Szmigielski, R., Surratt, J. D., Vermeylen, R., Szmigielska, K., Kroll, J. H., Ng, N. L., Murphy, S. M., Sorooshian, A., Seinfeld, J. H., and Claeys, M.: Characterization of 2-methylglyceric acid oligomers in secondary organic aerosol formed from the photooxidation of isoprene using trimethylsilylation and gas chromatography/ion trap mass spectrometry, *J. Mass Spectrometry*, 42, 101–116, <https://doi.org/10.1002/jms.1146>, <http://dx.doi.org/10.1002/jms.1146>, 2007.
- 10 Taraborrelli, D., Lawrence, M. G., Butler, T. M., Sander, R., and Lelieveld, J.: Mainz Isoprene Mechanism 2 (MIM2): an isoprene oxidation mechanism for regional and global atmospheric modelling, *Atmos. Chem. Phys.*, 9, 2751–2777, <https://doi.org/10.5194/acp-9-2751-2009>, <http://www.atmos-chem-phys.net/9/2751/2009/>, 2009.
- 15 Teng, A. P., Crouse, J. D., and Wennberg, P. O.: Isoprene Peroxy Radical Dynamics, *J. Am. Chem. Soc.*, 139, 5367–5377, 2017.
- Trainer, M., Williams, E. J., Parrish, D. D., Buhr, M. P., Allwine, E. J., Westberg, H. H., Fehsenfeld, F. C., and Liu, S. C.: Models and observations of the impact of natural hydrocarbons on rural ozone, *Nature*, 329, 705–707, <http://dx.doi.org/10.1038/329705a0>, 1987.
- Travis, K. R., Jacob, D. J., Fisher, J. A., Kim, P. S., Marais, E. A., Zhu, L., Yu, K., Miller, C. C., Yantosca, R. M., Sulprizio, M. P., Thompson, A. M., Wennberg, P. O., Crouse, J. D., St. Clair, J. M., Cohen, R. C., Laughner, J. L., Dibb, J. E., Hall, S. R., Ullmann, K., Wolfe, G. M., Pollack, I. B., Peischl, J., Neuman, J. A., and Zhou, X.: Why do models overestimate surface ozone in the Southeast United States?, *Atmos. Chem. Phys.*, 16, 13 561–13 577, <https://doi.org/10.5194/acp-16-13561-2016>, <http://www.atmos-chem-phys.net/16/13561/2016/>, 2016.
- 20 Tsigaridis, K., Daskalakis, N., Kanakidou, M., Adams, P. J., Artaxo, P., Bahadur, R., Balkanski, Y., Bauer, S. E., Bellouin, N., Benedetti, A., Bergman, T., Berntsen, T. K., Beukes, J. P., Bian, H., Carslaw, K. S., Chin, M., Curci, G., Diehl, T., Easter, R. C., Ghan, S. J., Gong, S. L., Hodzic, A., Hoyle, C. R., Iversen, T., Jathar, S., Jimenez, J. L., Kaiser, J. W., Kirkevåg, A., Koch, D., Kokkola, H., Lee, Y. H., Lin, G., Liu, X., Luo, G., Ma, X., Mann, G. W., Mihalopoulos, N., Morcrette, J.-J., Müller, J.-F., Myhre, G., Myriokefalitakis, S., Ng, N. L., O'Donnell, D., Penner, J. E., Pozzoli, L., Pringle, K. J., Russell, L. M., Schulz, M., Sciare, J., Seland, Ø., Shindell, D. T., Sillman, S., Skeie, R. B., Spracklen, D., Stavrou, T., Steenrod, S. D., Takemura, T., Tiitta, P., Tilmes, S., Tost, H., van Noije, T., van Zyl, P. G., von Salzen, K., Yu, F., Wang, Z., Wang, Z., Zaveri, R. A., Zhang, H., Zhang, K., Zhang, Q., and Zhang, X.: The AeroCom evaluation and intercomparison of organic aerosol in global models, *Atmos. Chem. Phys.*, 14, 10 845–10 895, <https://doi.org/10.5194/acp-14-10845-2014>, 2014.
- 30 Tuazon, E. C. and Atkinson, R.: A product study of the gas-phase reaction of methacrolein with the OH radical in the presence of NO<sub>x</sub>, *Int. J. Chem. Kinetics*, 22, 591–602, <https://doi.org/10.1002/kin.550220604>, <http://dx.doi.org/10.1002/kin.550220604>, 1990.
- Volkamer, R., Jimenez, J. L., San Martini, F., Dzepina, K., Zhang, Q., Salcedo, D., Molina, L. T., Worsnop, D. R., and Molina, M. J.: Secondary organic aerosol formation from anthropogenic air pollution: Rapid and higher than expected, *Geophys. Res. Lett.*, 33, <https://doi.org/10.1029/2006GL026899>, 2006.
- von Kuhlmann, R. and Lawrence, M. G.: Sensitivities in global scale modeling of isoprene, *Atmos. Chem. Phys.*, 4, 1–17, 2004.

- Vrekoussis, M., Wittrock, F., Richter, A., and Burrows, J. P.: Temporal and spatial variability of glyoxal as observed from space, *Atmosph. Chem. Phys.*, 9, 4485–4504, <https://doi.org/10.5194/acp-9-4485-2009>, 2009.
- Wang, K. Y. and Shallcross, D. E.: Modelling terrestrial biogenic isoprene fluxes and their potential impact on global chemical species using a coupled sim-ctm model, *Atmos. Environ.*, 34, 2909–2925, 2000.
- 5 Wang, S., Riva, M., Yan, C., Ehn, M., and Wang, L.: Primary formation of highly oxidized multifunctional products in the OH-initiated oxidation of isoprene: A combined theoretical and experimental study, *Environ. Sci. Technol.*, 52, 12 255–12 264, <https://doi.org/10.1021/acs.est.8b02783>, 2018.
- Wennberg, P. O., Bates, K. H., Crounse, J. D., Dodson, L. G., McVay, R. C., Mertens, L. A., Nguyen, T. B., Praske, E., Schwantes, R. H., Smarte, M. D., St Clair, J. M., Teng, A. P., Zhang, X., and Seinfeld, J. H.: Gas-phase reactions of isoprene and its major oxidation products, *Chem. Rev.*, 118, 3337–3390, <https://doi.org/10.1021/acs.chemrev.7b00439>, <https://doi.org/10.1021/acs.chemrev.7b00439>, 2018.
- 10 Whalley, L. K., Edwards, P. M., Furneaux, K. L., Goddard, A., Ingham, T., Evans, M. J., Stone, D., Hopkins, J. R., Jones, C. E., Karunaharan, A., Lee, J. D., Lewis, A. C., Monks, P. S., Moller, S. J., and Heard, D. E.: Quantifying the magnitude of a missing hydroxyl radical source in a tropical rainforest, *Atmos. Chem. Phys.*, 11, 7223–7233, <https://doi.org/10.5194/acp-11-7223-2011>, <https://www.atmos-chem-phys.net/11/7223/2011/>, 2011.
- 15 Wiedinmyer, C., Friedfeld, S., Baugh, W., Greenberg, J., Guenther, A., Fraser, M., and Allen, D.: Measurement and analysis of atmospheric concentrations of isoprene and its reaction products in central Texas, *Atmos. Environ.*, 35, 1001 – 1013, [https://doi.org/10.1016/S1352-2310\(00\)00406-4](https://doi.org/10.1016/S1352-2310(00)00406-4), 2001.
- Wiedinmyer, C., Tie, X., Guenther, A., Neilson, R., and Granier, C.: Future changes in biogenic isoprene emissions: how might they affect regional and global atmospheric chemistry?, *Earth Interactions*, 10, 1–19, <https://doi.org/10.1175/EI174.1>, <http://journals.ametsoc.org/doi/pdf/10.1175/EI174.1>, 2006.
- 20 Williams, P., Calabrese, E. J., and Moore, G. S.: The effect of methyl oleate hydroperoxide, a possible toxic ozone intermediate, on human normal and glucose-6-phosphate dehydrogenase-deficient erythrocytes, *Ecotoxicol. Environ. Safety*, 7, 242 – 248, [https://doi.org/https://doi.org/10.1016/0147-6513\(83\)90069-6](https://doi.org/https://doi.org/10.1016/0147-6513(83)90069-6), 1983.
- Wolfe, G. M., Kaiser, J., Hanisco, T. F., Keutsch, F. N., de Gouw, J. A., Gilman, J. B., Graus, M., Hatch, C. D., Holloway, J., Horowitz, L. W., Lee, B. H., Lerner, B. M., Lopez-Hilifker, F., Mao, J., Marvin, M. R., Peischl, J., Pollack, I. B., Roberts, J. M., Ryerson, T. B., Thornton, J. A., Veres, P. R., and Warneke, C.: Formaldehyde production from isoprene oxidation across NO<sub>x</sub> regimes, *Atmos. Chem. Phys.*, 16, 2597–2610, <https://doi.org/10.5194/acp-16-2597-2016>, 2016.
- Wu, S., Mickley, L. J., Jacob, D. J., Logan, J. A., Yantosca, R. M., and Rind, D.: Why are there large differences between models in global budgets of tropospheric ozone?, *J. Geophys. Res. - Atmos.*, 112, 2007.
- 30 Wu, S., Mickley, L. J., Kaplan, J. O., and Jacob, D. J.: Impacts of changes in land use and land cover on atmospheric chemistry and air quality over the 21st century, *Atmos. Chem. Phys.*, 12, 1597–1609, <https://doi.org/10.5194/acp-12-1597-2012>, 2012.
- Xie, Y., Paulot, F., Carter, W. P. L., Nolte, C. G., Luecken, D. J., Hutzell, W. T., Wennberg, P. O., Cohen, R. C., and Pinder, R. W.: Understanding the impact of recent advances in isoprene photooxidation on simulations of regional air quality, *Atmos. Chem. Phys.*, 13, 8439–8455, <https://doi.org/10.5194/acp-13-8439-2013>, <http://www.atmos-chem-phys.net/13/8439/2013/acp-13-8439-2013.pdf>, 2013.
- 35 Xu, L., Guo, H., Boyd, C. M., Klein, M., Bougiatioti, A., Cerully, K. M., Hite, J. R., Isaacman-VanWertz, G., Kreisberg, N. M., Knote, C., Olson, K., Koss, A., Goldstein, A. H., Hering, S. V., de Gouw, J., Baumann, K., Lee, S.-H., Nenes, A., Weber, R. J., and Ng, N. L.: Effect of anthropogenic emissions on aerosol formation from isoprene and monoterpenes in the southeastern United States, *Proc. Nat'l. Acad. Sci.*, 112, 37–42, 2015.

- Yu, K., Jacob, D. J., Fisher, J. A., Kim, P. S., Marais, E. A., Miller, C. C., Travis, K. R., Zhu, L., Yantosca, R. M., Sulprizio, M. P., Cohen, R. C., Dibb, J. E., Fried, A., Mikoviny, T., Ryerson, T. B., Wennberg, P. O., and Wisthaler, A.: Sensitivity to grid resolution in the ability of a chemical transport model to simulate observed oxidant chemistry under high-isoprene conditions, *Atmos. Chem. Phys.*, 16, 4369–4378, <https://doi.org/10.5194/acp-16-4369-2016>, 2016.
- 5 Yu, S., Mathur, R., Schere, K., Kang, D., Pleim, J., and Otte, T. L.: A detailed evaluation of the Eta-CMAQ forecast model performance for O<sub>3</sub>, its related precursors, and meteorological parameters during the 2004 ICARTT study, *J. Geophys. Res. - Atmos.*, 112, <https://doi.org/10.1029/2006JD007715>, 2007.
- Yu, S., Mathur, R., Sarwar, G., Kang, D., Tong, D., Pouliot, G., and Pleim, J.: Eta-CMAQ air quality forecasts for O<sub>3</sub> and related species using three different photochemical mechanisms (CB4, CB05, SAPRC-99): comparisons with measurements during the 2004 ICARTT
- 10 study, *Atmos. Chem. Phys.*, 10, 3001–3025, <https://doi.org/10.5194/acp-10-3001-2010>, 2010.
- Zeng, G., Williams, J. E., Fisher, J. A., Emmons, L. K., Jones, N. B., Morgenstern, O., Robinson, J., Smale, D., Paton-Walsh, C., and Griffith, D. W. T.: Multi-model simulation of CO and HCHO in the Southern Hemisphere: Comparison with observations and impact of biogenic emissions, *Atmos. Chem. Phys.*, 15, 7217–7245, <https://doi.org/10.5194/acp-15-7217-2015>, 2015.
- Zhang, H., Surratt, J. D., Lin, Y. H., Bapat, J., and Kamens, R. M.: Effect of relative humidity on SOA formation from isoprene/NO photoxidation: enhancement of 2-methylglyceric acid and its corresponding oligoesters under dry conditions, *Atmos. Chem. Phys.*, 11,
- 15 6411–6424, <https://doi.org/10.5194/acp-11-6411-2011>, <http://www.atmos-chem-phys.net/11/6411/2011/>, 2011.
- Zhang, Y., Chen, Y., Lambe, A. T., Olson, N. E., Lei, Z., Craig, R. L., Zhang, Z., Gold, A., Onasch, T. B., Jayne, J. T., Worsnop, D. R., Gaston, C. J., Thornton, J. A., Vizuete, W., Ault, A. P., and Surratt, J. D.: Effect of the aerosol-phase state on secondary organic aerosol formation from the reactive uptake of isoprene-derived epoxydiols (IEPOX), *Environ. Sci. Technol.*, 5, 167–174,
- 20 <https://doi.org/10.1021/acs.estlett.8b00044>, 2018.
- Zhou, X. and Lee, Y. N.: Aqueous solubility and reaction kinetics of hydroxymethyl hydroperoxide, *J. Phys. Chem.*, 96, 265–272, <https://doi.org/10.1021/j100180a051>, 1992.

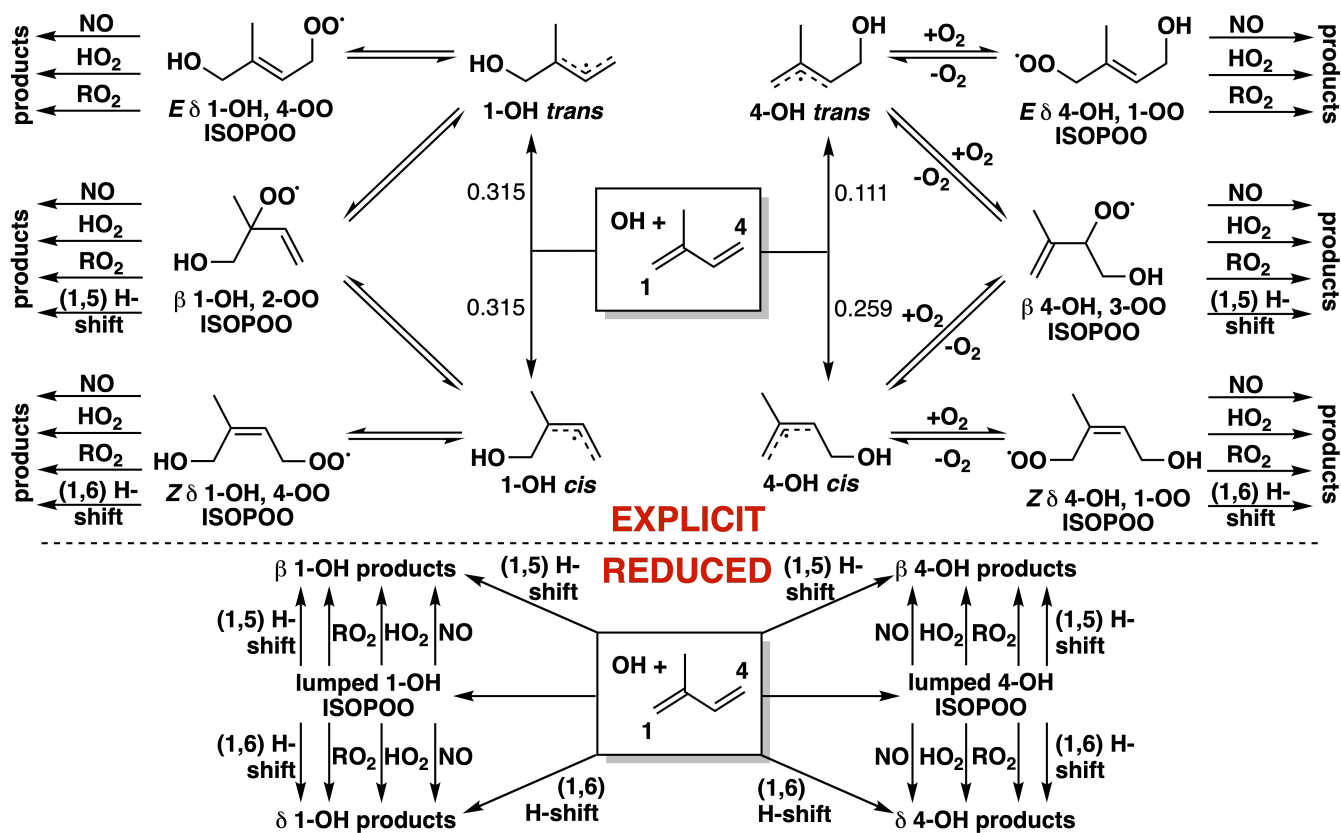


**Figure 1.** Fate of the allylic and peroxy radicals produced from the reaction of isoprene with OH in the presence of O<sub>2</sub>. The explicit Wennberg et al. (2018) scheme is on top and the Reduced Caltech Isoprene Mechanism (RCIM) scheme is on bottom.

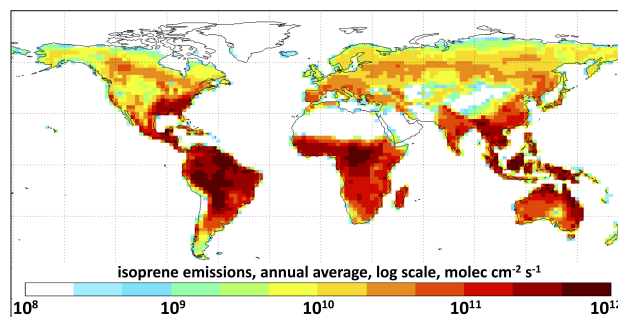


**Figure 2.** Annually averaged MEGAN v2.1 isoprene emissions for July 2014 – June 2015 as implemented in GEOS-Chem at  $2^\circ \times 2.5^\circ$  horizontal resolution.

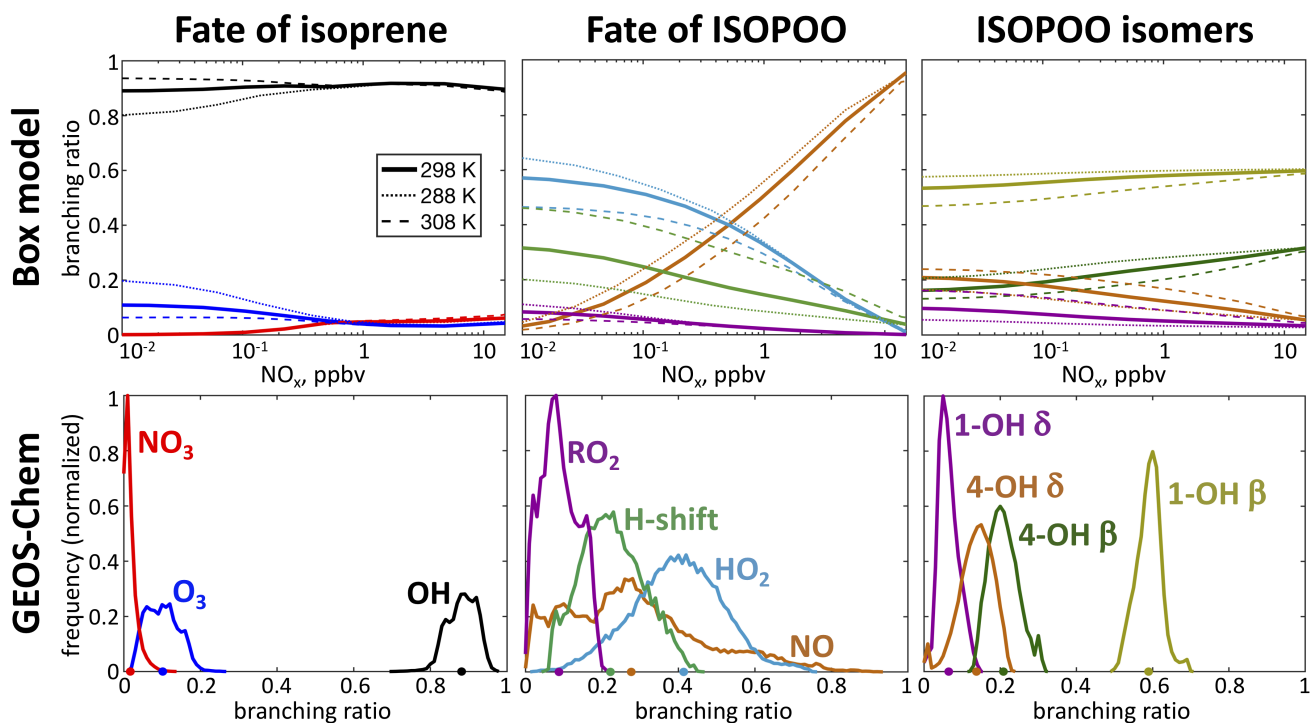


**Figure 3.** Fate of isoprene and isoprene hydroxy-peroxy radicals (ISOPOO) in the Reduced Caltech Isoprene Mechanism (RCIM). The figure shows isoprene oxidation pathway branching ratios in a diurnal-steady-state box model for clear-sky equatorial conditions (top) as a function of daytime mean  $\text{NO}_x$  concentration and temperature, and the global spatial frequency distribution of annual mean branching ratios in GEOS-Chem (bottom) at  $2^\circ \times 2.5^\circ$  horizontal resolution. The GEOS-Chem frequency distributions are weighted by the amount of isoprene reacting in each grid box. Dots on the x axis indicate the global annual total reacting via each pathway. The distributions of ISOPOO isomers are weighted by their subsequent reactivity.

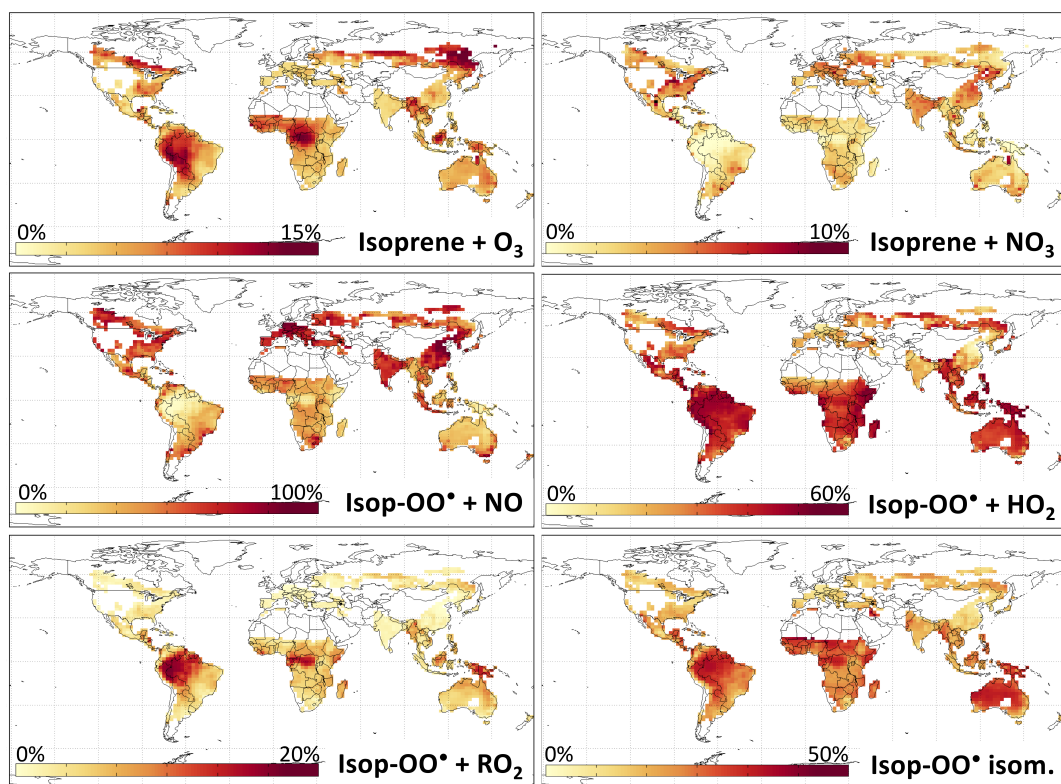


**Figure 4.** Percent of isoprene reacting with O<sub>3</sub> and NO<sub>3</sub>, and percent of the products from the reaction of isoprene with OH (ISOPOO hydroxy-peroxy radicals) reacting via each pathway. Values are annual averages from the Reduced Caltech Isoprene Mechanism (RCIM) as implemented in GEOS-Chem and for the bottom 1 km of the troposphere. Grid boxes with an average isoprene oxidation rate of  $< 1 \times 10^6$  molecules cm<sup>-3</sup> s<sup>-1</sup> are excluded. Note the different scales for each panel.

**Table 1.** Branching ratios (%) of isoprene oxidation pathways.<sup>a</sup>

Pathway		RCIM, global	v11-02c, global	Literature, global	RCIM, SE USA	RCIM, Amazon	RCIM, E China
Isoprene +	OH	88	83	85 <sup>b</sup> , 84 <sup>c</sup> , 80 <sup>d</sup>	85	86	91
	O <sub>3</sub>	10	15	9 <sup>b</sup> , 11 <sup>c</sup> , 15 <sup>d</sup>	11	13	4.5
	NO <sub>3</sub>	1.7	2.3	5 <sup>c</sup> , 5 <sup>b</sup> , 5 <sup>d</sup> , 6-7 <sup>e,f</sup>	4.2	0.2	5.1
ISOPOO +	HO <sub>2</sub>	41	42	53.5 <sup>g</sup>	31	45	14
	NO	28	31	33.5 <sup>g</sup>	46	6.4	73
	RO <sub>2</sub>	8.8	13		5.1	15	1.4
	H-shift	22	14	20 <sup>b</sup> , 9.6 <sup>g</sup> , 30 <sup>h</sup>	18	33	11
ISOPOO isomer <sup>i</sup>	<i>E/Z</i> -1-OH- $\delta$	6.5	2.4 <sup>j</sup>	16 <sup>k</sup>	5.5	10	4.1
	1-OH- $\beta$	59	51 <sup>j</sup>	44 <sup>k</sup>	59	55	61
	<i>E/Z</i> -4-OH- $\delta$	14	18 <sup>j</sup>	15 <sup>k</sup>	12	19	7.9
	4-OH- $\beta$	21	28 <sup>j</sup>	25 <sup>k</sup>	23	16	27

<sup>a</sup> Annual totals. Percentage values from the Reduced Caltech Isoprene Mechanism (RCIM) implemented in GEOS-Chem are compared to the standard GEOS-Chem v11-02c mechanism and to literature values. Regional domains are defined in the text; SE USA = Southeast United States. <sup>b</sup>Müller et al. (2018). <sup>c</sup>Taraborrelli et al. (2009). <sup>d</sup>Pfister et al. (2008). <sup>e</sup>Horowitz et al. (2007). <sup>f</sup>Ng et al. (2008). <sup>g</sup>Crounse et al. (2011). <sup>h</sup>Peeters et al. (2014). <sup>i</sup> Values represent the reacted fractions, which govern product formation. <sup>j</sup> Inferred from product distribution. <sup>k</sup>Paulot et al. (2009a).

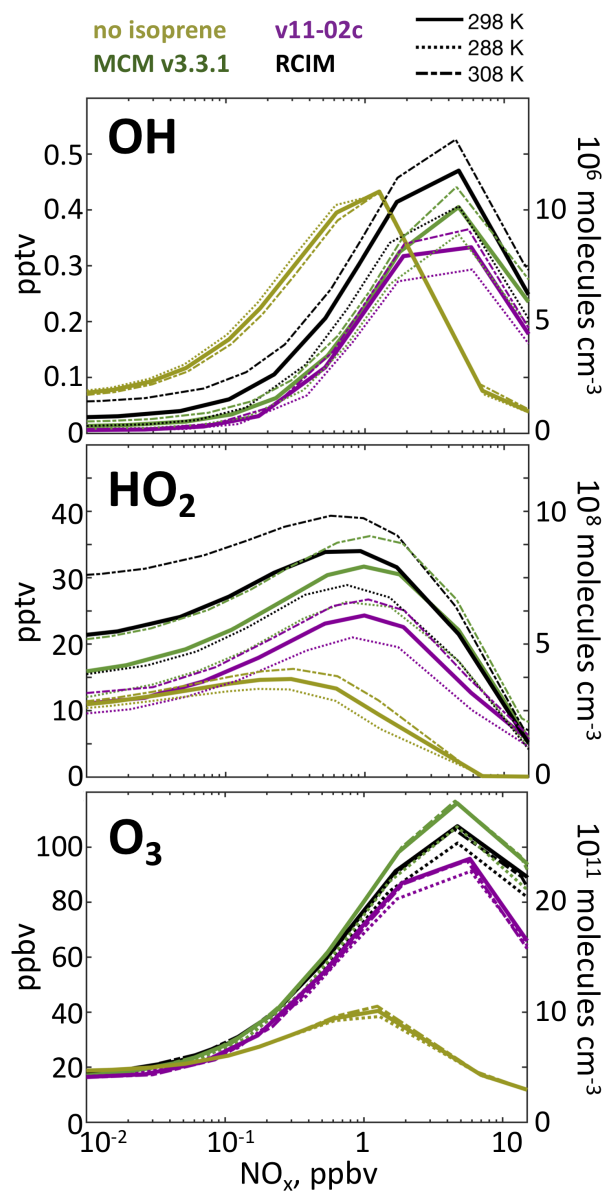


**Figure 5.** Effects of isoprene oxidation on OH, HO<sub>2</sub>, and ozone concentrations in a diurnal-steady-state box model for clear-sky equatorial conditions as a function of NO<sub>x</sub> and temperature. The RCIM, MCM, and GEOS-Chem v11-02c mechanisms are compared.

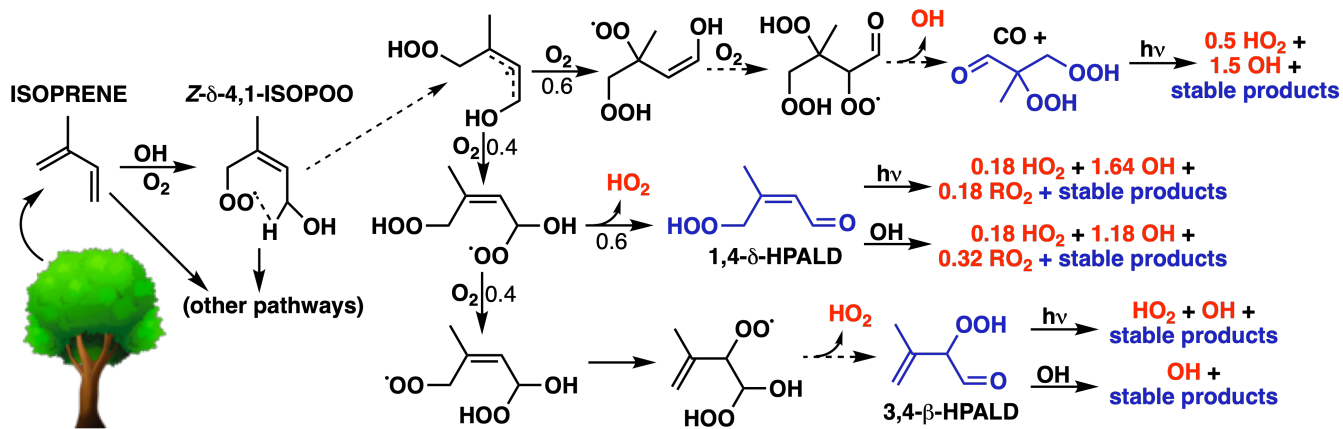


**Figure 6.** HO<sub>x</sub> production from H-shift chemistry in the Reduced Caltech Isoprene Mechanism (RCIM). The figure shows HO<sub>x</sub>-generating pathways following the 1,6-H-shift of Z- $\delta$ -1,4-ISOPOO. H-shift reactions are shown as dashed arrows, non-radical (closed-shell) products are shown in blue, and HO<sub>x</sub> production is shown in red. In RCIM, C<sub>4</sub>-dihydroperoxy-aldehydes (top-right) are assumed to photolyze rapidly, resulting in a first-generation HO<sub>x</sub> recycling yield of 2.2 (1.5 OH + 0.7 HO<sub>2</sub>) produced per ISOPOO H-shift.

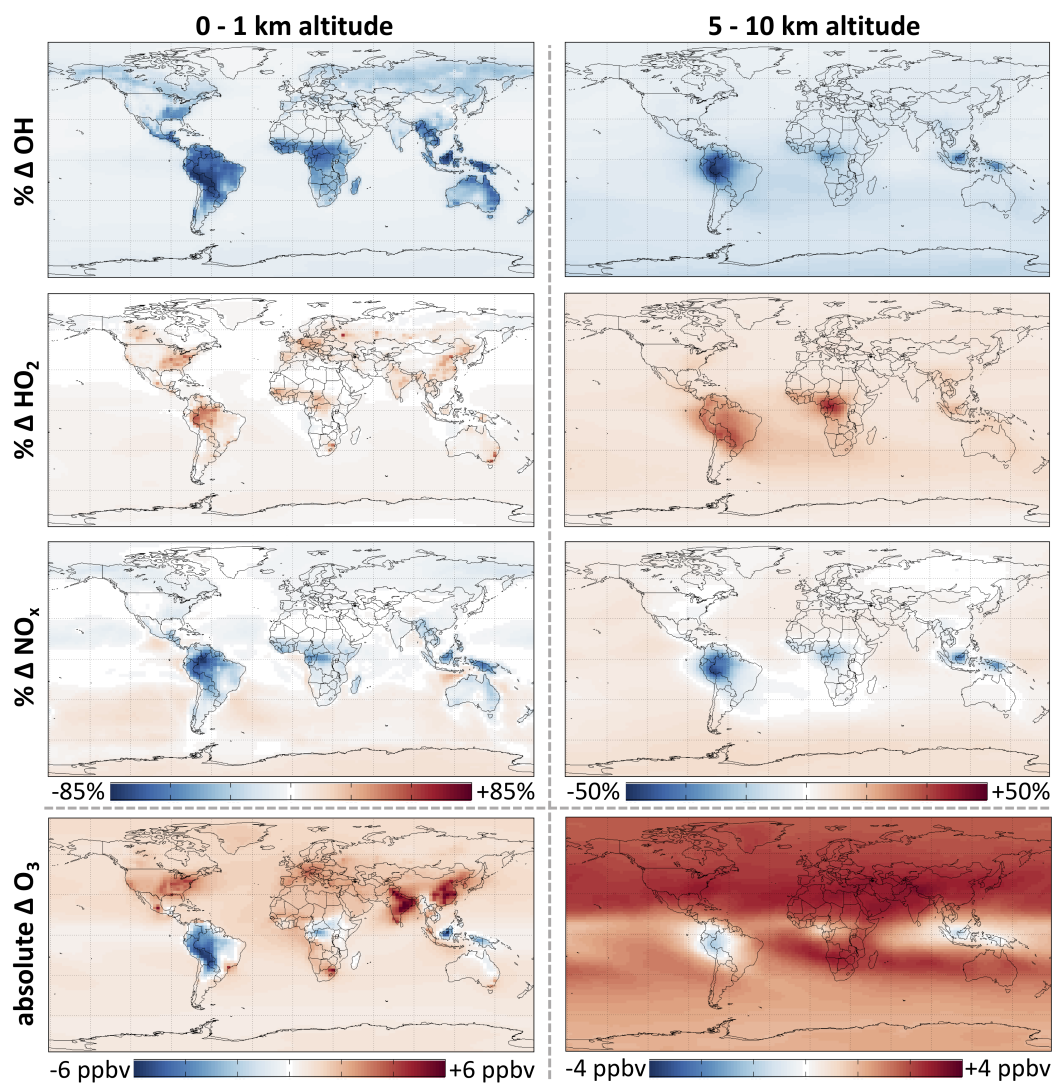


**Figure 7.** Effects of RCIM isoprene chemistry on OH, HO<sub>2</sub>, NO<sub>x</sub>, and ozone concentrations. The figure shows annual mean differences in GEOS-Chem simulations with versus without isoprene emissions.

**Table 2.** Percent changes in tropospheric concentrations due to isoprene.<sup>a</sup>

Species	Global	0-1 km, global	5-10 km, global	SE USA <sup>b</sup>	Amazon <sup>b</sup>	E China <sup>b</sup>
OH	-11	-15	-11	-49	-69	-14
HO <sub>2</sub>	6.5	4.0	8.4	28	31	17
NO <sub>x</sub>	-4.2	-4.9	-1.5	-9.7	-43	-3.6
O <sub>3</sub> <sup>c</sup>	4.2 (1.9)	3.6 (0.9)	4.1 (2.2)	7.2 (3.0)	-22 (-3.4)	9.1 (5.3)
CO	30	25	32	27	60	7.5
HCHO	22	38	1.9	180	340	33
PANs	25	16	29	65	3.8	68
Organonitrates <sup>d</sup>	39	90	18	240	86	22

<sup>a</sup> Annual mean differences between GEOS-Chem simulations with and without isoprene emissions. Isoprene chemistry uses RCIM.

<sup>b</sup> Regional results are for 0-1 km altitude; see Section 2.2 for precise geographic definitions; SE USA = Southeast United States.

<sup>c</sup> Numbers in parentheses are annual mean absolute changes in ppbv. <sup>d</sup> Not including PANs.

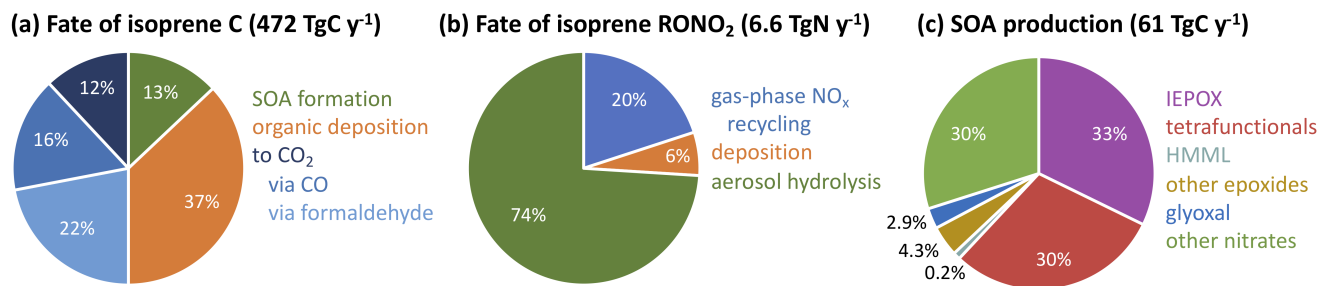


**Figure 8.** Accounting in the Reduced Caltech Isoprene Mechanism (RCIM) of (a) isoprene carbon, (b) the fate of isoprene-derived organonitrates (not including PANs), and (c) isoprene-derived SOA **production**. Values are global annual means from RCIM implemented in GEOS-Chem.

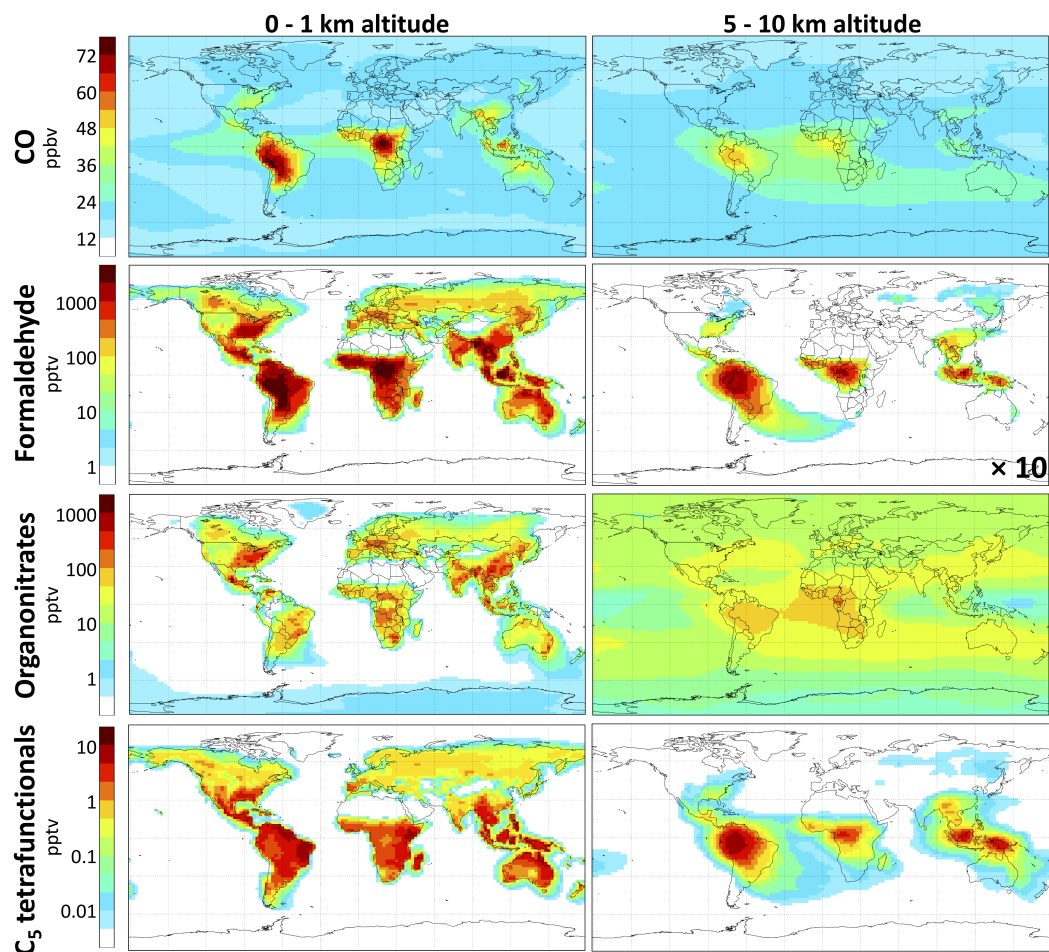


**Figure 9.** Contributions of isoprene to concentrations of CO, formaldehyde, organonitrates (including peroxyacyl nitrates), and C<sub>5</sub> tetrafunctional compounds using RCIM. Values are annual averages calculated as the differences between GEOS-Chem simulations with and without isoprene emissions. Color scale is linear for CO and logarithmic for other species.

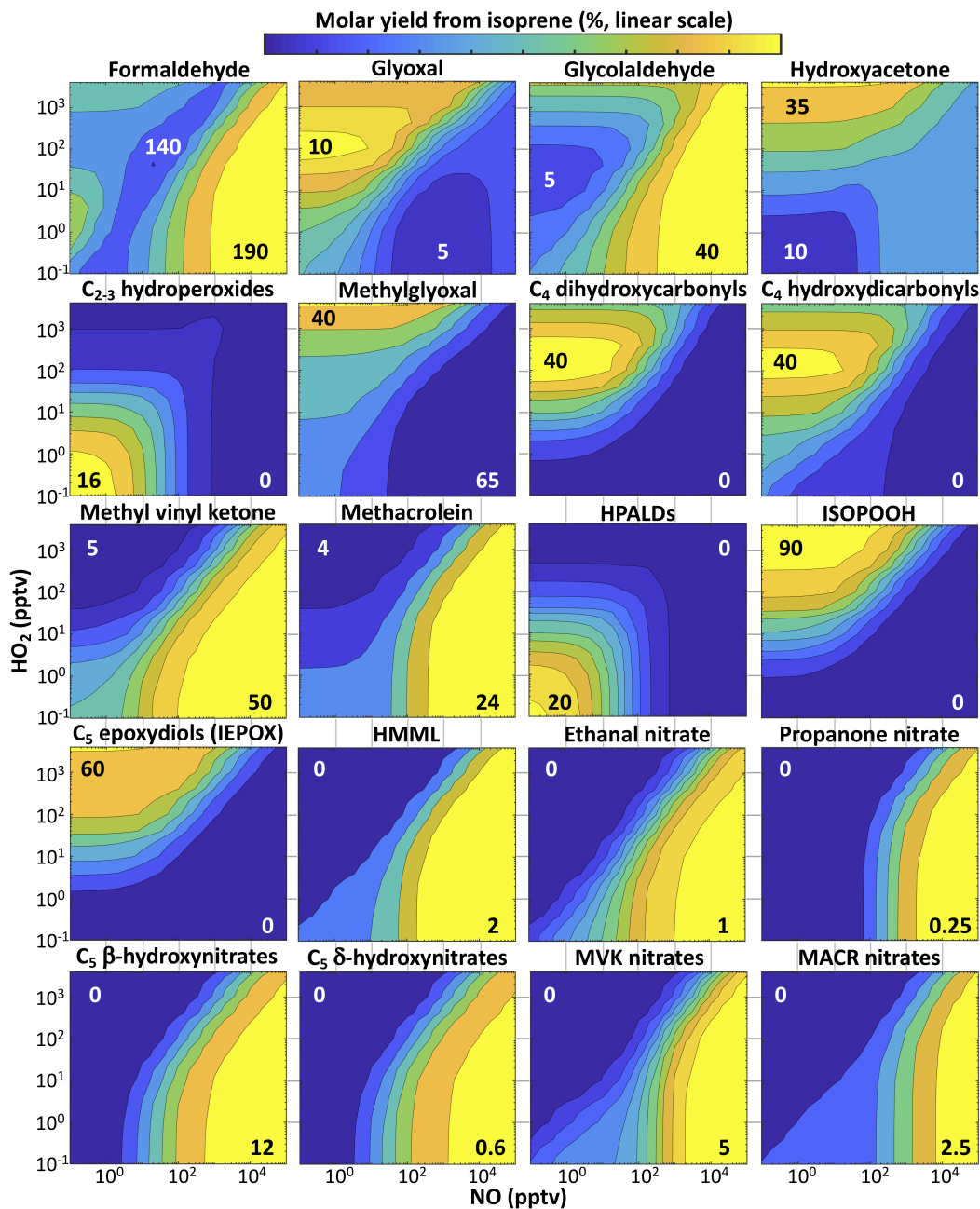


**Figure 10.** Percent yields of organic products from isoprene + OH oxidation as a function of NO and HO<sub>2</sub>. Results are from fixed-radical box model simulations with RCIM, run at 25 °C for clear-sky equatorial radiation at solar noon and an ozone column of 350 DU. The fixed-radical box model does not account for deposition or aerosol uptake. Contours are evenly spaced on a linear scale between the **minimum values (in white)** and **maximum values (in black)** located on each plot. HPALDs ≡ C<sub>5</sub> hydroperoxy-aldehydes; ISOPOOH ≡ C<sub>5</sub> hydroxy-hydroperoxides; HMML ≡ hydroxymethyl-methyl- $\alpha$ -lactone; MVK ≡ methyl vinyl ketone; MACR ≡ methacrolein.

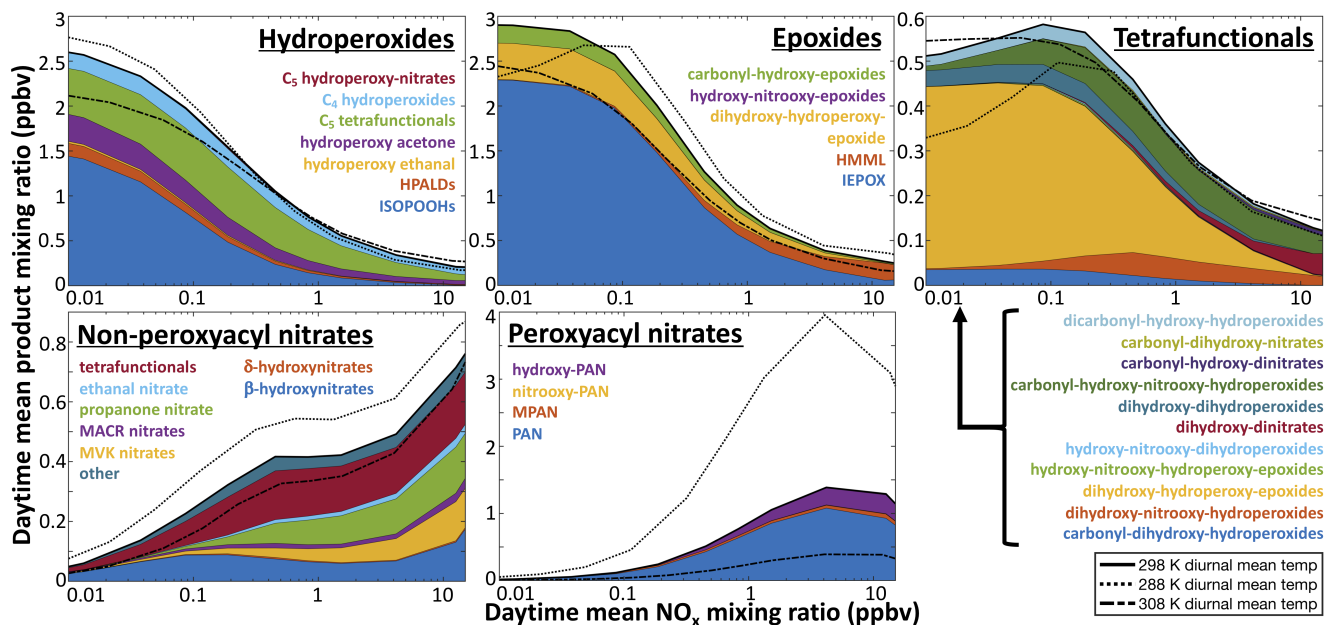


**Figure 11.** Daytime average concentrations of isoprene oxidation products as a function of  $\text{NO}_x$ . Results are from diurnal-steady-state box model simulations for equatorial conditions using RCIM. Y axis scales vary between panels.

# Supplement to “A new model mechanism for atmospheric oxidation of isoprene: global effects on oxidants, nitrogen oxides, organic products, and secondary organic aerosol”

Kelvin H. Bates\*<sup>1</sup> and Daniel J. Jacob<sup>2</sup>

<sup>1</sup>Faculty of Arts and Sciences, Harvard University, Cambridge, MA 02138, USA

<sup>2</sup>School of Engineering and Applied Sciences, Harvard University, Cambridge, MA 02138, USA

June 21, 2019

\*for correspondence: kelvin\_bates@fas.harvard.edu

## Contents

<b>S1 Additional details from global simulations</b>	<b>S2</b>
<b>S2 Light &amp; temperature sensitivities in fixed-radical box models</b>	<b>S6</b>
<b>S3 Emission sensitivities in global models</b>	<b>S11</b>
<b>S4 Isoprene oxidation at night</b>	<b>S12</b>
<b>S5 Comparisons to other mechanisms</b>	<b>S15</b>
S5.1 Isoprene reaction pathways . . . . .	S16
S5.2 HO <sub>x</sub> , NO <sub>x</sub> , and ozone . . . . .	S16
S5.3 Organic products . . . . .	S22
<b>S6 Mechanism simplification</b>	<b>S29</b>

## S1 Additional details from global simulations

Tables S1-S3 provide additional details from global simulations of RCIM. Tables S1-S2 show the percent changes in global annual average tropospheric burdens of compounds of interest between a standard global simulation and a perturbed simulation. Perturbations include removing isoprene chemistry altogether, using the GEOS-Chem v11-02c mechanism, and using the RCIM with different ISOPOO isomer branchings. Table S1 also shows changes due to the removal of specific isoprene and ISOPOO reaction pathways (e.g. isoprene + O<sub>3</sub> or ISOPOO + RO<sub>2</sub>), which gives a sense of the specific contributions of these pathways to the overall tropospheric effects of isoprene oxidation. Table S2 shows similar perturbations but with specific oxidation products (e.g. MVK, IEPOX) removed, which gives a sense of those products' contributions to isoprene's tropospheric effects, as well as perturbations to isoprene nitrate chemistry. Table S3 provides global annual average molar yields of VOCs from isoprene, using both RCIM and GEOS-Chem v11-02c, as well regional molar yields in the Southeast United States, the Amazon, and East China using RCIM.

Table S1: Percent changes in annual average tropospheric mixing ratios due to specific perturbations to the isoprene oxidation mechanism.

Species	No isoprene	Fixed		Single ISOPOO species <sup>b</sup>	No isoprene + O <sub>3</sub>		No isoprene + NO <sub>3</sub>		No ISOPOO + NO <sup>c</sup>		No ISOPOO + HO <sub>2</sub>		No ISOPOO H-shifts <sup>c</sup>		No ISOPOO + RO <sub>2</sub>	
		ISOPOO distrib. <sup>a</sup>	ISOPOO		isoprene + O <sub>3</sub>	isoprene + NO <sub>3</sub>	ISOPOO + NO <sup>c</sup>	ISOPOO + HO <sub>2</sub>	ISOPOO H-shifts <sup>c</sup>	ISOPOO + RO <sub>2</sub>						
OH	12.9	1.27	0.03	0.03	1.15	-0.17	6.64	3.36	-1.23	0.59						
HO <sub>2</sub>	-6.15	0.60	-0.20	-1.12	-0.26	-2.85	0.17	-1.81	-0.96							
NO	6.23	0.72	0.07	0.36	0.00	6.25	1.03	-1.28	0.23							
NO <sub>2</sub>	3.04	0.49	0.28	0.00	-0.38	5.74	0.45	-0.43	-0.02							
NO <sub>3</sub>	10.4	2.30	-0.41	-0.13	3.47	5.11	7.15	-5.46	-0.54							
O <sub>3</sub>	-3.37	0.50	0.04	-0.22	-0.40	-0.30	-0.40	-1.28	-0.42							
CO	-24.1	-0.23	-0.55	-3.05	-0.40	-10.8	-6.00	-2.33	-1.99							
Formaldehyde	-17.4	-0.05	-1.26	-4.37	-0.94	-7.59	-3.10	-2.50	-2.68							
Formic acid	-94.2	-6.01	1.20	-48.4	-4.16	-32.6	-13.3	19.2	-4.40							
Acetic acid	-58.6	4.51	-3.05	-4.28	-1.32	-25.4	-9.51	-12.5	-5.41							
Glycolaldehyde	-97.6	-17.0	-14.8	-5.82	-3.80	-62.6	-24.8	-0.33	-11.9							
Glyoxal	-43.1	44.1	-17.6	-1.27	-1.07	-14.0	-4.78	-17.2	-1.74							
Hydroxyacetone	-89.9	-2.10	20.8	-16.8	-1.55	-42.1	-30.8	-1.11	-11.24							
Methylglyoxal	-87.3	5.30	-5.78	-5.78	-2.37	-32.1	-15.8	-37.9	-6.12							
Methyl vinyl ketone	-100	-24.3	-17.3	-11.3	-2.50	-63.3	-29.2	10.5	-21.2							
Methacrolein	-99.3	-3.22	23.4	-35.0	-1.39	-45.3	-20.5	32.8	-20.0							
PANs <sup>d</sup>	-18.7	-0.74	-0.42	-1.76	-1.74	-10.28	-5.96	-0.82	-2.20							
C <sub>2+</sub> nitrates <sup>d, e</sup>	-97.4	-1.91	22.5	-9.96	-38.6	-24.3	-1.24	9.91	-4.32							
C <sub>2+</sub> hydroperoxides <sup>d</sup>	-100	-13.8	4.68	-4.27	-1.08	-38.4	-82.0	-8.67	-9.21							
Epoxides <sup>d</sup>	-99.5	-7.16	1.99	-4.98	-0.65	-32.9	-89.4	-8.3	-5.0							
Tetrafunctionals <sup>d</sup>	-100	-2.39	10.4	-1.71	-4.3	-21.3	-82.7	15.9	-0.45							
CH <sub>4</sub> lifetime	-13.6	-1.58	0.06	-1.12	0.27	-6.47	-3.42	1.57	-0.53							

All listed changes are relative to a simulation employing RCIM, from 4° × 5° horizontal resolution global simulations. <sup>a</sup>from Paulot et al. (2009); <sup>b</sup>as in GEOS-Chem v10-01 (Mao et al., 2013); <sup>c</sup>in these comparisons, the reaction in question remains in the mechanism with its standard rate, but forms no products and does not consume the co-reactant; <sup>d</sup>percent differences in lumped classes of compounds are calculated by mole, not mass; <sup>e</sup>includes only non-PAN organonitrates.

Table S2: Percent changes in annual average tropospheric mixing ratios due to specific perturbations to the isoprene oxidation mechanism.

Species	No isoprene	No MVK <sup>a</sup>	No MCAR <sup>a</sup>	No IEPOX <sup>a</sup>	No isoprene hydroxy-nitrates <sup>a</sup>	Full nitrate removal <sup>b</sup>	Slow nitrate hydrolysis <sup>c</sup>
OH	12.9	1.35	0.86	1.46	-0.48	-15.7	0.99
HO <sub>2</sub>	-6.15	-2.41	-1.20	-0.09	0.13	-4.27	0.32
NO	6.23	1.73	0.61	0.58	-0.47	-9.24	0.70
NO <sub>2</sub>	3.04	0.28	-0.03	0.26	-0.41	-10.5	0.78
NO <sub>3</sub>	10.4	-3.64	-1.63	4.72	0.74	-22.3	2.21
O <sub>3</sub>	-3.37	-1.88	-1.01	-0.18	-0.43	-12.2	0.82
CO	-24.1	-5.11	-3.03	-2.58	0.18	9.63	-0.49
Formaldehyde	-17.4	-5.58	-2.23	-0.46	-0.48	-14.0	0.71
Formic acid	-94.2	-33.6	-10.3	-3.42	-1.47	-25.9	2.48
Acetic acid	-58.6	-19.5	-10.1	-4.23	0.26	-5.25	0.58
Glycolaldehyde	-97.6	-87.4	0.43	-3.18	-1.74	-39.0	3.45
Glyoxal	-43.1	-18.3	0.53	-0.72	1.46	-1.06	1.07
Hydroxyacetone	-89.9	-6.52	-54.5	-15.5	0.38	10.3	1.19
Methylglyoxal	-87.3	-28.4	-12.8	-6.55	-0.48	-16.9	1.44
Methyl vinyl ketone	-100	-2.24	-1.65	-3.40	-0.22	2.67	-1.36
Methacrolein	-99.3	-4.24	-3.35	-4.04	-0.14	27.1	-1.71
PANs <sup>d</sup>	-18.7	-15.0	-5.35	-2.53	-1.00	-25.0	1.87
C <sub>2</sub> + nitrates <sup>d, e</sup>	-97.4	-8.02	-41.7	2.23	-6.75	-53.7	32.1
C <sub>2</sub> + hydroperoxides <sup>d</sup>	-100	-7.96	-2.61	-0.49	1.41	51.5	-1.88
Epoxides <sup>d</sup>	-99.5	-5.07	-10.4	3.89	2.08	24.4	-0.25
Tetrafunctionals <sup>d</sup>	-100	-2.81	-1.40	18.5	-3.22	21.6	16.9
CH <sub>4</sub> lifetime	-13.6	-1.22	-0.80	-1.50	0.51	20.5	-1.04

All listed changes are relative to a simulation employing RCM, from 4° × 5° horizontal resolution global simulations. <sup>a</sup>in these comparisons, the species in question is still produced in the isoprene oxidation mechanism, but is not allowed to react; <sup>b</sup>this simulation assumes the limiting case that all ISOPROO + NO reactions lead to the formation of non-NO<sub>x</sub> recycling nitrates; <sup>c</sup>referring only to the 1-OH,2-ONO<sub>2</sub> isoprene hydroxynitrate, the heterogeneous hydrolysis rate of which is reduced by an order of magnitude for this comparison; <sup>d</sup>percent differences in lumped classes of compounds are calculated by mole, not mass; <sup>e</sup>includes only non-PAN organonitrates.

Table S3: Molar yields of VOCs and SOA precursors of interest from isoprene<sup>a</sup>

Species	Molar yield from isoprene, %, RCIM (GEOS-Chem v11-02c)			
	Global	SE USA	Amazon	E China
CO	190 (180)	150 (121)	138 (101)	213 (197)
Formaldehyde	111 (107)	97.7 (77.0)	79.4 (44.3)	148 (141)
Formic acid	5.76 (6.33)	5.28 (4.53)	4.12 (4.05)	7.59 (7.05)
Acetic acid	5.49 (4.18)	2.93 (2.04)	3.34 (2.59)	4.59 (3.11)
Hydroxymethyl hydroperoxide	3.94 (-)	4.55 (-)	4.71 (-)	2.53 (-)
Glycolaldehyde	11.5 (16.2)	11.1 (13.41)	5.00 (12.1)	23.7 (20.1)
Glyoxal	1.63 (5.47)	1.06 (3.85)	1.08 (2.17)	2.06 (6.51)
Hydroxyacetone	12.3 (11.1)	10.6 (10.0)	7.72 (5.00)	15.2 (17.2)
Methylglyoxal	20.1 (24.5)	16.1 (18.2)	13.4 (15.3)	25.3 (29.3)
Methyl vinyl ketone	27.9 (21.5)	31.1 (25.7)	22.0 (15.5)	42.2 (35.8)
Methacrolein	15.9 (17.3)	17.9 (20.6)	15.1 (14.2)	21.3 (26.5)
C <sub>4</sub> dihydroxycarbonyls	6.32 (3.67)	4.99 (2.31)	3.59 (1.86)	4.58 (2.85)
C <sub>4</sub> hydroxydicarbonyls	10.6 (-)	7.60 (-)	6.49 (-)	8.43 (-)
C <sub>2+</sub> nitrates <sup>c,d</sup>	5.99 (6.96)	9.08 (9.95)	1.30 (1.09)	15.1 (19.1)
C <sub>5</sub> nitrates <sup>c</sup>	4.82 (4.79)	7.55 (7.16)	1.02 (0.848)	11.8 (11.9)
C <sub>5</sub> hydroxynitrates	3.60 (2.61)	5.31 (3.82)	0.782 (0.488)	9.25 (6.68)
C <sub>4</sub> nitrates <sup>c</sup>	0.878 (1.70)	1.10 (2.03)	0.234 (0.185)	2.42 (5.85)
Propanone nitrate	0.188 (0.412)	0.304 (0.675)	0.0277 (0.0483)	0.627 (1.20)
C <sub>2+</sub> hydroperoxides <sup>c</sup>	52.3 (42.6)	43.9 (33.1)	58.7 (47.2)	24.9 (18.1)
ISOPOOH	35.3 (33.8)	29.7 (29.7)	41.2 (37.1)	14.0 (13.8)
C <sub>5</sub> hydroperoxy aldehydes	6.77 (5.80)	4.93 (3.56)	8.49 (7.89)	3.42 (2.08)
Epoxides <sup>c</sup>	25.7 (25.8)	23.3 (21.4)	20.9 (18.1)	15.3 (20.9)
IEPOX	20.1 (19.9)	18.3 (16.8)	17.1 (15.7)	9.84 (10.5)
HMML	0.732 (5.85)	0.937 (4.62)	0.154 (2.40)	2.42 (10.3)
Tetrafunctionals <sup>c</sup>	4.07 (4.11)	3.73 (3.32)	3.26 (3.80)	2.63 (3.62)
IDHPE <sup>e</sup>	2.20 (-)	1.86 (-)	2.12 (-)	0.847 (-)
IDHDP <sup>f</sup>	0.530 (0.0992)	0.438 (0.0808)	0.486 (0.0830)	0.159 (0.0480)
ICPDH <sup>g</sup>	0.458 (0.584)	0.346 (0.341)	0.380 (0.719)	0.185 (0.149)
IDCHP <sup>h</sup>	0.384 (-)	0.349 (-)	0.190 (-)	0.359 (-)
ICHNP <sup>i</sup>	0.232 (-)	0.319 (-)	0.0353 (-)	0.479 (-)
IDHPN <sup>j</sup>	0.218 (0.466)	0.348 (0.538)	0.0386 (0.0890)	0.411 (0.596)

<sup>a</sup>Results from 2° × 2.5° horizontal resolution global simulations using RCIM. Yields of species with additional non-isoprene precursors are calculated by taking the difference in production between a simulation with isoprene and one without isoprene emissions. Yields of CO and formaldehyde calculated with this method are then corrected for differences in total methane oxidation between the simulations. <sup>b</sup>Using the GEOS-Chem v11-02c mechanism instead of RCIM. <sup>c</sup>Yields of lumped species may include multiple generations of a single oxidation pathway (e.g., separately counting both IEPOX and its oxidation product, isoprene hydroxycarbonyl epoxides). <sup>d</sup>Includes only non-PAN organonitrates. <sup>e</sup>C<sub>5</sub> dihydroxy-hydroperoxy-epoxides. <sup>f</sup>C<sub>5</sub> dihydroxy-dihydroperoxides. <sup>g</sup>C<sub>5</sub> dihydroxy-carbonyl-hydroperoxides. <sup>h</sup>C<sub>5</sub> dicarbonyl-hydroxy-hydroperoxides. <sup>i</sup>C<sub>5</sub> carbonyl-hydroxy-hydroperoxy-nitrates. <sup>j</sup>C<sub>5</sub> dihydroxy-hydroperoxy-nitrates.

## S2 Light & temperature sensitivities in fixed-radical box models

Figures S1-S5 show the effects of varying light and temperature on  $\text{HO}_x$ , ozone, oxidation pathways, and VOC yields in fixed-radical box models. In addition to the simulations described in the main text, the model was run with every permutation of (a) temperature set to 283.15 K, 298.15 K, and 313.15 K, and (b) solar radiation for photolysis set to clear-sky equatorial midday with an ozone column of 350 DU,  $0.1 \times$  equatorial midday, and 0. The primary effect of temperature is to increase the rates of H-shift reactions, which substantially increases their relative contribution to the fate of the ISOPOO radicals (Figure S1). This leads to an increase in overall net  $\text{HO}_x$  recycling from isoprene oxidation (Figure S2). Increased photolysis rates from higher photon fluxes also lead to increased net  $\text{HO}_x$  recycling (Figure S2) and net potential ozone production (Figure S3) from isoprene oxidation.

The effects of temperature on VOC yields (Figure S4) are largely mediated by the temperature dependence of H-shift reactions (Peeters and Nguyen, 2012; Peeters et al., 2014; Crounse et al., 2011; Praske et al., 2018) and of nitrate formation branching ratios in reactions of peroxy radicals with NO (Arey et al., 2001; Carter and Atkinson, 1985, 1989). Thus, overall yields from isoprene of ISOPOO H-shift products (e.g.  $\text{C}_2$ - $\text{C}_5$  hydroperoxyaldehydes) increase with temperature, while those of organonitrates decrease. The effects of light on VOC yields (Figure S5) are generally smaller than those of temperature, but among the most pronounced are a decrease in formaldehyde yields and an increase in methylglyoxal yields under low-light conditions.

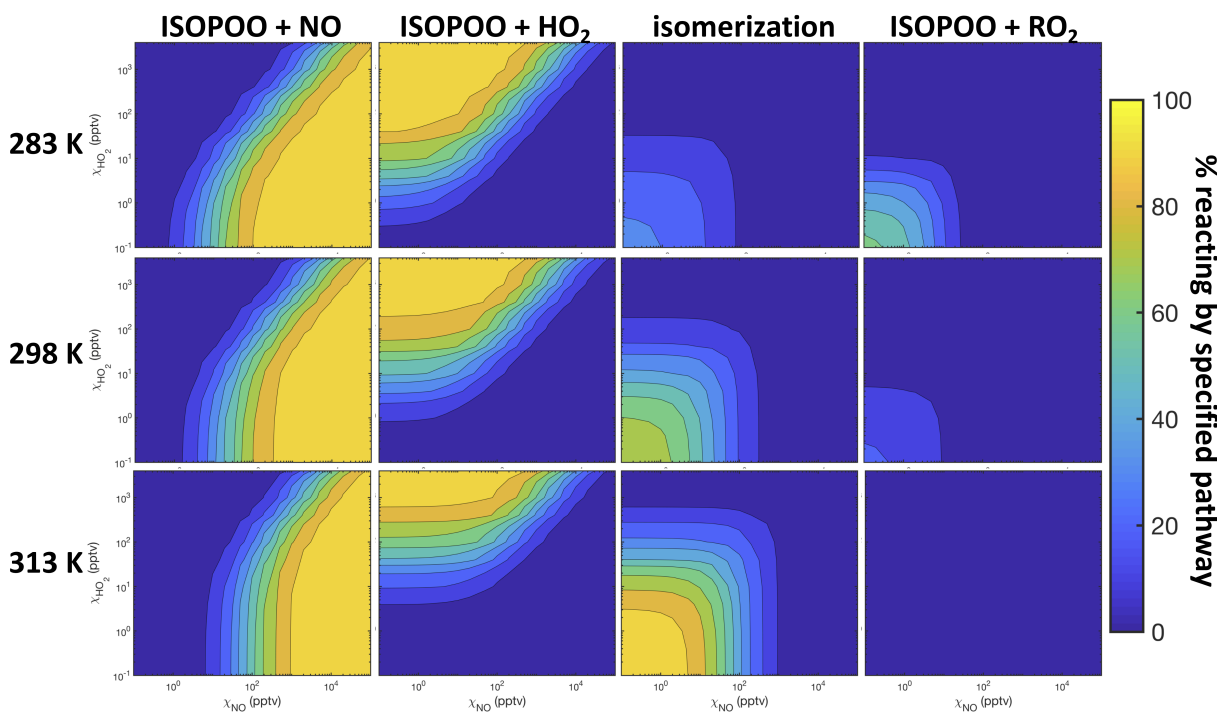


Figure S1: Temperature dependence of the percent of isoprene hydroxy peroxy radicals reacting via each pathway as a function of NO and  $\text{HO}_2$ , from fixed-radical box modeling of RCIM.

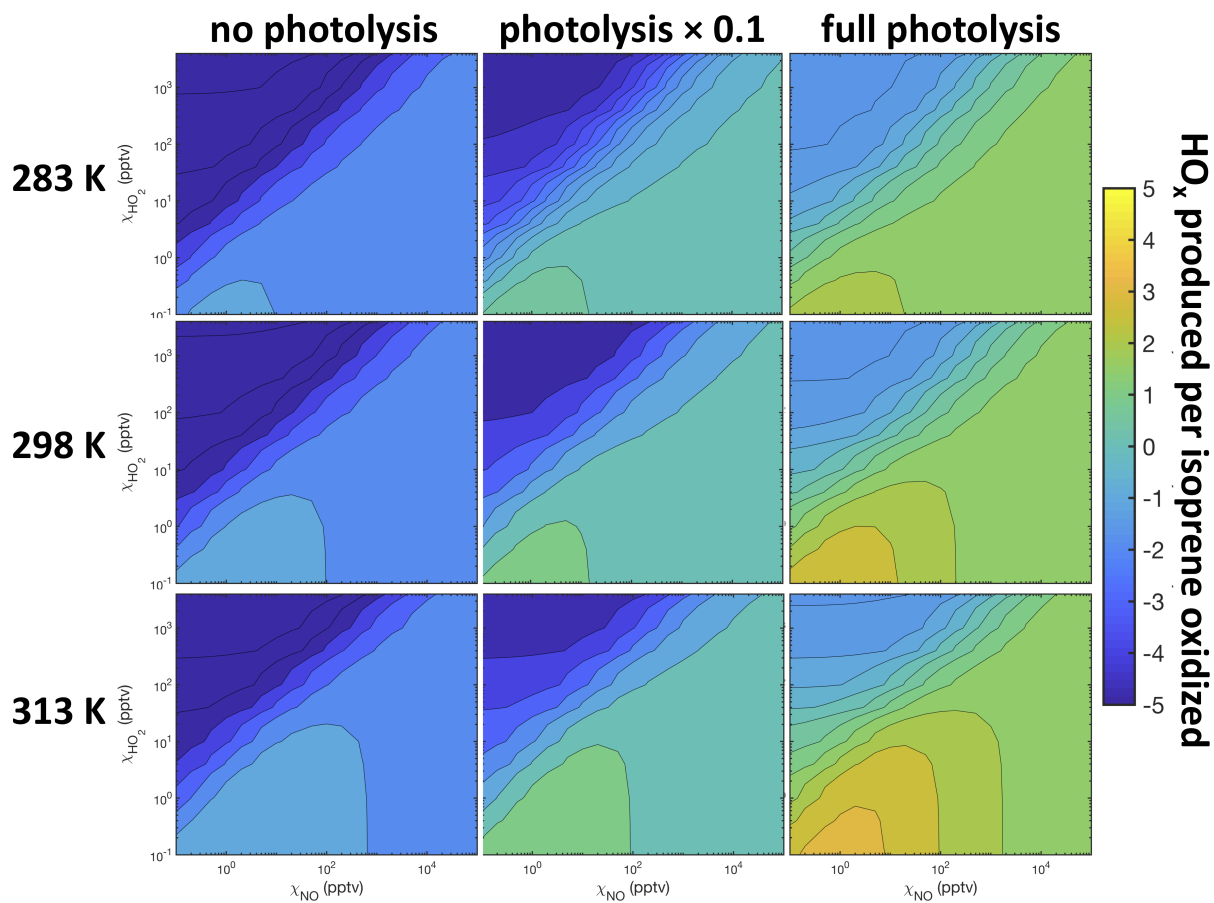


Figure S2: Net effects of isoprene oxidation on  $\text{HO}_x$  under various temperature and light conditions as a function of  $\text{NO}$  and  $\text{HO}_2$ , from fixed-radical box modeling of RCIM.

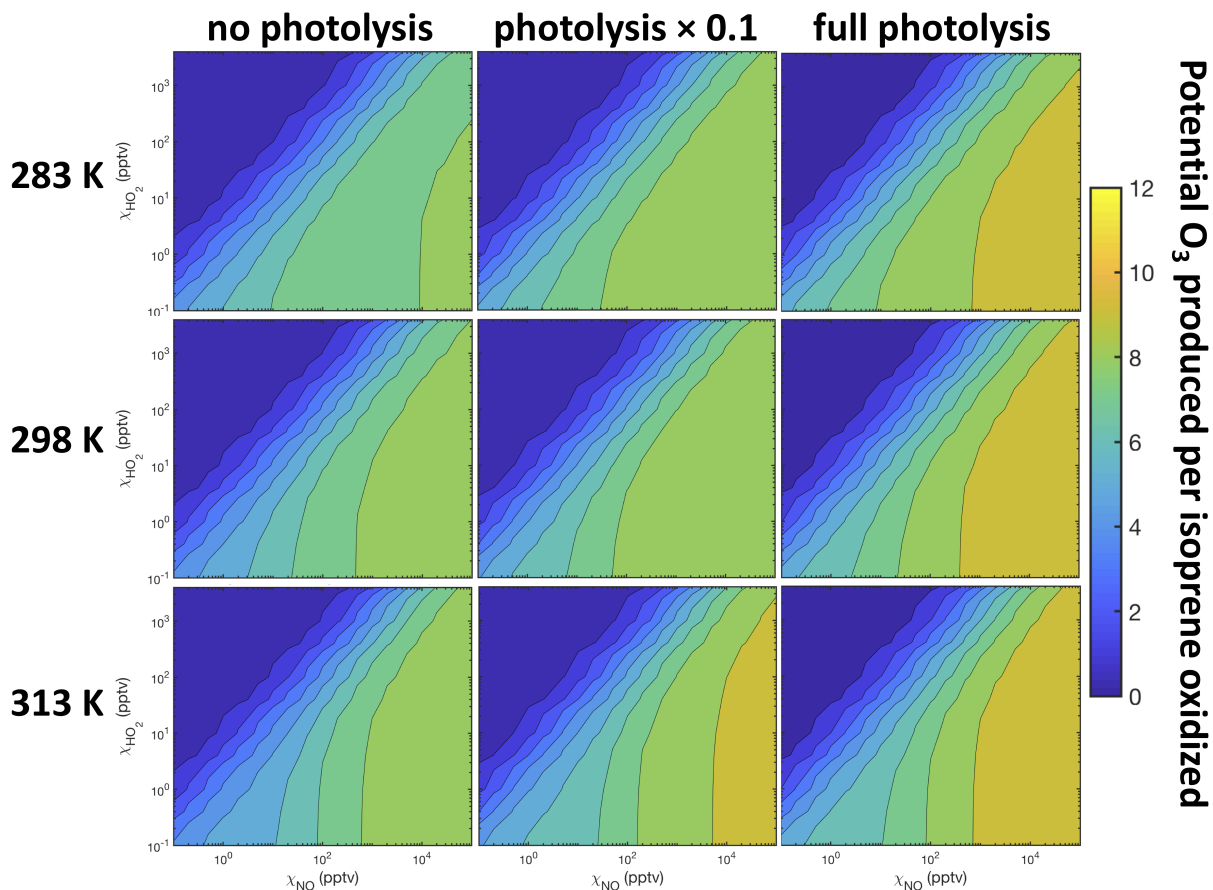


Figure S3: Net effects of isoprene oxidation on potential O<sub>3</sub> – estimated as the sum of the ozone, NO<sub>2</sub>, and HO<sub>2</sub> (times the fraction of HO<sub>2</sub> that would go on to react with NO) produced over the course of its oxidation – under various temperature and light conditions as a function of NO and HO<sub>2</sub>, from fixed-radical box modeling of RCIM.

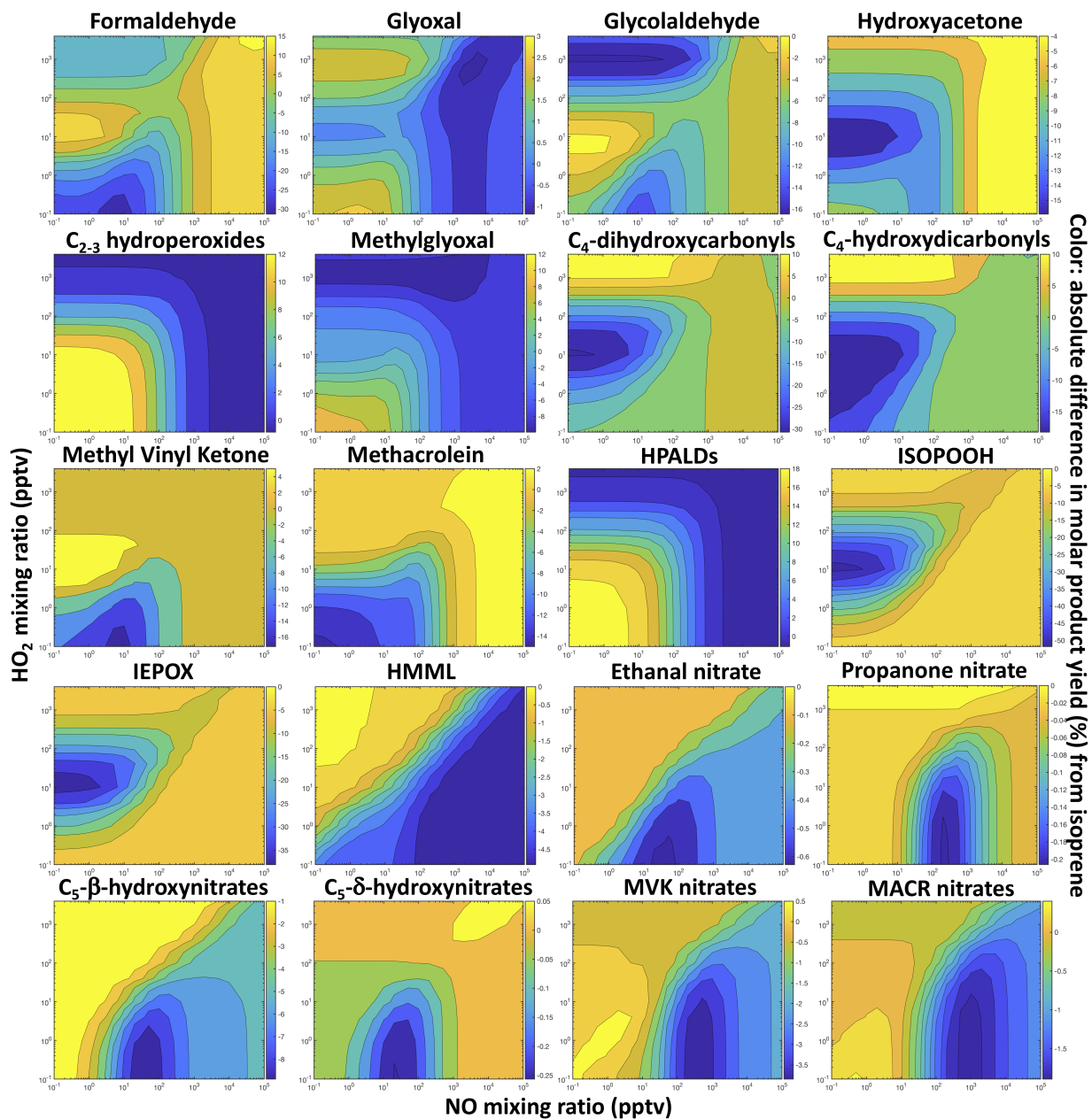


Figure S4: Absolute changes in percent yields of compounds of interest from isoprene when switching from fixed-radical box models run at 10 °C to simulations run at 40 °C. All box models are run with full photolytic sunlight flux (equatorial midday) and using RCIM.

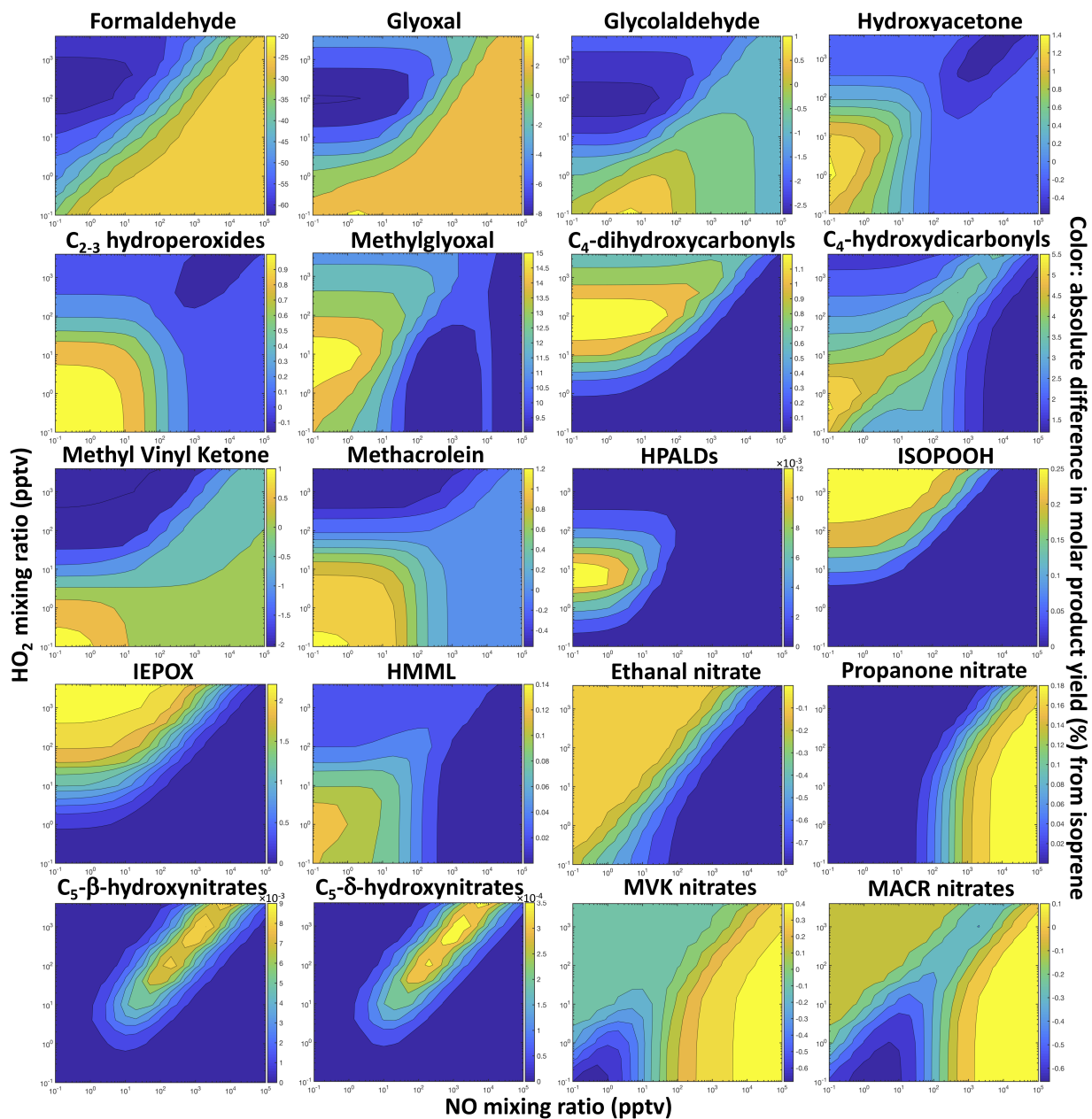


Figure S5: Absolute changes in percent yields of compounds of interest from isoprene when switching from fixed-radical box models with full photolytic sunlight flux (equatorial midday) to simulations with no photolytic light flux. All box models are run at 25 °C and using RCIM.

### S3 Emission sensitivities in global models

Sensitivity simulations were performed with 10% increases and decreases to both isoprene and  $\text{NO}_x$  emissions worldwide, to examine the effects of these perturbations on the results reported herein. Changes in isoprene oxidation pathways due to emission changes can be found in Table S4, while changes in tropospheric average mixing ratios of species of interest can be found in Table S5. The contributions of isoprene oxidation pathways – including the initial oxidants, the ISOPOO fate, and the ISOPOO isomer reactivity – are largely insensitive to 10% perturbations in either  $\text{NO}_x$  or isoprene emissions, with the largest relative changes in the fraction of isoprene reacting with  $\text{NO}_3$ .

Table S4: Global contributions of isoprene oxidation pathways with changed isoprene and  $\text{NO}_x$  emissions.<sup>a</sup>

Pathway		isoprene +10%	isoprene -10%	$\text{NO}_x$ +10%	$\text{NO}_x$ -10%	no anthro- pogenic $\text{NO}_x$	no anthrop. or BB $\text{NO}_x$
isop +	OH	87	88	88	88	89	90
	$\text{O}_3$	11	10	10	10	10	10
	$\text{NO}_3$	1.7	1.8	1.8	1.7	0.9	0.5
$\text{RO}_2^b$ +	$\text{HO}_2$	42	41	41	41	45	47
	NO	27	29	29	27	18	13
	$\text{RO}_2$	8.8	8.2	8.5	8.6	11	13
	H-shift	22	22	22	23	26	28
isomer	<i>E/Z</i> -1-OH- $\delta$	6.5	6.5	6.4	6.5	7.5	8.0
	1-OH- $\beta$	59	59	59	59	58	58
	<i>E/Z</i> -4-OH- $\delta$	14	14	14	14	16	16
	4-OH- $\beta$	21	21	21	21	19	18

<sup>a</sup>Reported percentages are global tropospheric annual averages, from  $4^\circ \times 5^\circ$  horizontal resolution GEOS-Chem simulations using RCIM; numbers may not add to 100% due to rounding; <sup>b</sup>Referring only to the  $\text{RO}_2$  radicals formed in the reaction of isoprene with OH and  $\text{O}_2$ .

Table S5: Changes in tropospheric burdens due to perturbations to isoprene and NO<sub>x</sub> emissions (%)<sup>a</sup>

Species	isoprene +10%	isoprene -10%	NO <sub>x</sub> +10% <sup>b</sup>	NO <sub>x</sub> -10% <sup>b</sup>	no anthro- pogenic NO <sub>x</sub> <sup>b</sup>	no anthrop. or BB NO <sub>x</sub> <sup>b</sup>
OH	-0.42	0.82	1.6 (1.0)	-1.3 (-1.8)	-4.5 (-4.0)	-0.12 (0.86)
HO <sub>2</sub>	0.32	-0.40	0.18 (0.50)	-0.27 (0.06)	-10 (-9.3)	-15 (-14)
NO	-0.27	0.41	2.8 (3.2)	-2.5 (-2.2)	-17 (-17)	-20 (-20)
NO <sub>2</sub>	-0.21	0.13	5.1 (5.4)	-5.0 (-4.8)	-44 (-44)	-50 (-50)
NO <sub>3</sub>	-0.42	0.38	3.8 (3.9)	-3.9 (-3.9)	-34 (-31)	-39 (-31)
O <sub>3</sub>	0.21	-0.17	1.0 (0.63)	-1.0 (-1.3)	-16 (-15)	-20 (-19)
CO	1.2	-1.6	-1.1 (0.60)	0.84 (2.3)	-28 (-26)	-47 (-43)
Formaldehyde	1.0	-1.2	0.86 (0.68)	-1.1 (-1.2)	-14 (-13)	-15 (-13)
PANs <sup>c</sup>	1.0	-2.5	1.5 (2.0)	-3.0 (-1.9)	-54 (-53)	-62 (-61)
C <sub>2+</sub> nitrates <sup>c</sup>	0.81	-2.4	1.4 (1.8)	-3.1 (-2.0)	-67 (-59)	-75 (-64)
Epoxides <sup>c</sup>	11	-11	-0.86	1.6	-22	-33
Tetrafunctionals <sup>c</sup>	4.4	-12	-5.0	-2.7	29	53
Isoprene SOA	15	-8	2.9	3.9	48	74
CH <sub>4</sub> lifetime	0.82	-0.59	-1.5 (-1.1)	1.9 (1.9)	9.8 (7.8)	6.3 (4.22)

<sup>a</sup>Percent differences are annual averages from 4° × 5° horizontal resolution GEOS-Chem simulations using RCIM; <sup>b</sup>for simulations with changed NO<sub>x</sub> emissions, numbers in parentheses are the percent change that results from the same change in NO<sub>x</sub> emissions between two simulations with no isoprene emissions; <sup>c</sup>percent differences in lumped classes of compounds are calculated by mole, not mass.

## S4 Isoprene oxidation at night

Figures S6-S10 show the results of diurnal-steady-state and fixed-radical simulations of nighttime isoprene chemistry, which was also updated substantially in Wennberg et al. (2018) following the recommendations of Schwantes et al. (2015). For diurnal-steady-state simulations, figures S6 and S7 show average mixing ratios of isoprene oxidation products over the period 20:00-04:00 on the seventh simulated night; in general, due to the persistence of isoprene + OH oxidation products, these exhibit on minimal differences from daytime averages. Notably, the diurnal-steady-state simulations do not include nighttime changes to the mixed layer height or depositional and aerosol-phase losses, which may cause substantial biases.

In fixed-radical simulations, a series of simulations investigating NO<sub>3</sub>-initiated isoprene oxidation were performed alongside those investigating OH-initiated oxidation. They were run similarly to those described in Section 2.2 of the main text, but instead of initializing with 1 ppbv isoprene, they were initialized with 1 total ppbv of isoprene + NO<sub>3</sub> + O<sub>2</sub> peroxy radicals, distributed across the peroxy radical isomers as in Wennberg et al. (2018). RCIM does not include many reactions of NO<sub>3</sub> with stable isoprene oxidation products, because the rates and products of these reactions are poorly constrained. Instead, the mechanism emphasizes reactions of first-generation isoprene + NO<sub>3</sub> products with OH, which are expected to occur in the morning. The fixed-radical simulations were there run with 0.1 pptv OH and 10% of Equatorial midday light flux to target these morning conditions.

Figure S8 shows the yields of major products of isoprene + NO<sub>3</sub> oxidation as simulated in fixed-radical box models with RCIM, including functionalized nitrates and the epoxides produced in their reactions with OH (Jacobs et al., 2014; Schwantes et al., 2015). Figure S9 compares these yields to those of fixed-radical simulations using the MCM v3.3.1 isoprene oxidation mechanism, which exhibits much higher formation of carbonyl nitrates and much lower production of C<sub>4</sub> nitrates, ethanal nitrate, and epoxides. Figure S10 compares RCIM to the GEOS-Chem v11-02c mechanism in fixed-radical nighttime simulations. The GEOS-Chem mechanism includes a smaller pool of functional products from isoprene + NO<sub>3</sub> oxidation, with high yields of C<sub>5</sub> hydroxy- and hydroperoxy-nitrates and only minor yields of the other products shown in RCIM.

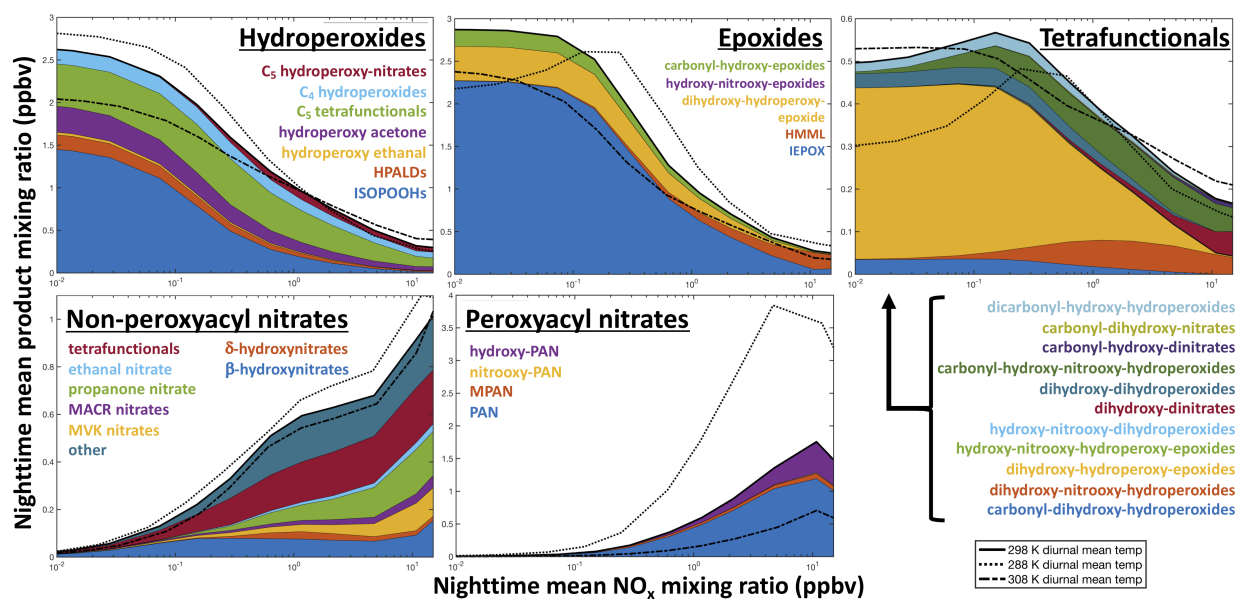


Figure S6: Nighttime average mixing ratios of major classes of compounds from isoprene oxidation in diurnal-steady-state box models as functions of  $\text{NO}_x$  and temperature, using RCIM. Y axis scales vary between graphs.

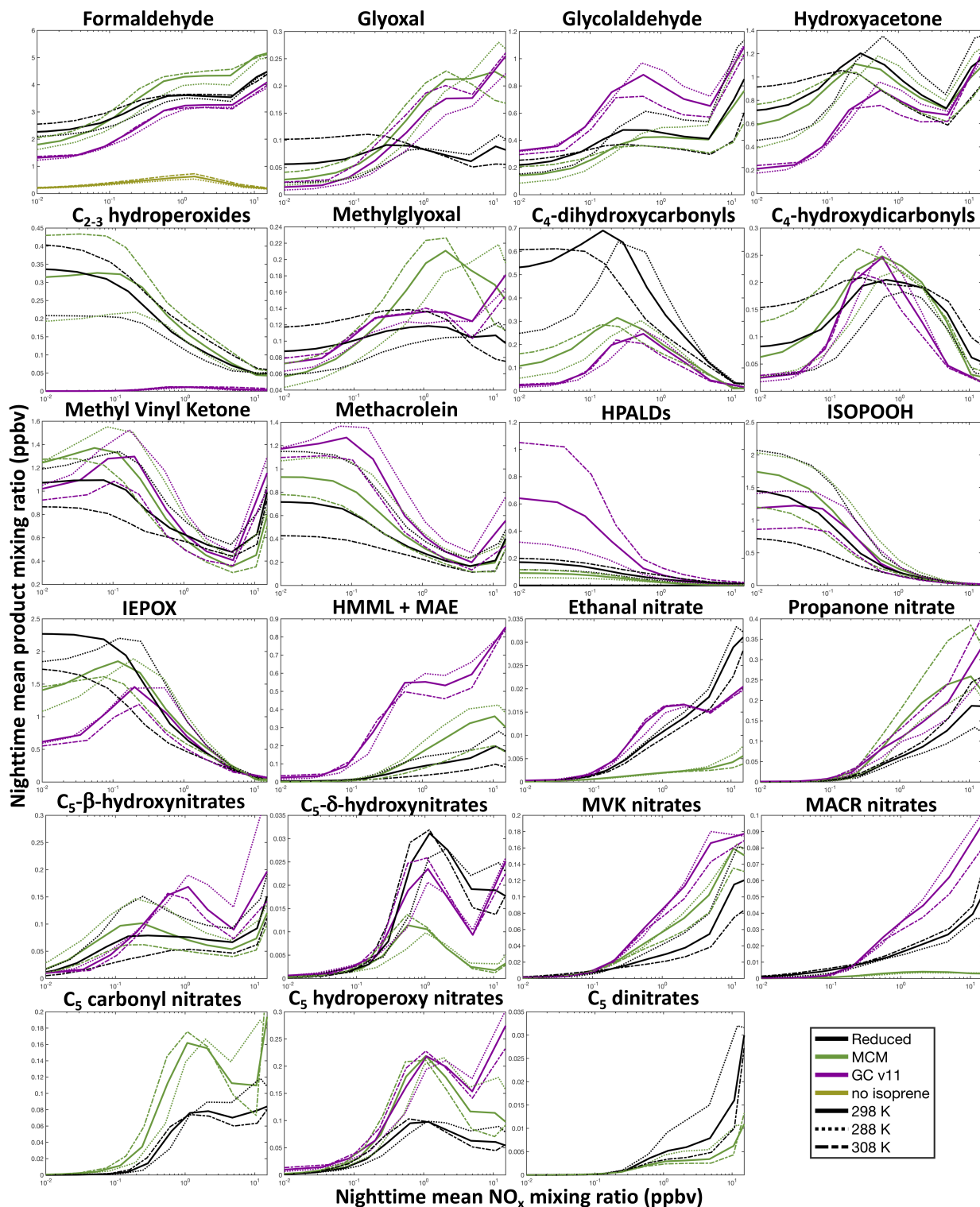


Figure S7: Nighttime average mixing ratios of major products of isoprene oxidation in diurnal-steady-state box models as functions of  $\text{NO}_x$  and temperature, using RCIM. Y axis scales vary between graphs. For formaldehyde, the model assumes a background mixing ratio of 300 pptv, with some additional contribution from methane oxidation. For HPETHNL + HPAC,  $\approx 10\%$  of the total is contributed by HPETHNL under all conditions.

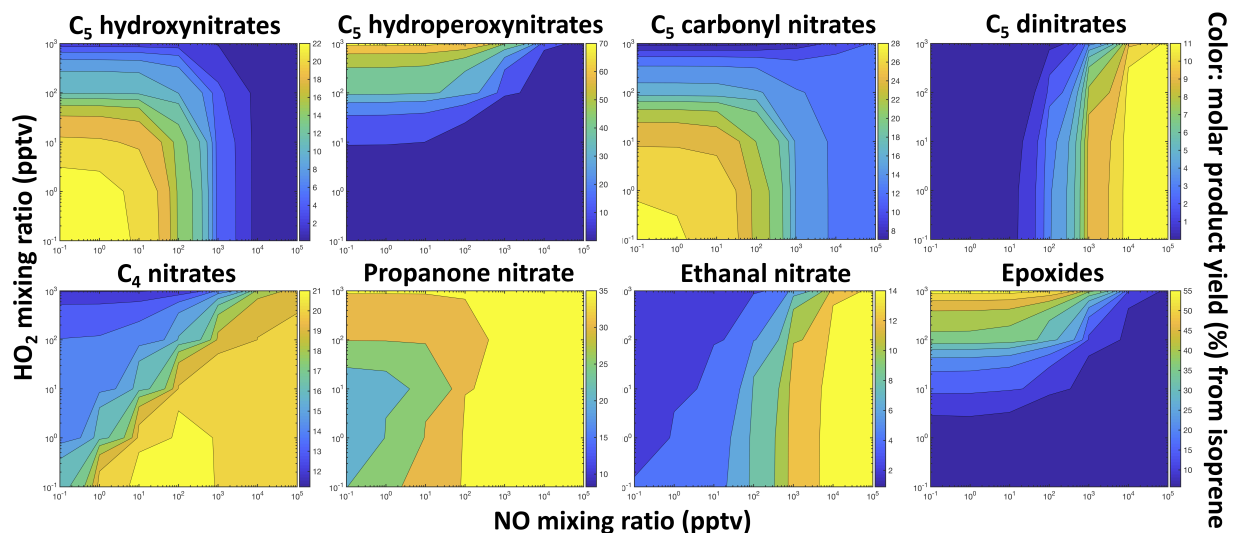


Figure S8: Percent yields of compounds of interest from isoprene + NO<sub>3</sub> oxidation in RCIM. All box models are run at 25 °C and 10% of equatorial midday photolytic light flux.

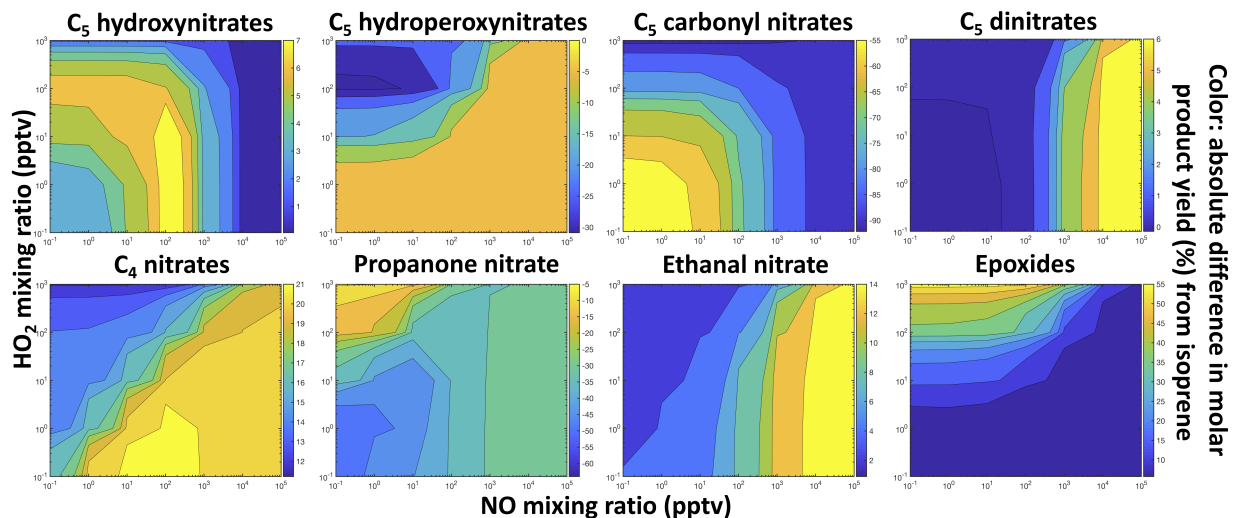


Figure S9: Absolute changes in percent yields of compounds of interest from isoprene + NO<sub>3</sub> oxidation when switching from fixed-radical box models with the MCM v3.3.1 mechanism (Jenkin et al., 2015) to RCIM. All box models are run at 25 °C and 10% of equatorial midday photolytic light flux.

## S5 Comparisons to other mechanisms

Figures S11-S24 and Tables S3 and S6 show detailed comparisons between RCIM, MCM v3.3.1, and the GEOS-Chem v11-02c isoprene oxidation mechanisms in box models, and between RCIM and v11-02c in global simulations. Many differences between the mechanisms stem from variability in the initial reactive pathway branching of isoprene, shown in Section S5.1, and from differences between the OH-recycling tendencies of the mechanisms under low-NO conditions (Section S5.2). These differences then carry over into variability in the yields of organic products (Section S5.3).

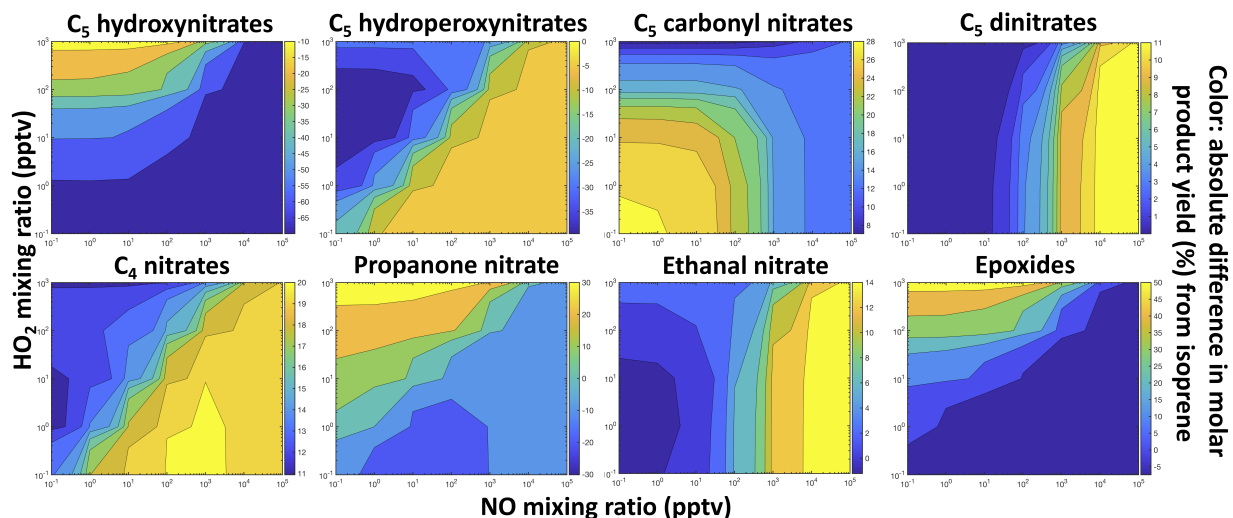


Figure S10: Absolute changes in percent yields of compounds of interest from isoprene +  $\text{NO}_3$  oxidation when switching from fixed-radical box models with the GEOS-Chem v11-02c mechanism to RCIM. All box models are run at 25 °C and 10% of equatorial midday photolytic light flux.

## S5.1 Isoprene reaction pathways

Figure S11 shows the contributions of specific reactive pathways to the overall fate of isoprene in diurnal-steady-state box models with the three isoprene oxidation mechanisms. Lower OH recycling under low-NO conditions in the MCM and GEOS-Chem mechanisms relative to RCIM means that less OH is available to react with isoprene, and leads to a higher reactivity with ozone, by up to a factor of 2 in the MCM mechanism and over a factor of 3 in the GEOS-Chem v11-02c mechanism. This effect is also visible in global chemical transport simulations with RCIM and v11-02c (Figure S12). The increased OH recycling in RCIM also sustains higher  $\text{HO}_2$  mixing ratios, which leads to a larger fraction of ISOPOO reacting with  $\text{HO}_2$  than in the other mechanisms. Fixed-radical simulations (Figure S13 and S14) show that when NO and  $\text{HO}_2$  are held constant, RCIM results in a larger proportion of ISOPOO reacting via H-shifts than the other two mechanisms, and only deviates substantially from MCM in the fraction reacting via each isomer under extremely high-NO conditions.

## S5.2 $\text{HO}_x$ , $\text{NO}_x$ , and ozone

Figures S15 and S16 show the differences in net production of  $\text{HO}_x$ ,  $\text{NO}_x$  and ozone due to isoprene oxidation by the three different mechanisms in fixed-radical box models. As described in the main manuscript, the main difference between the mechanisms is the higher  $\text{HO}_x$  recycling in RCIM under conditions where H-shift chemistry dominates. This can also be seen in global simulations comparing GEOS-Chem v11-02c and RCIM (Figure S17 and Table S6), which show that RCIM sustains OH concentrations up to three times those of the GEOS-Chem v11-02c mechanism in remote regions of high isoprene emission such as the Amazon, and that the reduced MPAN formation rate in RCIM leads to much lower  $\text{NO}_x$  titration over the Amazon.

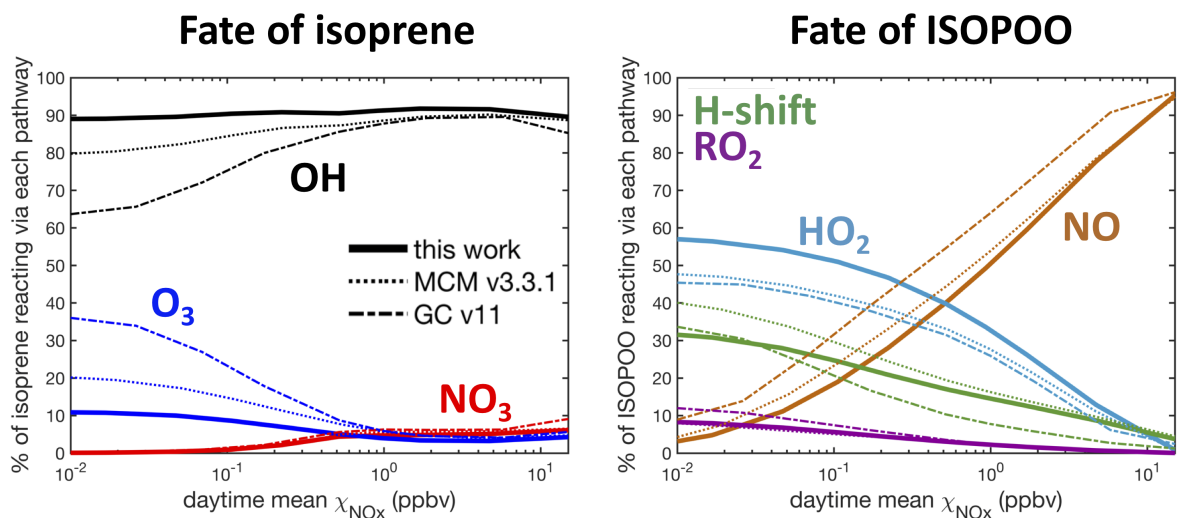


Figure S11: Isoprene oxidation pathway branchings in diurnal-steady-state box models as a function of  $\text{NO}_x$  mixing ratio, using RCIM (solid), MCM v3.3.1 (dashed), and GEOS-Chem v11-02c (dotted).

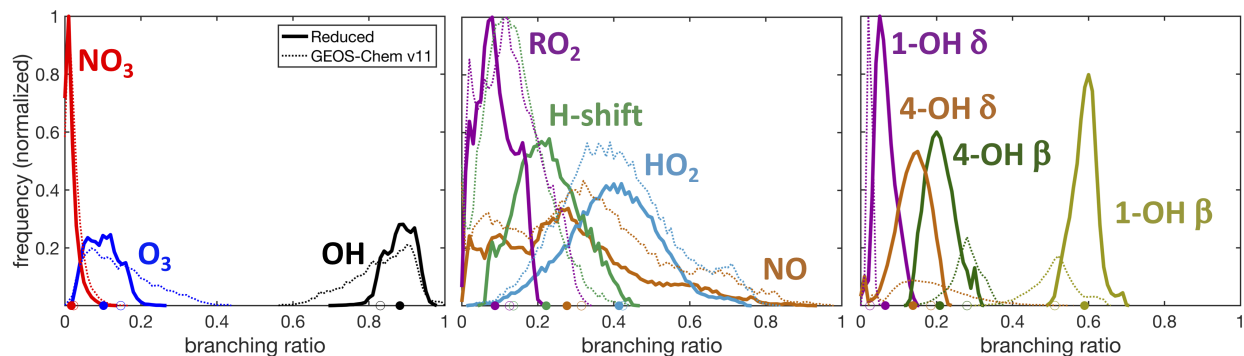


Figure S12: Isoprene oxidation pathway branchings in GEOS-Chem using RCIM (solid lines, filled dots) and GEOS-Chem v11-02c (dotted lines, open dots), at  $2^\circ \times 2.5^\circ$  horizontal resolution, on an annual average. The curves represent probability density functions of the models grid boxes, weighted by the amount of isoprene reacting in each grid box, while the dots on the x axis represent the global annual total reacting via each pathway.

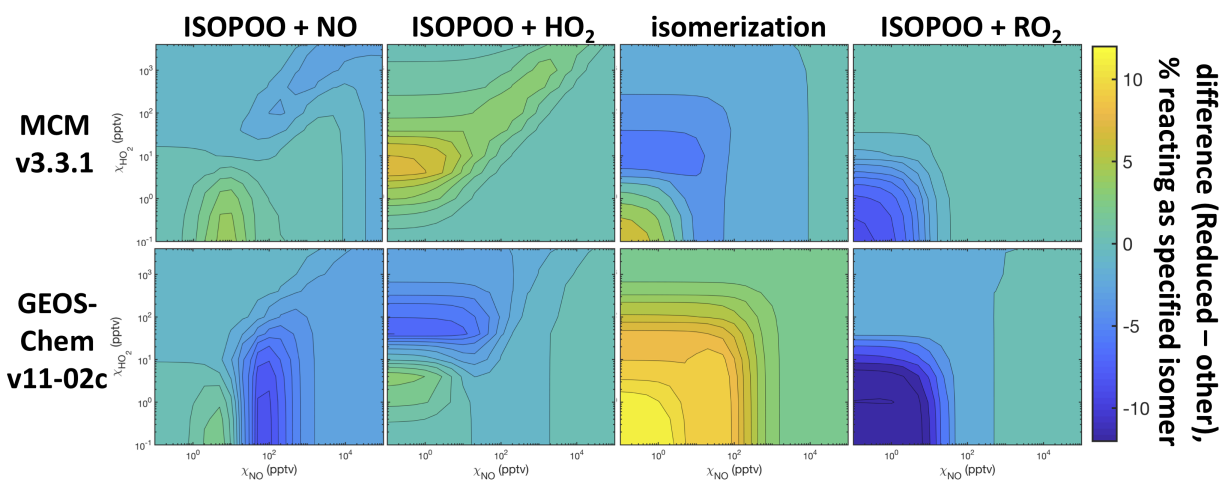


Figure S13: Absolute difference between RCIM and MCM v3.3.1 (top) and GEOS-Chem v11-02c (bottom) in the percent of isoprene hydroxy peroxy radicals reacting via each pathway as a function of NO and HO<sub>2</sub>, from fixed-radical box modeling of all three mechanisms at 298 K and full photolytic sunlight flux (equatorial midday).

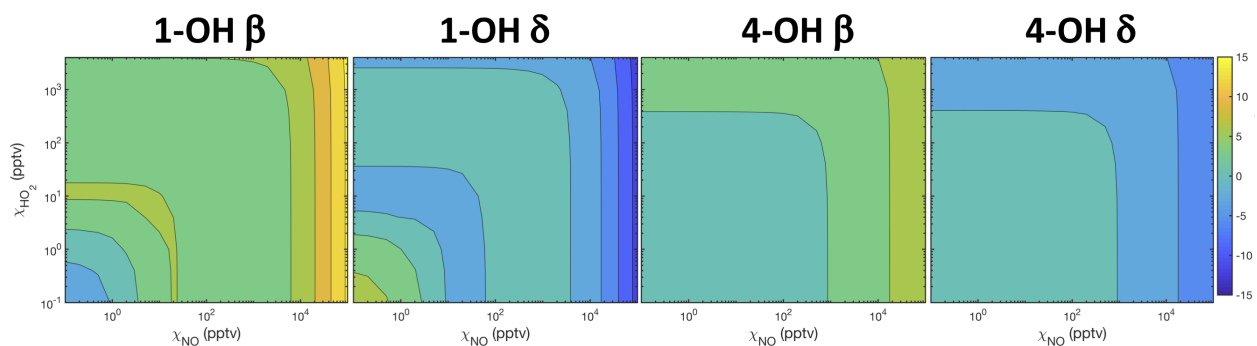


Figure S14: Absolute difference between RCIM and MCM v3.3.1 mechanism in the percent of isoprene hydroxy peroxy radicals reacting via each isomer as a function of NO and HO<sub>2</sub>, from fixed-radical box modeling of all three mechanisms at 298 K and full photolytic sunlight flux (equatorial midday).

Table S6: Differences (%) in annual average mixing ratios between GEOS-Chem simulations using RCIM and the GEOS-Chem v11-02c mechanism<sup>a</sup>

species	troposphere	0-1 km	5-10 km	SE USA <sup>b</sup>	Amazon <sup>b</sup>	E China <sup>b</sup>
OH	1.2 <sup>c</sup>	-0.57	-0.70	-12	-63	-3.3
HO <sub>2</sub>	2.0	0.75	1.9	-0.41	-24	-0.26
NO	-2.4	0.27	-3.9	2.2	0.2	-0.45
NO <sub>2</sub>	0.69	0.97	-2.8	1.7	-16	0.44
NO <sub>3</sub>	6.6	4.3	-1.5	-1.5	-26	2.7
O <sub>3</sub>	2.5	2.7	1.8	1.5	14	1.0
CO	-1.1	-1.4	-0.90	-1.7	-8.2	-0.22
HCHO	-0.99	-7.0	3.8	-11	-44	-1.4
Formicacid	9.3	-14	59	-23	-48	-9.8
Aceticacid	-14	-23	3.6	-30	-42	-24
Glycolaldehyde	60	42	130	27	100	-6.3
Glyoxal	130	87	430	310	47	26
Hydroxyacetone	1.3	-11	43	-0.40	-47	12
Methylglyoxal	8.9	-5.6	83	7.4	-43	6.5
Methyl vinyl ketone	-5.5	-17	52	-7.9	-34	-12
Methacrolein	33	19	105	26	-1.8	20
C <sub>4</sub> dihydroxycarbonyls	-34	-47	30	-48	-65	-36
PANs <sup>d</sup>	50	34	52	39	400	7.8
C <sub>2+</sub> nitrates <sup>d,e</sup>	160	240	68	220	1100	86
C <sub>5</sub> nitrates <sup>d</sup>	490	360	420	270	700	230
C <sub>5</sub> hydroxynitrates	640	530	440	450	870	470
C <sub>4</sub> nitrates <sup>d</sup>	860	700	1300	410	1500	300
Propanone nitrate	120	100	87	100	100	71
C <sub>2+</sub> hydroperoxides <sup>d</sup>	65	33	360	29	11	31
ISOPOOH	25	0.035	370	16	-25	13
C <sub>5</sub> hydroperoxy aldehydes	400	290	1100	140	330	62
Epoxides <sup>d</sup>	96	34	420	38	-30	120
IEPOX	29	-1.0	190	5.2	-41	24
HMML	900	630	1600	430	780	360
Tetrafunctionals <sup>d</sup>	2500	1800	2900	980	2600	2300
SOA	-39	-61	48	-75	-81	-33

<sup>a</sup>Results from 2° × 2.5° horizontal resolution global simulations. Positive percentages indicate higher mixing ratios in GEOS-Chem v11-02c than RCIM. <sup>b</sup>Average mixing ratios from 0-1 km altitude. <sup>c</sup>Causing a 1.16% decrease in the tropospheric methane lifetime. <sup>d</sup>Yields of lumped species may include multiple generations of a single oxidation pathway (e.g., separately counting both IEPOX and its oxidation product, isoprene hydroxycarbonyl epoxides). <sup>e</sup>Includes only non-PAN organonitrates.

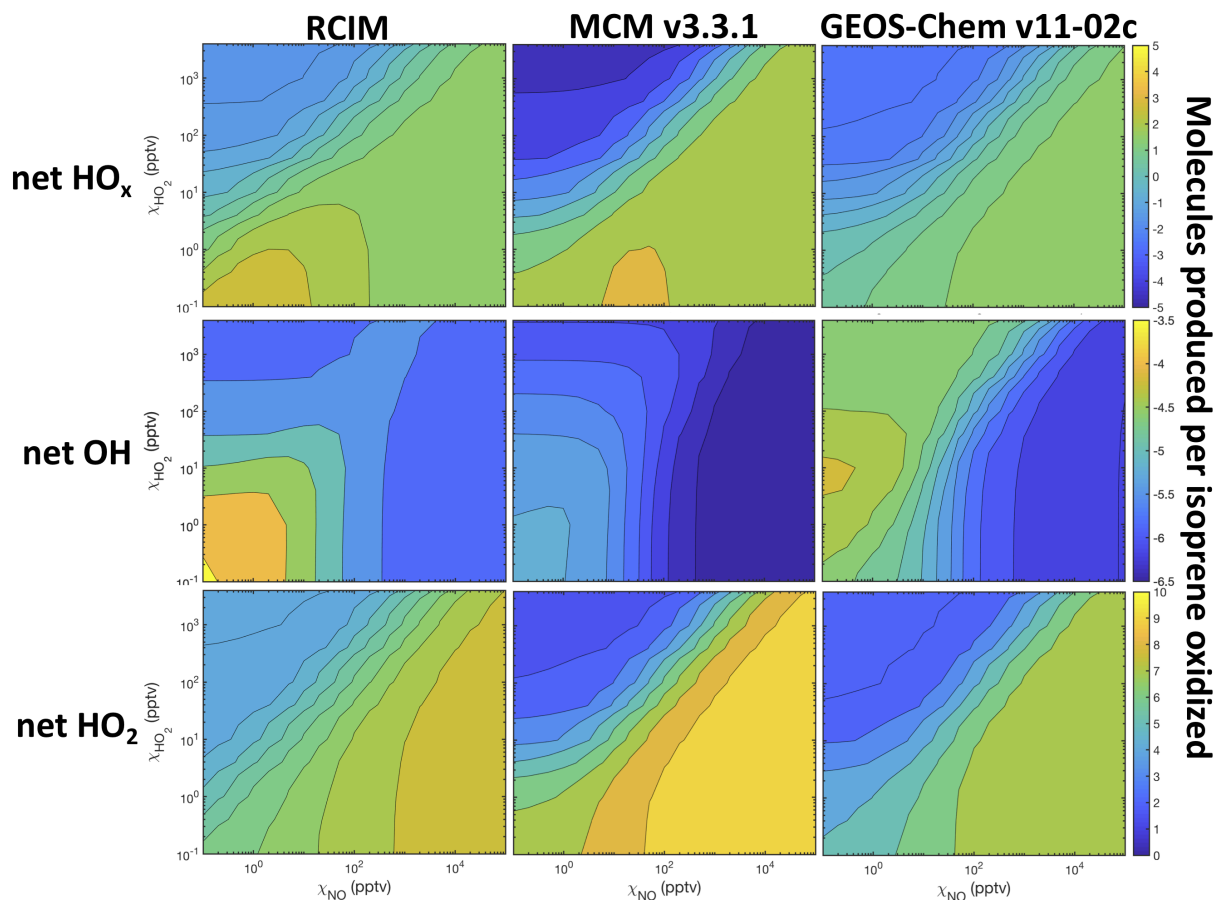


Figure S15: Net molar production or consumption of HO<sub>x</sub>, OH, and HO<sub>2</sub> from isoprene oxidation as a function of NO and HO<sub>2</sub> in RCIM (top), MCM v3.3.1 (middle) and GEOS-Chem v11-02c (bottom), from fixed-radical box modeling of all three mechanisms at 298 K and full photolytic sunlight flux (equatorial midday).

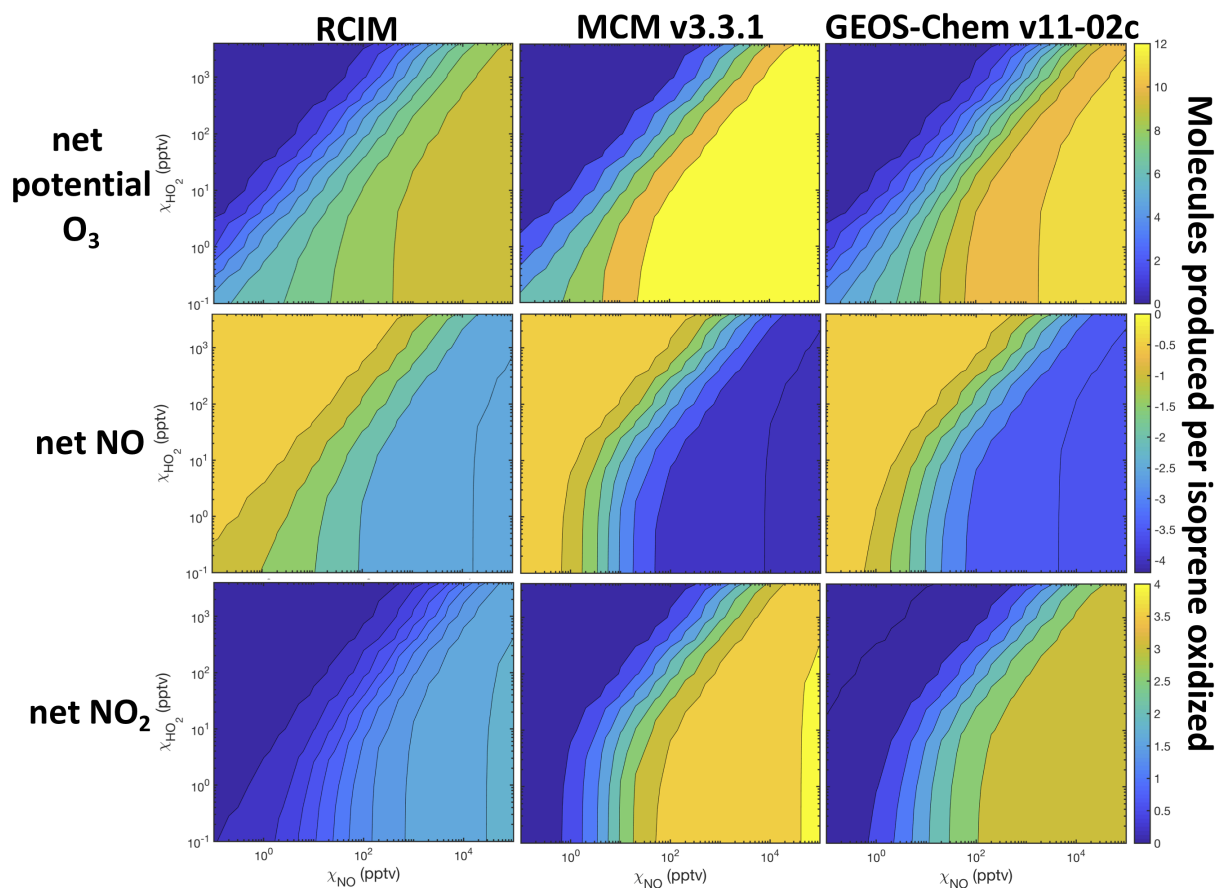


Figure S16: Net molar production or consumption of potential  $O_3$ ,  $NO$ , and  $NO_2$  from isoprene oxidation as a function of  $NO$  and  $HO_2$  in RCIM (top), MCM v3.3.1 (middle) and GEOS-Chem v11-02c (bottom), from fixed-radical box modeling of all three mechanisms at 298 K and full photolytic sunlight flux (equatorial midday). Net potential  $O_3$  is estimated as the sum of net production of ozone,  $NO_2$ , and  $HO_2$  (times the fraction of  $HO_2$  that would go on to react with  $NO$  based on the relative concentrations of its potential reaction partners).

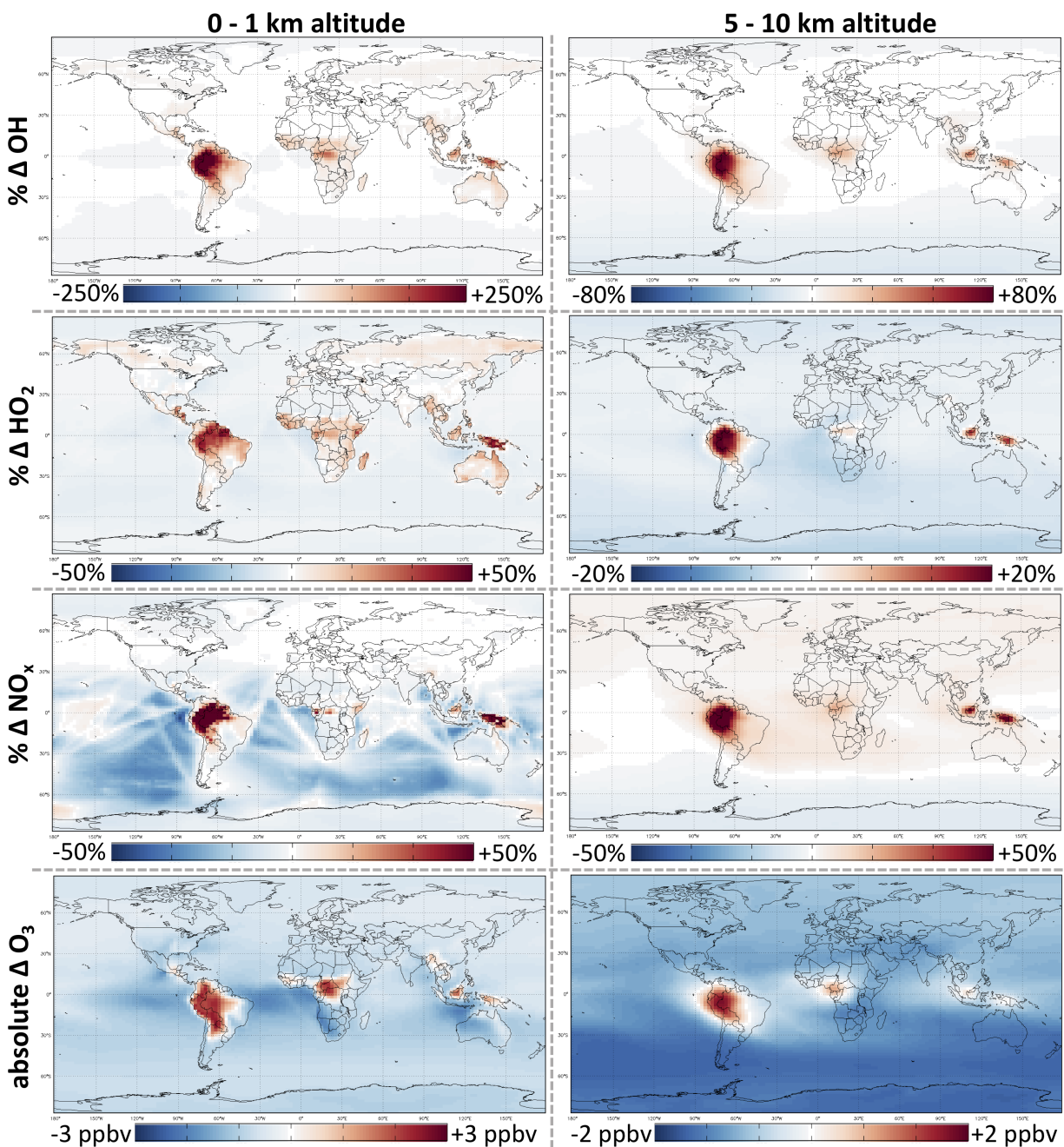


Figure S17: Changes in annual average mixing ratios of OH, HO<sub>2</sub>, NO<sub>x</sub>, and O<sub>3</sub> from a 2° × 2.5° horizontal resolution GEOS-Chem simulation with the GEOS-Chem v11-02c mechanism to one with RCIM.

### S5.3 Organic products

Figures S18 and S19 show the differences in yields of organic products between RCIM, MCM v3.3.1, and GEOS-Chem v11-02c in fixed-radical box model simulations. Figures S20-S23 show differences in daytime mixing ratios of organic products between the mechanisms in diurnal-steady-state simulations. Table S3 shows differences in mean annual yields of organic isoprene oxidation products between GEOS-Chem v11-02c and RCIM in global chemical transport simulations, while Figure S24 and Table S6 show differences in mean

annual mixing ratios of organic isoprene oxidation products from the same simulations. The maps in Figure S24 show the higher formaldehyde production from local isoprene oxidation over remote forests as well as the strong effects of the decreased MPAN formation rate in RCIM, along with smaller corresponding decreases in PAN formation and in the lifetimes of tertiary nitrates due to rapid hydrolysis. The major differences between product yields are noted in the main manuscript; these figures are provided as a reference for those seeking a more detailed accounting of individual products.

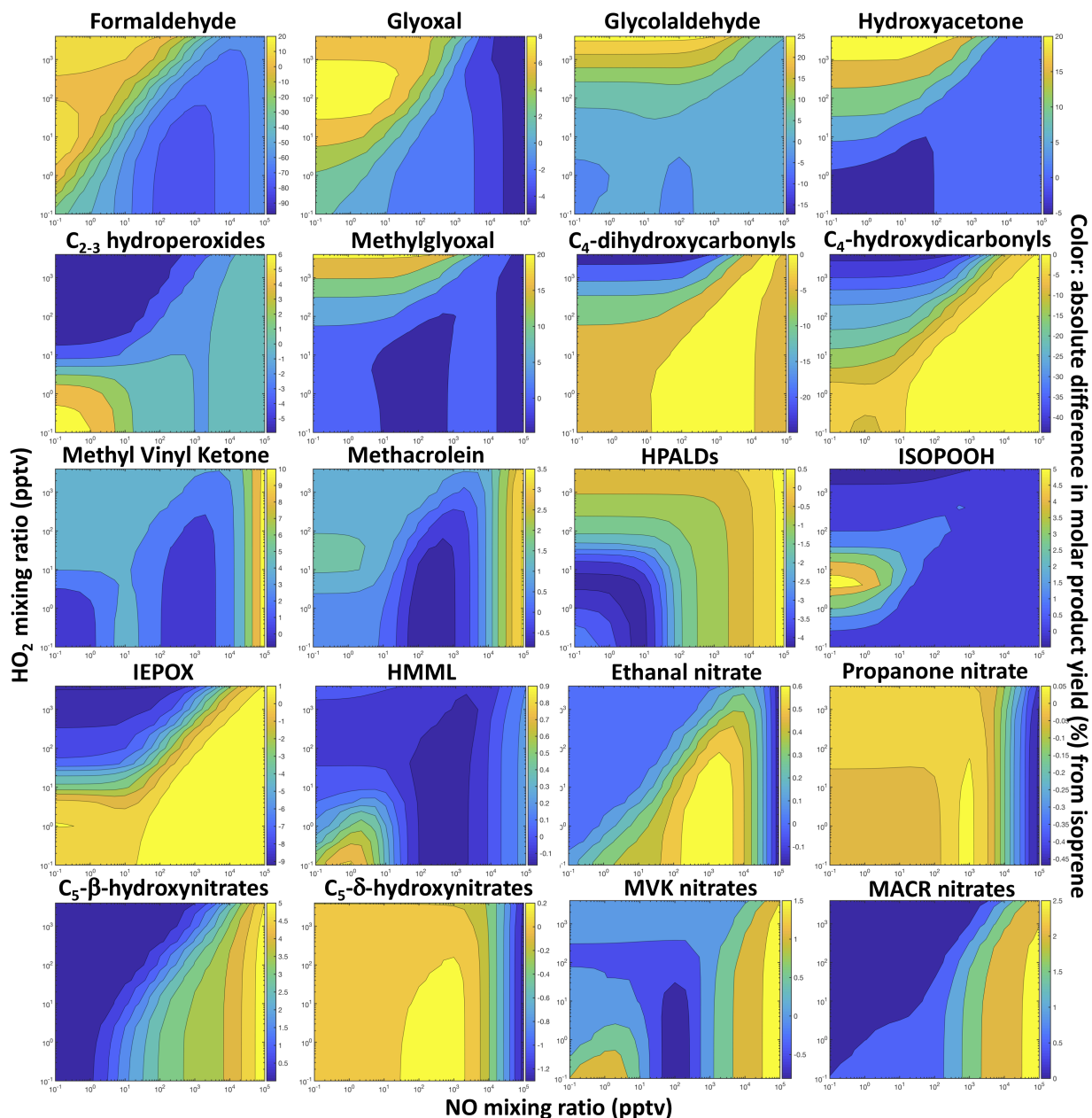


Figure S18: Absolute changes in percent yields of compounds of interest from isoprene + OH oxidation when switching from fixed-radical box models with MCM v3.3.1 (Jenkin et al., 2015) to RCIM. All box models are run at 25 °C and equatorial midday photolytic light flux.

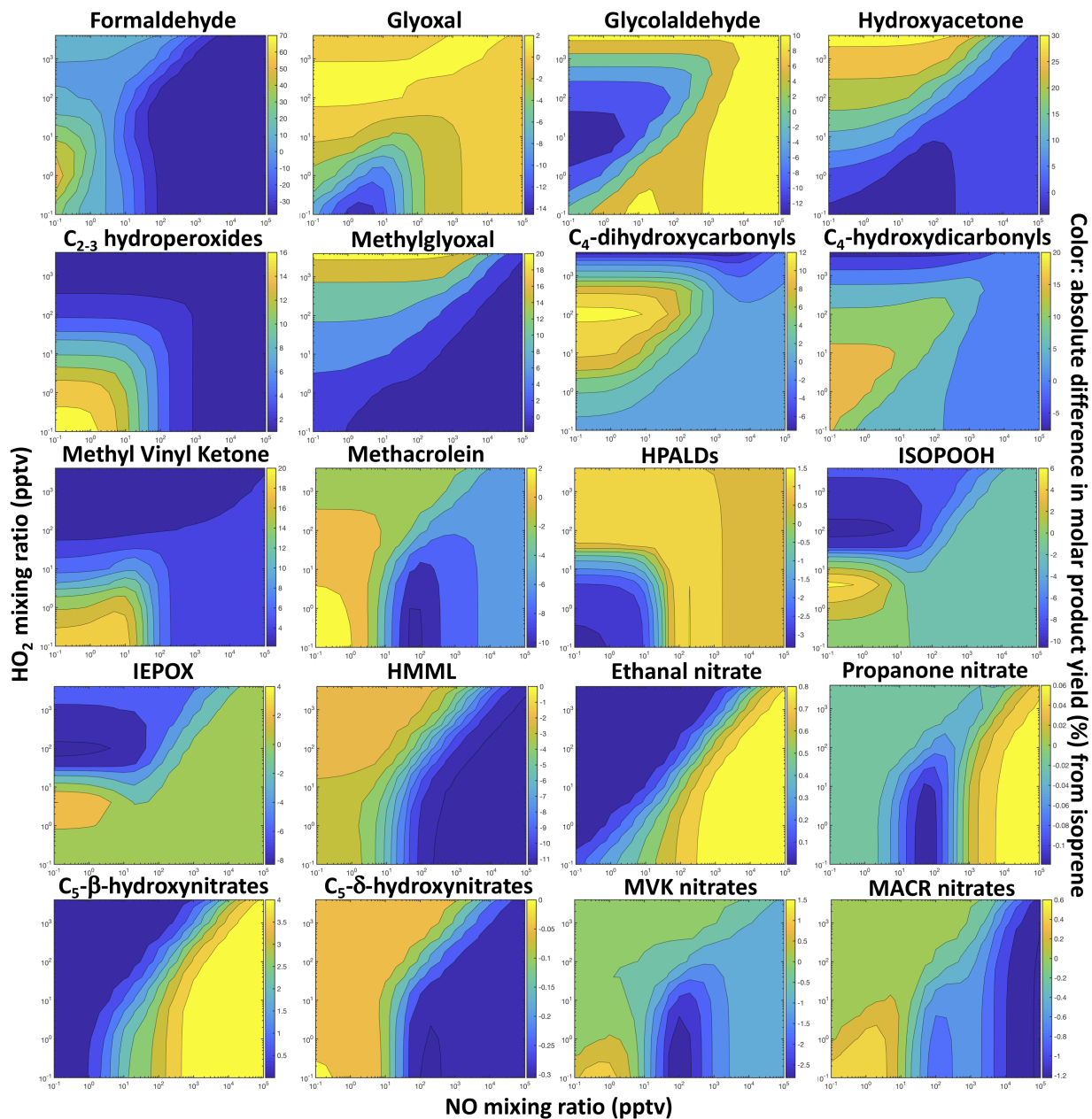


Figure S19: Absolute changes in percent yields of compounds of interest from isoprene + OH oxidation when switching from fixed-radical box models with GEOS-Chem v11-02c to RCIM. All box models are run at 25 °C and equatorial midday photolytic light flux.

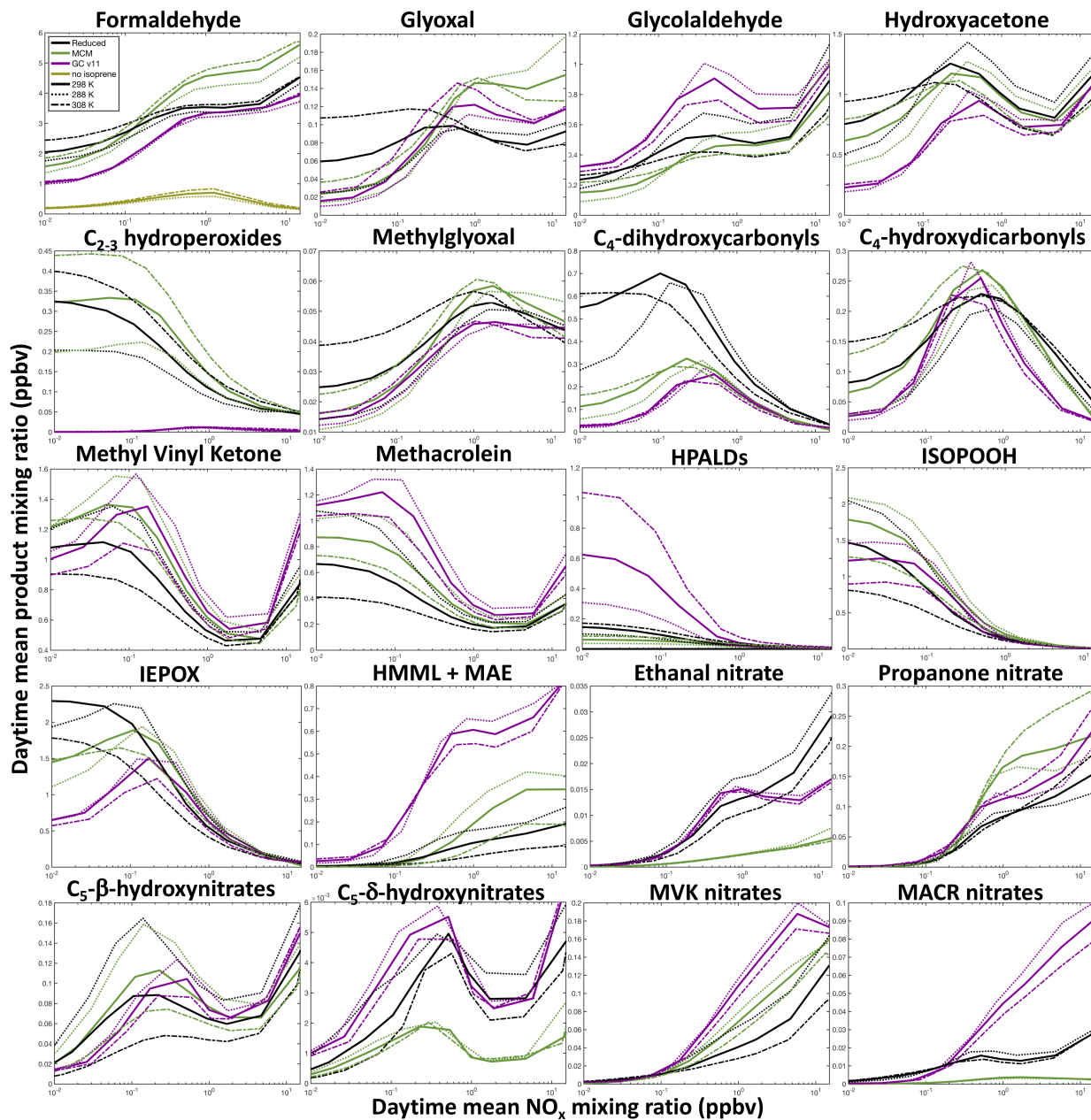


Figure S20: Daytime average mixing ratios of isoprene oxidation products in diurnal-steady-state box models as a function of  $\text{NO}_x$  mixing ratio (X axis) and temperature (line style), using RCIM (black), MCM v3.3.1 (green), and GEOS-Chem v11-02c (purple).

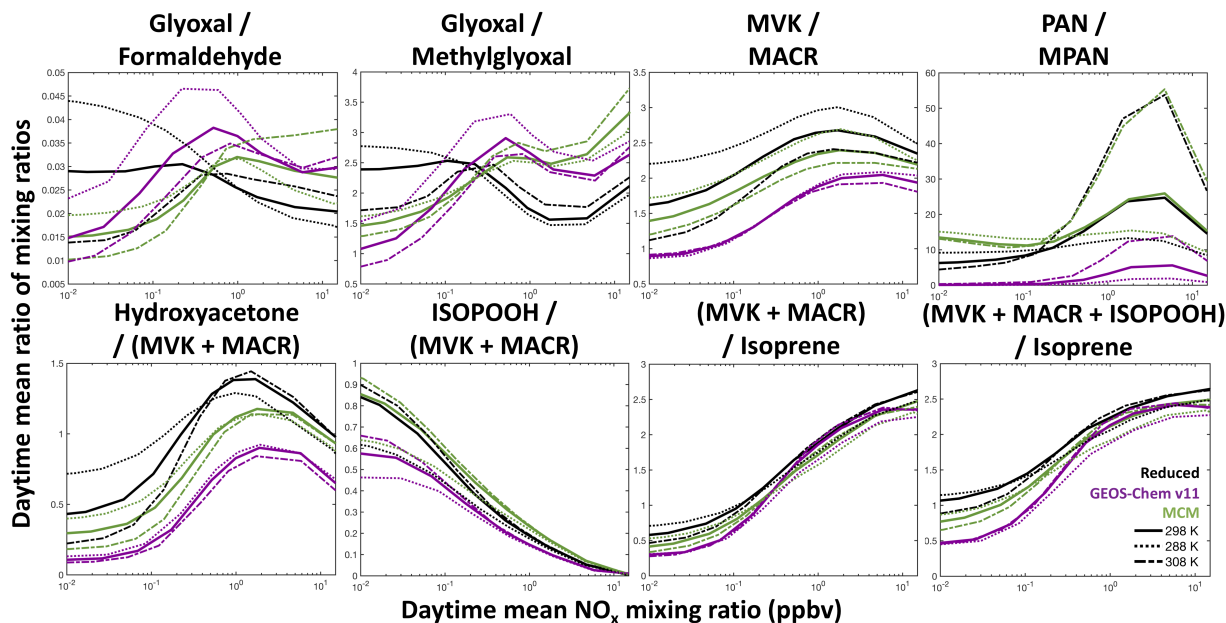


Figure S21: Commonly reported ratios between daytime average mixing ratios of isoprene oxidation products in diurnal-steady-state box models as a function of  $\text{NO}_x$  mixing ratio (X axis) and temperature (line style), using RCIM (black), MCM v3.3.1 (green), and GEOS-Chem v11-02c (purple).

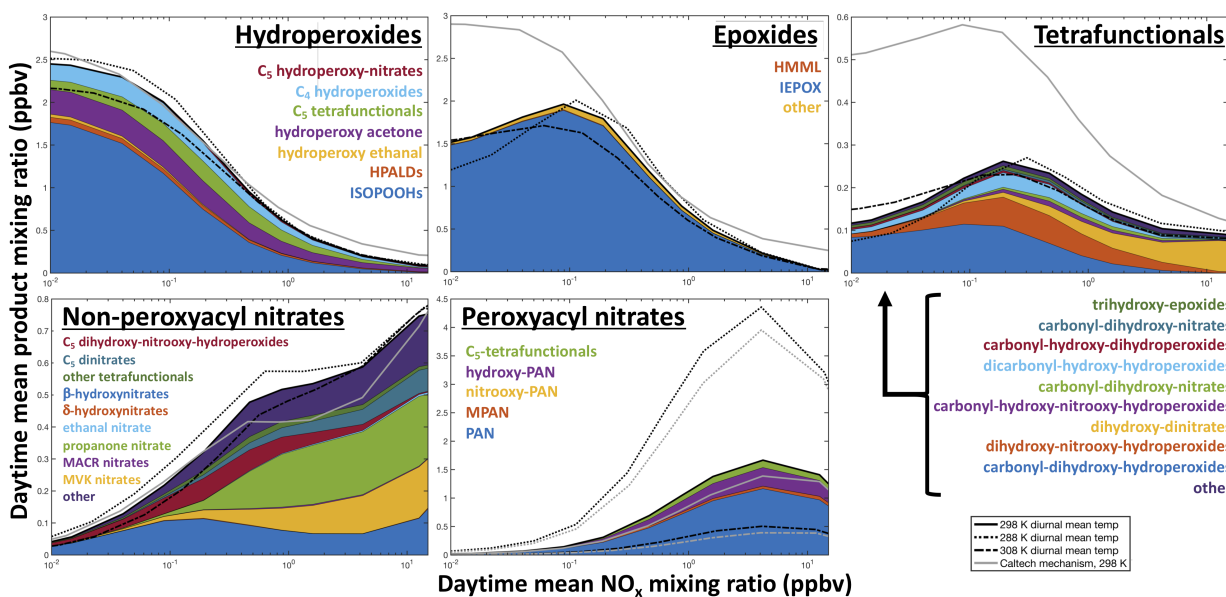


Figure S22: Daytime average mixing ratios of major classes of compounds from isoprene oxidation in diurnal-steady-state box models as functions of  $\text{NO}_x$  (X axis) and temperature (black lines), using MCM v3.3.1. Y axis scales vary between graphs. Grey lines denote corresponding mixing ratios using the RCIM for comparison.

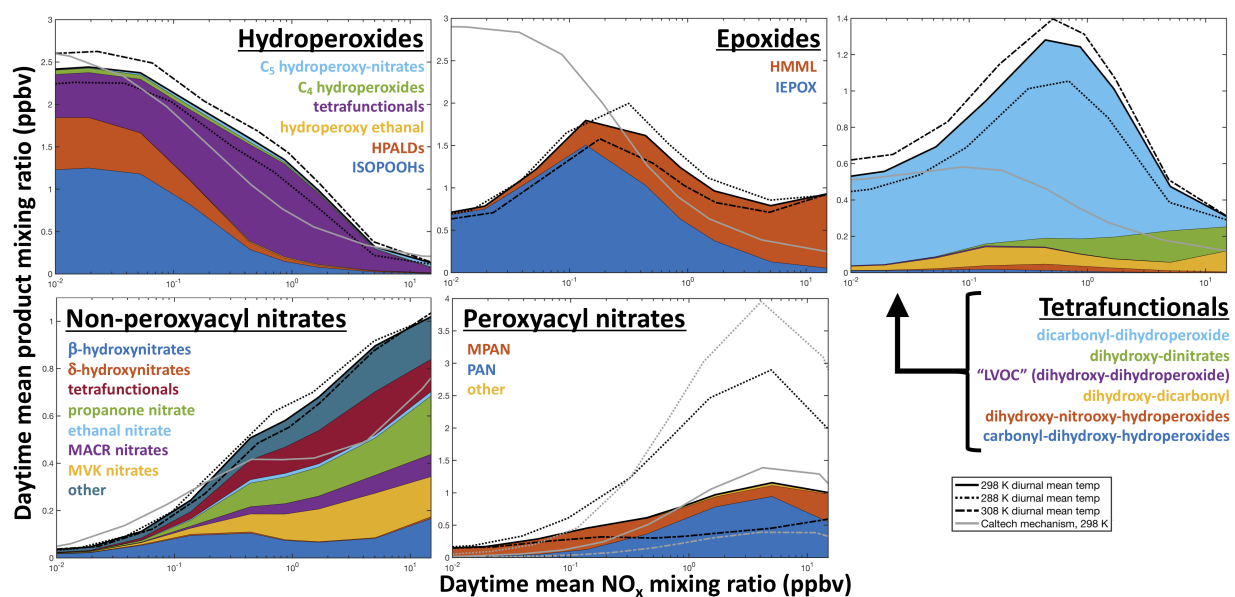


Figure S23: Daytime average mixing ratios of major classes of compounds from isoprene oxidation in diurnal-steady-state box models as functions of  $\text{NO}_x$  (X axis) and temperature (black lines), using GEOS-Chem v11-02c. Y axis scales vary between graphs. Grey lines denote corresponding mixing ratios using RCIM for comparison.

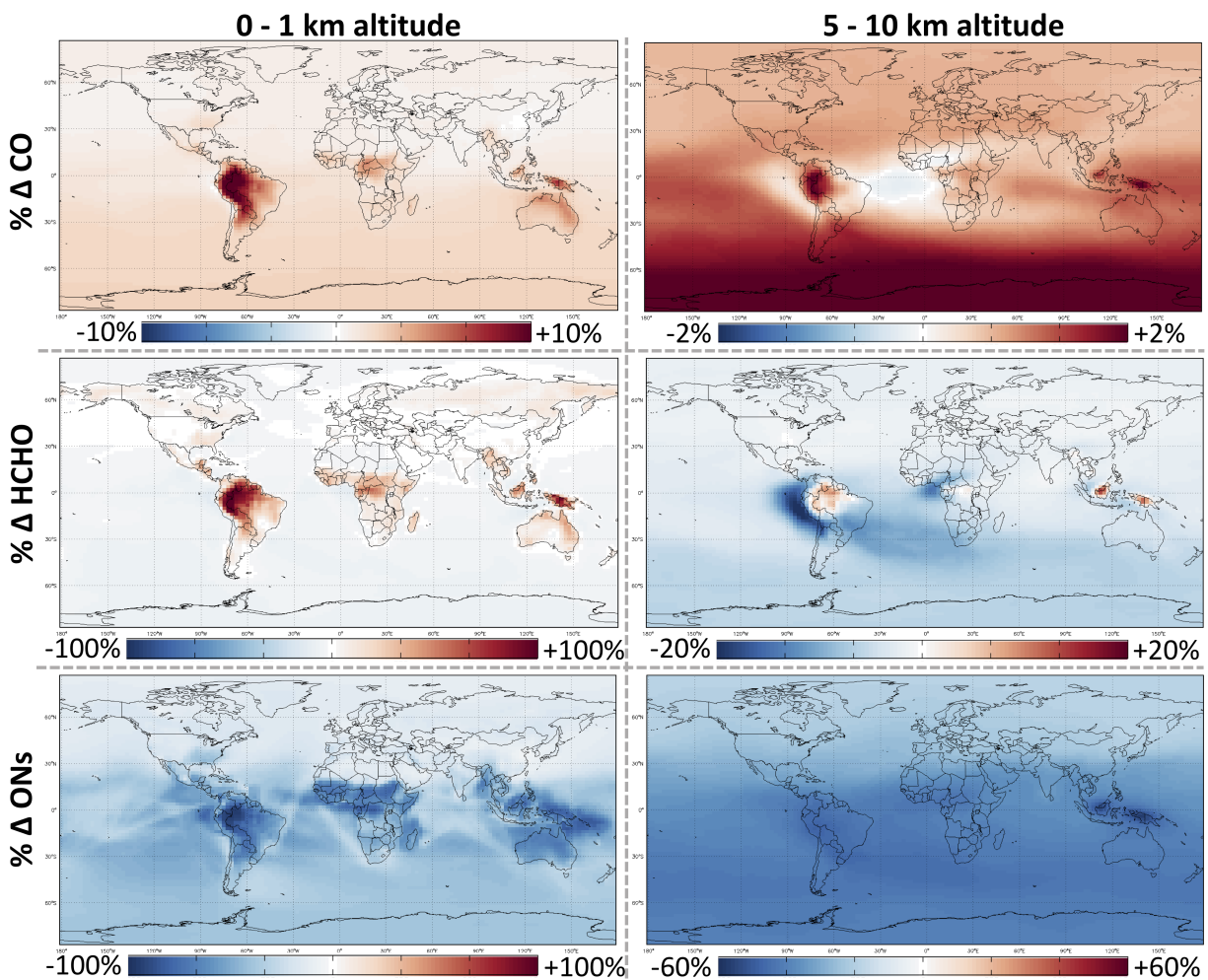


Figure S24: Percent changes in annual average mixing ratios of CO (top), formaldehyde (middle), and total organonitrates (bottom) from a  $2^\circ \times 2.5^\circ$  horizontal resolution GEOS-Chem simulation with the GEOS-Chem v11-02c mechanism to one with RCIM.

## S6 Mechanism simplification

Table S7 provides the differences in tropospheric and regional production and mixing ratios of species between annual GEOS-Chem simulations using RCIM and Mini-CIM. As described in the main text, the changes between the two mechanisms are minimal ( $\sim 0.1\%$ ), particularly for  $\text{HO}_x$ ,  $\text{NO}_x$ ,  $\text{O}_3$ ,  $\text{CO}$ , and  $\text{HCHO}$ . Larger reductions in  $\text{C}_{2+}$  organonitrate (2.8 %) and  $\text{C}_5$  tetrafunctional (12 %) production are largely due to the removal of multigenerational steps (e.g. the conversion of one tetrafunctional species into another), and therefore do not carry over substantially to changes in mixing ratios. Further, the moderate percent reduction (4.4 %) in mixing ratios of organonitrates over the Amazon represents only a tiny absolute difference, since the region experiences very little nitrate formation.

Table S7: Differences (%) in annual production and mixing ratios between GEOS-Chem simulations using RCIM and Mini-CIM

species	tropospheric production	tropospheric loading	loading, 0-1 km	loading, Amazon	loading, SE USA	loading, E China
OH	-	-0.14	-0.12	-0.17	-0.03	-0.01
$\text{HO}_2$	-	-3.2E-3	-0.022	-0.020	0.079	0.025
$\text{NO}_x$	-	-0.17	-0.02	-0.22	0.020	0.016
$\text{O}_3$	-	-0.11	-0.097	-0.42	-0.074	-0.028
CO	-0.11	-0.078	0.054	0.038	0.014	5.1E-3
HCHO	-0.13	-0.096	-0.11	-0.12	-0.13	-0.047
GLYC	-0.66	-0.53	-0.67	-0.63	-0.68	-0.30
GLYX	0.43	0.58	0.47	-1.2	2.1	0.076
HAC	0.14	0.089	0.33	0.55	-0.24	-0.42
MGLY	-0.35	-0.17	-0.077	-0.11	0.22	0.084
PANs	-	-0.34	-0.18	-0.50	-0.28	-0.067
$\text{C}_{2+}$ nitrates <sup>a</sup>	-2.8	-0.68	0.77	4.4	2.4	0.02
$\text{C}_{2+}$ hydroperoxides	-0.65	0.43	0.44	0.14	1.4	2.9
epoxides	1.7E-3	0.32	0.21	0.11	0.28	0.38
SOA	0.17	0.23	0.082	-0.10	0.17	0.023
$\text{C}_5$ tetrafunctionals	-12	-0.048	-0.21	-0.074	-0.64	2.2

<sup>a</sup>Includes only non-PAN organonitrates

Table S8 shows the annual global and regional molar product yields from isoprene of species removed from RCIM to create Mini-CIM. We also provide a complete list of the simplifications made to create Mini-CIM below. Naming conventions follow those laid out in Wennberg et al. (2018) and used in RCIM. More details, along with a complete listing of the reactions and species in both RCIM and Mini-CIM, can be found online in the mechanism repository (DOI 10.22002/D1.247)

The following simplifications apply to species that meet the simplification criteria of  $< 0.1\%$  yield from isoprene globally and  $< 1\%$  yield from isoprene regionally in the Amazon, the Southeast United States, and East China:

- ISOP3CO4OH is replaced with ISOP1OH2OO3CO4OH; because  $\text{ISOP3CO4OH} + \text{OH} = \text{ISOP1OH-2OO3CO4OH} + \text{OH}$  is the only loss process of ISOP3CO4OH, this replacement is OH-neutral.
- The acylperoxy radical of hydroxyethane ( $\text{HOCH}_2\text{C}(\text{O})\text{OO}\bullet$ ) is replaced with the peroxyacetyl radical ( $\text{CH}_3\text{C}(\text{O})\text{OO}\bullet$ ), and the products of its reactions with  $\text{HO}_2$  and  $\text{NO}_2$  ( $\text{HOCH}_2\text{C}(\text{O})\text{OOH}$ ,  $\text{HOCH}_2\text{C}(\text{O})\text{OH}$ , and  $\text{HOCH}_2\text{C}(\text{O})\text{OONO}_2$ ) are removed.
- The acylperoxy radical of nitrooxyethane ( $\text{O}_2\text{NOCH}_2\text{C}(\text{O})\text{OO}\bullet$ ) is replaced with the peroxyacetyl radical ( $\text{CH}_3\text{C}(\text{O})\text{OO}\bullet$ ) plus  $\text{NO}_2$ , and the products of its reactions with  $\text{HO}_2$  and  $\text{NO}_2$  ( $\text{O}_2\text{NOCH}_2\text{C}(\text{O})\text{OOH}$ ,  $\text{O}_2\text{NOCH}_2\text{C}(\text{O})\text{OH}$ , and  $\text{O}_2\text{NOCH}_2\text{C}(\text{O})\text{OONO}_2$ ) are removed.

- The three isoprene carbonyl nitrate isomers are lumped into a single species (ICN) representing 70% ISOP1N4CO, 30% ISOP1CO4N, and 0% ISOP3CO4N, the proportion in which they are produced in GEOS-Chem simulations; the subsequent reaction rates and products of the single ICN species are scaled according to these proportions.
- ICN3OO (ISOP1OH2OO3CO4N) is removed, as it is no longer produced from IC3N.
- ICN1OO (ISOP1N2OH3OO4CO) and ICN2OO (ISOP1CO2OO3OH4N) are found to undergo rapid H-shifts under almost all ambient conditions (Möller et al., 2019), and are therefore replaced with the H-shift products.
- The acylperoxy radical products of ICN + OH are lumped into a single species (ICNOO) representing 70% ICN4OO (ISOP1N4CO4OO) and 30% ICN5OO (ISOP1CO1OO4N), the proportions in which they are produced in GEOS-Chem simulations; the subsequent reaction rates and products of the single ICNOO species are scaled according to these proportions.
- MVK-derived nitrates are lumped into a single species (MVKN) representing 69% MVK3N4OH, 29% MVK3OH4N, 1% MVK3OOH4N, and 1% MVK3CO4N, the proportions in which they are produced in GEOS-Chem simulations; the subsequent reaction rates and products of the single MVKN species are scaled according to these proportions.
- MACR1OOH2N3OH is replaced with MACR2N3OH, which has nearly identical subsequent reactions.
- Minor isomers of methacrolein-derived nitrates are lumped into a single species (MACRN) representing 75% MACR2OH3N, 25% MACR2OOH3N, and 0% MACR1OH2N3OH, the proportions in which they are produced in GEOS-Chem simulations; the subsequent reaction rates and products of the single MACRN species are scaled according to these proportions.
- All dinitrates are lumped into a single species (IDN) representing 50% dihydroxy-dinitrates (IDHDN), 50% dinitrates retaining a double bond (IDN), 0% isoprene-hydroxy-hydroperoxy-dinitrates (IHPDN), and 0% isoprene-carbonyl-hydroxy-dinitrates (ICHDN), the proportions in which they are produced in GEOS-Chem simulations; the subsequent reaction rates and products of the single IDN species are scaled according to these proportions.
- All tri- and tetra-functionalized C<sub>5</sub> hydroxynitrates are lumped into a single species (ITHN) representing 90% isoprene-dihydroxy-hydroperoxy-nitrate (IDHPN), 10% isoprene-hydroxy-nitrooxy-epoxide (IHNE), 0% isoprene-hydroxy-dihydroperoxy-nitrates (IHNDP), and 0% isoprene-hydroxy-hydroperoxy-nitrooxy-epoxides (IHNPE), the proportions in which they are produced in GEOS-Chem simulations; the subsequent reaction rates and products of the single ITHN species are scaled according to these proportions. Because the hydroxy-nitrates have similar photolytic and OH loss pathways, this combination minimizes changes to the species' lifetimes.
- Isoprene-carbonyl-nitrooxy-epoxides (ICNE) and isoprene-dihydroxy-carbonyl-nitrates (IDHCN) are replaced with isoprene-carbonyl-hydroxy-hydroperoxy-nitrates (ICHNP), which is renamed as ITCN to reflect the lumped isoprene tri- and tetra-functionalized carbonyl nitrates. Because the carbonyl-nitrates have similar photolytic and OH loss pathways, this combination minimizes changes to the species' lifetimes.
- IHNEOO, the peroxy radical from isoprene-hydroxy-nitrooxy-epoxides (IHNE) + OH, is replaced with the peroxy radical from NO<sub>3</sub>-derived beta-hydroxy nitrates + OH (IDHNBOO), which reacts similarly.
- The lumped  $\beta$ -hydroxynitrates from isoprene + NO<sub>3</sub> oxidation (IHNB) are combined with the lumped beta-hydroperoxynitrates from isoprene + NO<sub>3</sub> oxidation (INPB); the subsequent reaction rates and products of the single INPB species are scaled (33% IHNB, 67% INPB) according to the proportions in which they are produced in GEOS-Chem simulations.
- Hydroxy-nitrooxy-methacryloylperoxynitrate (MPANH) is replaced with methacryloylperoxynitrate (MPAN) + NO<sub>2</sub>.

- The acid (MACR1OH) and peracid (MACR1OOH) from the methacryloylperoxy radical reaction with HO<sub>2</sub> are lumped into a single species (MACR1OOH) representing 75% MACR1OOH and 25% MACR1OH, the proportions in which they are produced in GEOS-Chem simulations; the subsequent reaction rates and products of the single ITHN species are scaled according to these proportions.
- SOA from methylglyoxal (SOAMG) and from HMML (SOAME) are combined, respectively, with SOA from glyoxal (SOAGX) and IEPOX (SOAIE). This simplification applies only to GEOS-Chem, not the gas-phase mechanism found in the online repository.

The following simplifications apply to species that do not meet the yield criteria described above, but are isobaric and have the same loss rates, such that combining them does not affect the species' atmospheric lifetime:

- ISOP1CO4OH and ISOP1OH4CO are lumped into a single C<sub>5</sub>- $\delta$ -hydroxy-carbonyl species (HC5) representing 65% ISOP1CO4OH and 35% ISOP1OH4CO, the proportions in which they are produced in GEOS-Chem simulations; the subsequent reaction rates and products of the single HC5 species are scaled according to these proportions.
- MVKENOL and MCRENOL are lumped into a single C<sub>4</sub>-enol species (MCRENOL) representing 75% MCRENOL and 25% MVKENOL, the proportions in which they are produced in GEOS-Chem simulations; the subsequent reaction rates and products of the single enol species are scaled according to these proportions.
- MACR2OH3CO and MVK3OH4CO have identical reaction pathways, and are therefore lumped into a single C<sub>4</sub>-hydroxy-dicarbonyl species (MVKHCB).
- MACR2OOH3OH and MACR2OH3OOH are lumped into a single hydroxy-hydroperoxy-methacrolein species (MACRHP) representing 77% MACR2OOH3OH and 23% MACR2OH3OOH, the proportions in which they are produced in GEOS-Chem simulations; the subsequent reaction rates and products of the single MACRHP species are scaled according to these proportions.
- MVK3OOH4OH and MVK3OH4OOH are lumped into a single hydroxy-hydroperoxy-MVK species (MVKHP) representing 53% MVK3OOH4OH and 47% MVK3OH4OOH, the proportions in which they are produced in GEOS-Chem simulations; the subsequent reaction rates and products of the single MVKHP species are scaled according to these proportions.

Table S8: Annual mean molar yields (%) from isoprene of species removed from the simplified mechanism<sup>a</sup>

species	global	Amazon	SE USA	E China
HOCH <sub>2</sub> CO <sub>2</sub> H	1.7E-4	1.9E-6	1.8E-5	1.2E-5
HOCH <sub>2</sub> CO <sub>3</sub> H	3.3E-4	2.4E-6	3.1E-5	2.1E-5
O <sub>2</sub> NOCH <sub>2</sub> CO <sub>2</sub> H	5.8E-4	2.0E-5	3.7E-4	5.6E-4
O <sub>2</sub> NOCH <sub>2</sub> CO <sub>3</sub> H	9.3E-4	2.5E-5	6.2E-4	9.3E-4
O <sub>2</sub> NOCH <sub>2</sub> CO <sub>3</sub> NO <sub>2</sub>	0.012	2.6E-4	0.017	0.080
HOCH <sub>2</sub> CO <sub>3</sub> NO <sub>2</sub>	8.7E-4	1.1E-5	6.7E-4	9.9E-4
MPANHN	0.018	1.5E-3	0.037	0.049
MVK3OOH4N	6.9E-3	5.6E-4	0.013	0.023
MVK3CO4N	5.2E-3	1.7E-4	7.6E-3	0.011
MACR2OOH3N	0.023	1.3E-3	0.045	0.059
MACR1OH2N3OH	2.2E-3	7.3E-4	1.5E-3	7.3E-4
MACR1OOH2N3OH	2.5E-3	6.8E-4	2.1E-3	1.2E-3
ISOP3CO4OH	0.069	0.037	0.059	0.036
ISOP1CO4N	0.088	8.2E-3	0.21	0.32
ISOP3CO4N	9.1E-3	7.8E-4	0.024	0.024
dinitrooxy-isoprene	0.035	4.0E-3	0.092	0.20
nighttime $\beta$ -hydroxynitrates	0.053	4.9E-3	0.13	0.13
C <sub>5</sub> dihydroxy-dinitrates	0.035	2.1E-3	0.068	0.17
C <sub>5</sub> hydroxy-hydroperoxy-dinitrates	2.1E-3	6.8E-5	2.9E-3	1.3E-3
C <sub>5</sub> carbonyl-hydroxy-dinitrates	1.3E-3	3.7E-6	3.9E-4	8.0E-4
C <sub>5</sub> hydroxy-nitrooxy-epoxides	0.027	2.1E-3	0.037	0.013
C <sub>5</sub> hydroxy-nitrooxy-dihydroperoxides	5.4E-3	3.9E-4	4.7E-3	1.0E-3
C <sub>5</sub> hydroxy-nitrooxy-hydroperoxy-epoxides	2.0E-3	2.5E-4	3.3E-3	8.0E-4
C <sub>5</sub> carbonyl-nitrooxy-epoxides	1.4E-3	2.5E-5	6.1E-4	2.6E-4
C <sub>5</sub> carbonyl-dihydroxy-nitrates	0.011	1.5E-4	3.9E-3	7.6E-3
MVK3OH4N <sup>b</sup>	0.17	0.015	0.21	0.48
ISOP1OH4CO <sup>b</sup>	0.31	0.24	0.38	0.57
MVK3OH4OOH <sup>b</sup>	2.5	1.1	1.3	1.1
MVKENOL <sup>b</sup>	0.37	0.65	0.22	0.12
MACR2OH3CO <sup>b</sup>	0.25	0.026	0.12	0.13
MACR2OH3OOH <sup>b</sup>	0.24	0.13	0.20	0.24
MACR1OH <sup>b</sup>	0.36	0.25	0.14	0.064
SOA from HMML/MAE <sup>c</sup>	0.023	2.6E-3	7.9E-3	0.030
SOA from methylglyoxal <sup>c</sup>	2.1E-3	2.0E-3	2.1E-3	0.015

<sup>a</sup>Species names are derived from Wennberg et al. (2018) and the mechanism posted in the online repository; <sup>b</sup>While these species' yields exceed the threshold set for exclusion, their lifetimes and loss pathways are sufficiently similar to those of other species in the mechanism to facilitate their combination (see text); <sup>c</sup>These simplification applies only to GEOS-Chem, not the gas-phase mechanism found in the online repository.

## References

- Arey, J., Aschmann, S. M., Kwok, E. S., and Atkinson, R.: Alkyl nitrate, hydroxyalkyl nitrate, and hydroxycarbonyl formation from the NO<sub>x</sub>-air photooxidations of C<sub>5</sub>-C<sub>8</sub> n-alkanes, *J. Phys. Chem. A*, 105, 1020–1027, 2001.
- Carter, W. P. L. and Atkinson, R.: Atmospheric chemistry of alkanes, *J. Atmos. Chem.*, 3, 377–405, <https://doi.org/10.1007/BF00122525>, 1985.
- Carter, W. P. L. and Atkinson, R.: Alkyl nitrate formation from the atmospheric photooxidation of alkanes: A revised estimation method, *J. Atmos. Chem.*, 8, 165173, 1989.
- Crouse, J. D., Paulot, F., Kjaergaard, H. G., and Wennberg, P. O.: Peroxy radical isomerization in the oxidation of isoprene, *Phys. Chem. Chem. Phys.*, 13, 13607–13613, 2011.
- Jacobs, M. I., Burke, W. J., and Elrod, M. J.: Kinetics of the reactions of isoprene-derived hydroxynitrates: Gas phase epoxide formation and solution phase hydrolysis, *Atmos. Chem. Phys.*, 14, 8933–8946, <https://doi.org/10.5194/acp-14-8933-2014>, 2014.
- Jenkin, M. E., Young, J. C., and Rickard, A. R.: The MCM v3.3.1 degradation scheme for isoprene, *Atmos. Chem. Phys.*, 15, 11433–11459, <https://doi.org/10.5194/acp-15-11433-2015>, 2015.
- Mao, J., Paulot, F., Jacob, D. J., Cohen, R. C., Crouse, J. D., Wennberg, P. O., Keller, C. A., Hudman, R. C., Barkley, M. P., and Horowitz, L. W.: Ozone and organic nitrates over the eastern United States: Sensitivity to isoprene chemistry, *J. Geophys. Res.*, 118, 11256–11268, 2013.
- Möller, K. H., Bates, K. H., and Kjaergaard, H. G.: The importance of peroxy radical hydrogen-shift reactions in atmospheric isoprene oxidation, *J. Phys. Chem. A*, 123, 920–932, <https://doi.org/10.1021/acs.jpca.8b10432>, 2019.
- Paulot, F., Crouse, J. D., Kjaergaard, H. G., Kroll, J. H., Seinfeld, J. H., and Wennberg, P. O.: Isoprene photooxidation: new insights into the production of acids and organic nitrates, *Atmos. Chem. Phys.*, 9, 1479–1501, 2009.
- Peeters, J. and Nguyen, T. L.: Unusually fast 1,6-H shifts of enolic hydrogens in peroxy radicals: formation of the first-generation C<sub>2</sub> and C<sub>3</sub> carbonyls in the oxidation of isoprene, *J. Phys. Chem. A*, 116, 6134–6141, <https://doi.org/10.1021/jp211447q>, 2012.
- Peeters, J., Muller, J. F., Stavrou, T., and Nguyen, V. S.: Hydroxyl radical recycling in isoprene oxidation driven by hydrogen bonding and hydrogen tunneling: The upgraded LIM1 mechanism, *J. Phys. Chem. A*, 118, 8625–8643, <https://doi.org/10.1021/jp5033146>, 2014.
- Praske, E., Otkjær, R. V., Crouse, J. D., Hethcox, J. C., Stoltz, B. M., Kjaergaard, H. G., and Wennberg, P. O.: Atmospheric autoxidation is increasingly important in urban and suburban North America, *Proc. Natl. Acad. Sci.*, 115, 64–69, <https://doi.org/10.1073/pnas.1715540115>, 2018.
- Schwantes, R. H., Teng, A. P., Nguyen, T. B., Coggon, M. M., Crouse, J. D., Clair, J. M. S., Zhang, X., Schilling, K. A., Seinfeld, J. H., and Wennberg, P. O.: Isoprene NO<sub>3</sub> oxidation products from the RO<sub>2</sub> + HO<sub>2</sub> pathway, *J. Phys. Chem. A*, 119, 10158–10171, <https://doi.org/10.1021/acs.jpca.5b06355>, 2015.
- Wennberg, P. O., Bates, K. H., Crouse, J. D., Dodson, L. G., McVay, R. C., Mertens, L. A., Nguyen, T. B., Praske, E., Schwantes, R. H., Smarte, M. D., St Clair, J. M., Teng, A. P., Zhang, X., and Seinfeld, J. H.: Gas-phase reactions of isoprene and its major oxidation products, *Chem. Rev.*, 118, 3337–3390, <https://doi.org/10.1021/acs.chemrev.7b00439>, 2018.